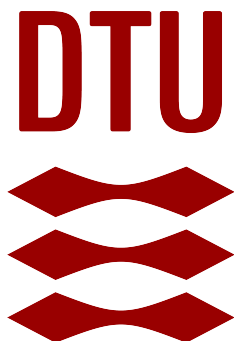


TECHNICAL UNIVERSITY OF DENMARK



Quantum Reaction Dynamics for Early- and Late-Barrier Reactions

Student:
SCHMIDT, O.

Student number:
s194193

Supervisor: Niels Engholm Henriksen,
Department of Chemistry

ABSTRACT

The understanding of how chemical reactions occur has been a subject of considerable debate among scientists since the discovery of molecules. Guidelines play a crucial role in facilitating the development of new molecules. Among these guidelines are the Polanyi rules, which suggest that vibrational excitation of the reactant is more effective in enhancing reaction probability for late-barrier reactions, while increasing translational energy is more effective for early-barrier reactions. However, the validity of the Polanyi rules has recently been questioned in several papers, along with proposed restrictions. One restriction is that reactions favour translational energy over vibrational for small energies and vice versa. This thesis shows that this may be true for early-barrier reactions, but is not necessarily the case for late-barrier reactions. Furthermore, the validity of the Transition State Theory is questioned, at least for great energies.

ACKNOWLEDGEMENT

The following thesis is part of the Master's degree curriculum in Applied Chemistry at the Technical University of Denmark (DTU). The work was carried out during the period of September 28th 2023 - January 28th 2024 under the supervision of Niels Engholm Henriksen at the Department of Chemistry.

First and foremost, while unconventional I will extend my thanks beyond the scope of this thesis to my supervisor. My thanks goes to Professor Niels Engholm Henriksen, whom I had the pleasure of having as my student supervisor in 2019, supervisor for a collaborative chemical project in 2020 and supervisor during my bachelor thesis in 2021-2022. Conventionally, within the scope of this thesis, I would like to thank him for his continuous support and theoretical insights. As always, it has been a delight and it goes without saying that I had chosen him as my supervisor again, should the opportunity arise. Furthermore, I would like to thank Ph.D. Stdt. Kasper Linger Effersøe for his continuous support and computational remarks. It has been a rewarding experience to discuss the various Matlab implementations. Moreover, I would like to thank my friends within and outside of academia, whose editorial support cannot be stopped by time of day or night. Your remarks and additions to the format of this thesis shall not go unmentioned. Finally, in best physiochemical manner, I would like to mention one more person by name: Celine Thustrup Hansen, your spirit, support and motivation remained proportional to the geographical displacement between us throughout writing of this thesis.

Preliminary Concepts and Definitions

The main objective of this thesis is to understand chemical reaction dynamics of early- and late barrier reactions. In doing so requires understanding quantum theory, which in turn requires a mathematical framework. Since definitions vary using different sources, this chapter provides a common framework, which will be used throughout this thesis. The idea of this section is not to provide generalized proofs of the axioms, definitions, postulates and approximations, but rather to present the notation of these. In the *mathematical foundation* section, the Hilbert space and linear bounded operators are defined, because these are mathematical cornerstones of quantum mechanics. In the *quantum mechanical* section, postulates of quantum mechanics along with operators and commutators are provided.

MATHEMATICAL FOUNDATION

In order to solve any problem, one first has to define the framework of the problem. In mathematics, this framework is the vector space (space, for short). An understanding of the space, and therefore the framework, of the physical system is required in order to understand the problem to be solved in hopes of solving it. Quantum mechanics include so-called wavefunctions, which are defined in the Hilbert space, \mathcal{H} . Hence this section is dedicated to understanding the axioms and definitions of the Hilbert space. While derivations in the field of pure topology can be fun in and of itself, they have been left out in order not to shift the focus from later sections, but can be seen in O. Christensen's *Functions, Spaces and Expansions* [1–3]. While this book is the main source for this section, some slight changes in definitions have been made in order to create a more smooth transition to the quantum mechanical terminology in later sections. To account for this, footnotes have been provided where definitions have been adjusted.

AXIOMS AND DEFINITIONS

This section defines the Hilbert space, the linear operator and the hermitian operator as well as prerequisite definitions of these.

(Vector) space axiom : *Let a nonempty set, V , be equipped with the following operations: addition and scalar multiplication. Then V forms a (vector) space, if the following equations are satisfied:*

$$\psi + \phi = \phi + \psi, \quad \text{for all } \psi, \phi \in V \quad (0.1a)$$

$$(\psi + \phi) + \varphi = \psi + (\phi + \varphi), \quad \text{for all } \psi, \phi, \varphi \in V \quad (0.1b)$$

$$\text{There exists an element, } 0 \text{ such that } \psi + 0 = \psi, \quad \text{for all } \psi \in V \quad (0.1c)$$

$$\text{There exists an element, } -\psi \in V \text{ such that } \psi + (-\psi) = 0, \quad \text{for all } \psi \in V \quad (0.1d)$$

$$\text{For all } \alpha, \beta \in \mathbb{C}, \quad \alpha(\beta\psi) = (\alpha\beta)\psi, \quad \text{for all } \psi \in V \quad (0.1e)$$

$$\text{For all } \alpha, \beta \in \mathbb{C}, \quad (\alpha + \beta)\psi = \alpha\psi + \beta\psi, \quad \text{for all } \psi \in V \quad (0.1f)$$

$$\text{For all } \alpha \in \mathbb{C}, \quad \alpha(\psi + \phi) = \alpha\psi + \alpha\phi, \quad \text{for all } \psi, \phi \in V \quad (0.1g)$$

$$\text{There exists an element, } 1 \text{ such that } 1\psi = \psi, \quad \text{for all } \psi \in V \quad (0.1h)$$

Norm definition¹ : *Let V be a complex space. A normed space, V , is a space equipped with the norm function:*

$$\|\cdot\| : V \rightarrow \mathbb{R} \quad (0.2)$$

that satisfies the following 4 conditions:

$$0 \leq \|\psi\|, \quad \text{for all } \psi \in V \quad (0.3a)$$

$$\|\psi\| = 0 \Leftrightarrow \psi = 0, \quad \text{for all } \psi \in V \quad (0.3b)$$

$$\text{Let } \alpha \in \mathbb{C}, \quad \|\alpha\psi\| = |\alpha| \|\psi\|, \quad \text{for all } \psi \in V \quad (0.3c)$$

$$\|\psi + \phi\| \leq \|\psi\| + \|\phi\|, \quad \text{for all } \psi, \phi \in V \quad (0.3d)$$

Cauchy sequence definition : *Let V be a normed space and $\{\psi_k\}_{k \in \mathbb{N}}$ be a sequence of elements in V . If for each $\varepsilon > 0$, there exists an $N \in \mathbb{N}$ such that*

$$\|\psi_m - \psi_n\| \leq \varepsilon \quad (0.4)$$

for every $m, n > N$, then $\{\psi_k\}_{k \in \mathbb{N}}$ is a Cauchy sequence.

Banach space definition : *A complete normed space, V , where each Cauchy sequence, $\{\psi_k\}_{k \in \mathbb{N}} \in V$, converges toward some $\psi \in V$, is called a Banach space.*

Inner product space definition : *Let V be a space. The inner product is defined as the*

¹The specific norm used is denoted as a subscript in the norm function, $\|\cdot\|_N$, where N is a specific norm. In this thesis, the L^2 norm is used in section 1 and the l^2 norm is used in section 2.

following mapping on V :

$$\langle \cdot | \cdot \rangle : V \times V \rightarrow \mathbb{C} \quad (0.5)$$

If the inner product satisfies the following equations:

$$\langle \alpha\psi + \beta\phi | \varphi \rangle = \bar{\alpha}\langle \psi | \varphi \rangle + \bar{\beta}\langle \phi | \varphi \rangle, \quad \text{for all } \psi, \phi, \varphi \in V, \quad \alpha, \beta \in \mathbb{C}; \quad (0.6a)$$

$$\langle \psi | \phi \rangle = \overline{\langle \phi | \psi \rangle}, \quad \text{for all } \psi, \phi \in V; \quad (0.6b)$$

$$0 \leq \langle \psi | \psi \rangle, \quad \text{for all } \psi \in V; \quad (0.6c)$$

$$\langle \psi | \psi \rangle = 0 \Leftrightarrow \psi = 0 \quad (0.6d)$$

then V is an inner product space.

Hilbert space definition : An inner product and Banach space with the following inner product norm:

$$\| \psi \| = \langle \psi | \psi \rangle^{0.5}, \quad \psi \in \mathcal{H} \quad (0.7)$$

is called a Hilbert space and denoted \mathcal{H} .

Orthogonal system and orthonormal system definitions : Let \mathcal{H} be a Hilbert space.

Two elements, $\psi, \phi \in \mathcal{H}$ are said to be orthogonal, if $\langle \psi | \phi \rangle_{\mathcal{H}} = 0$.

Let $\{\psi_n\}_{n \in \mathbb{N}} \in \mathcal{H}$ be a collection of vectors² and $\langle \psi_n | \psi_m \rangle = 0$ for all $n \neq m$. Then $\{\psi_n\}_{n \in \mathbb{N}}$ is an orthogonal system.

Let $\{\psi_n\}_{n \in \mathbb{N}} \in \mathcal{H}$ be an orthogonal system and $\| \psi_n \|_N = 1$ for all $n \in \mathbb{N}$. Then $\{\psi_n\}_{n \in \mathbb{N}}$ is an orthonormal system.

Bounded linear operator definition : Let V_1 and V_2 be normed spaces and $\psi, \phi \in V_1$. An operator $\hat{A} : V_1 \rightarrow V_2$ is linear, if it satisfies:

$$\hat{A}(\alpha\psi + \beta\phi) = \alpha\hat{A}\psi + \beta\hat{A}\phi, \quad \text{for all } \alpha, \beta \in \mathbb{C} \quad (0.8)$$

And bounded, if there exists a c such that:

$$|\hat{A}\psi| \leq c \|\psi\|_N, \quad \text{for all } \psi \in V_1 \quad (0.9)$$

Hermitian operator : Let \hat{A} be a linear bounded operator operating on $\psi \in \mathcal{H}$. If the

²Please note that a collection of vectors is not excluded from complex vectorfunctions, $\psi \in \mathbb{C}^n$, and that the collection itself can go towards infinity. However, each element must converge. This is due to the following: The Hilbert space is a Banach space by definition. Thus, a Banach space needs to have each Cauchy sequence converging toward some element in the sequence by definition.

following holds true

$$\hat{A}^\dagger = \hat{A} \quad (0.10)$$

then it follows that \hat{A} is a Hermitian operator.

Furthermore, if eq. (0.10) is satisfied, it follows that \hat{A} is self-adjoint, contains real eigenvalues, a_n , and \hat{A} is diagonalizable, respectively:

$$\langle \psi_m | \hat{A} \psi_n \rangle = \langle \hat{A} \psi_m | \psi_n \rangle \quad (0.11a)$$

$$\hat{A} |\psi_n\rangle = a_n |\psi_n\rangle \quad (0.11b)$$

$$\hat{A} = P D P \quad (0.11c)$$

where $D = \text{diag}(a_1, \dots, a_l)$ is the diagonal of the set of eigenvalues, $\{a_i\}_{i \in \mathbb{N}}$ and P is an invertible matrix consisting of the eigenvectors.

TRANSFORMATIONS AND DISTRIBUTIONS

This section defines the Fourier transformation and the delta distribution.

Fourier transformation : Let $\psi, \phi \in \mathcal{L}^2(\mathbb{R}^n)$, then the Fourier transformation and its inverse are denoted $\mathcal{F}, \mathcal{F}^{-1}$ and defined by [4]:

$$\mathcal{F}[\psi] : \mathbb{R}^n \rightarrow \mathbb{C}^n, \mathcal{F}[\psi] = \int_{\mathbb{R}^n} \phi(k) \exp(2\pi i x k) dk \quad (0.12a)$$

$$\mathcal{F}^{-1}[\phi] : \mathbb{C}^n \rightarrow \mathbb{R}^n, \mathcal{F}^{-1}[\phi] = \int_{\mathbb{R}^n} \psi(x) \exp(-2\pi i x k) dx \quad (0.12b)$$

δ (delta) distribution³ : Let $a \in \mathbb{R}$. The delta distribution, δ_a , is defined as a linear functional, which fulfills $\delta_a(\psi) = \psi(a)$. From eq. (0.9), it follows that $|\delta_a\psi| = \|\psi\|_{0,0} \in \mathcal{F}$. There does not exist a function, $g(x) \in \mathcal{L}^2(\mathbb{R}^n)$ such that $\delta_a(\psi) = \int_{\mathbb{R}^n} g(x)\psi(x) dx$ for all $\psi \in \mathcal{F}$, but there is a pure point measure⁴, $\mu_a(x)$, which is incorporated into the notation in the following way:

$$\delta_a(\psi) = \int_{\mathbb{R}^n} \psi(x) d\mu_a = \int_{\mathbb{R}^n} \psi(x)\delta(x-a) dx \quad (0.13)$$

QUANTUM MECHANICAL FOUNDATION

As stated in the mathematical foundation section, the framework of the problem has to be defined to solve the problem. Quantum mechanics can be boiled down to 3-7 postulates dependent on the source [10, 11], which define the starting point of quantum mechanical derivations. To continue from this, quantum mechanical operators are defined. These are defined in such a way that the value of a laboratory measurement can show the validity of the measurement. While the *axioms and definitions* and *transformations, distributions and spaces* sections defined the spaces and how to map elements of these spaces to other spaces using transformations, the following *postulates of quantum mechanics* section defines the specific spaces and their operators. The *quantum mechanical operators* section defines the validation of the measurement values. While coupled in many ways, this thesis pursues to distinguish the mathematics from quantum

³The field of abstract mathematics is - as the name suggests - abstract. While not necessary in order to define the δ distribution, explicit representations of the delta distribution and the different notations of previously mentioned distribution can help understanding it. The delta distribution is also famously known as Dirac's delta function, who defined it as $\delta(x) = 1$, when $x \neq 0$ while $\int_{-\infty}^{\infty} x\delta(x) dx = 1$ in the paper *The Physical Interpretation of the Quantum Dynamics* in 1927 [5]. The change of definition in this study seeks only to elaborate on this definition from a "Real Analysis"-point of view, whose field have been expanded since the delta function was first defined. Dirac, however, did contribute considerably to the field of quantum mechanics and this paper compensates the lack of recognition of the delta function by naming 3 out of the 5 postulates defined in section 1.2.1 to Dirac and Born for their shared contributions to the field of quantum mechanics. In the field of signals and systems, the delta distribution is also called the unit impulse function and defined in the time domain similarly to Dirac: $\delta = \lim_{\epsilon \rightarrow 0} I(t) = \frac{1}{\epsilon}$, where $t \in [\frac{\epsilon}{2}; \frac{\epsilon}{2}]$ and 0 otherwise as can be seen in *Structural Dynamics Fundamentals and Advanced Applications* by Alvar M. Kabe and Brian H. Sako [6]. As a final example, the delta distribution can be represented as a sequence of exponential functions $\{\psi_j(x)\}$ where $\psi_j(x) = \lim_{j \rightarrow \infty} \frac{j}{\sqrt{2\pi}} \exp\left(\frac{-(x-j)^2}{2}\right)$ for $x \in \mathbb{C}$ and $j \in \mathbb{N}_0$. Recall the limit law of products and the comparison test theorem and see that $\lim_{j \rightarrow \infty} \frac{j}{\sqrt{2\pi}}$ diverges towards ∞ at slower pace than $\lim_{j \rightarrow \infty} \exp\left(\frac{-(xj)^2}{2}\right)$, which converges towards 0. It is very easy to Fourier transform complex exponential functions using eqs. (0.12a) or (0.12b), which is the main reason for using this notation as can be seen in *Generalized Delta Functions and Their Use in Quantum Optics* by R.A. Brewster and J.D. Franson [7, 8].

⁴Measure theory exceeds the span of this thesis but elaborate descriptions can be found in Y. M. Berezansky et al's *Measures in the Products of Spaces. Fubini Theorem*: [9].

mechanics in this way. Many books have coupled mathematics to quantum mechanics and one of these is V. Moretti's *Spectral Theory and Quantum Mechanics* [12, 13].

THE POSTULATES OF QUANTUM MECHANICS

This section proposes the postulates of quantum mechanics [14].

Schrödinger's postulate I : *The wave-function completely specifies the state of a quantum-mechanical system, $|\Psi\rangle \in \mathcal{L}^2(\mathbb{R}^n)$ and evolves in time according to the time-dependent Schrödinger equation [11, 15]:*

$$\hat{H} |\Psi\rangle = i\hbar \frac{d}{dt} |\Psi\rangle \quad (0.14)$$

Born-Dirac's postulates II.a, II.b and II.c : *In a unity normalized state represented by the $|\Psi\rangle$, the probability of an observable \hat{A} having the eigenvalue a is given by [16, 17]⁵:*

$$\mathcal{P}(A|\mathcal{L}^2(\mathbb{R}^n)) = |\langle a|\Psi\rangle|^2 \quad (0.15)$$

$$\hat{A} |\Psi\rangle = a |\Psi\rangle \quad (0.16)$$

$$\langle \hat{A} \rangle = \langle \Psi | \hat{A} | \Psi \rangle \quad (0.17)$$

Neumann postulate III : *Let \hat{A} be a linear Hermitian operator that represents a physically observable property, then the eigenstate $|\Psi\rangle$ of \hat{A} forms a complete set. [13, 19].*

QUANTUM MECHANICAL OPERATORS AND COMMUTATORS

This section introduces quantum mechanical operators and commutators used in this thesis.

Position operator definition⁶ : *Let $\psi, \phi \in \mathcal{L}^2(\mathbb{R}^n)$ be represented by the complete position orthogonal system, $\{x_n\}_{n \in \mathbb{N}}$ and $\{k_n\}_{n \in \mathbb{N}}$, respectively, then:*

$$\hat{X} |\psi\rangle : \mathcal{L}^2(\mathbb{R}^n) \rightarrow \mathcal{L}^2(\mathbb{R}^n), \quad \hat{X} |\psi\rangle = x |\psi\rangle \quad (0.18a)$$

$$\hat{X} |\phi\rangle : \mathcal{L}^2(\mathbb{R}^n) \rightarrow \mathcal{L}^2(\mathbb{R}^n), \quad \hat{X} |\phi\rangle = -i\hbar \frac{d}{dk} |\phi\rangle \quad (0.18b)$$

⁵The original paper of the Born rule, $\langle \hat{A} \rangle = \langle \Psi | \hat{A} | \Psi \rangle$, was in german but has since been translated to english using the following source: [18]

⁶By convention, ψ is used to denote wavefunctions represented as linear combination of the coordinate basis arising from the position operator as $|\psi\rangle$ [10, 20, 21].

Momentum operator definition⁷ : Let $\phi \in \mathcal{L}^2(\mathbb{R}^n)$ be represented by the complete momentum orthogonal system, $\{k_n\}_{n \in \mathbb{N}}$ then:

$$\hat{P} |\phi\rangle : \mathcal{L}^2(\mathbb{R}^n) \rightarrow \mathcal{L}^2(\mathbb{R}^n), \quad \hat{P} |\phi\rangle = k |\phi\rangle \quad (0.19)$$

$$\hat{P} |\psi\rangle : \mathcal{L}^2(\mathbb{R}^n) \rightarrow \mathcal{L}^2(\mathbb{R}^n), \quad \hat{P} |\psi\rangle = -i\hbar \frac{d}{dx} |\psi\rangle \quad (0.20)$$

Hamiltonian definition : Let $\psi \in \mathcal{L}^2(\mathbb{R}^n)$, then :

$$\begin{aligned} \hat{H} |\psi\rangle &: \mathcal{L}^2(\mathbb{R}^n) \rightarrow \mathcal{L}^2(\mathbb{R}^n), \\ \hat{H} |\psi\rangle &= \left[-\frac{\hbar^2}{2} \sum_i \frac{1}{m_i} \nabla_i^2 + V \right] |\psi\rangle \end{aligned} \quad (0.21)$$

Canonical commutation relation : Let \hat{X} be defined by eqs. (0.18a) and (0.18b). Furthermore, let \hat{P} be defined by eqs. (0.19) and (0.19). Then their canonical commutation relation is:

$$[\hat{X}, \hat{P}] = i\hbar \quad (0.22)$$

⁷By convention, ϕ is used to denote wavefunctions represented as linear combination of the momentum basis arising from the momentum operator as $|\phi\rangle$ [10, 20, 21].

Contents

Introduction	1
1 Reaction Dynamics	2
1.1 Potential Energy Surfaces	2
1.1.1 Morse Potential	2
1.1.2 London-Eyring-Polanyi (LEP) Potential	6
1.1.3 London-Eyring-Polanyi-Sato (LEPS) Potential	7
1.2 Hamiltonian and Wavefunction	8
1.2.1 The Hamiltonian	8
1.2.2 The Wavefunction	10
1.3 LEPS Energy Barriers	11
1.4 Normal Modes	13
1.4.1 Second Derivative Test	13
1.4.2 Normal Mode Frequencies and Representations	14
1.5 Transition State Theory - Rate Constant	16
2 Numerical Methods	21
2.1 Splitting-Operator Method	21
2.1.1 The Strang-Marchuk Algorithm	22
2.2 Reactive Flux and Complex Absorbing Potentials	25
2.2.1 Complex Absorbing Potential (CAP)	25
2.2.2 Reactive Flux	27
2.2.3 Cumulative Flux Method and Trapezoidal Rule	30
2.3 Test Cases	32
2.3.1 Standard Deviation of Gaussian Wave Packet	32
2.3.2 Choice of Step size, Δt and Grid spacing	35
3 Results and Discussion	36
3.1 Thermoneutral Reaction, $H + H_2 \rightarrow H_2 + H$	38
3.2 Early-Barrier Reactions	39
3.2.1 $O + H_2 \rightarrow OH + H$	39
3.2.2 $F + H_2 \rightarrow HF + H$	40
3.2.3 $F + HCl \rightarrow HF + Cl$	41
3.3 Late-Barrier Reactions	42
3.3.1 $OH + H \rightarrow O + H_2$	42
3.3.2 $HF + H \rightarrow F + H_2$	43
3.3.3 $HF + Cl \rightarrow F + HCl$	44
3.4 Discussion	46

Conclusion	48
Bibliography	49
A Normal Mode Analysis	55
B Morse Parameters	57
C Jacobi Coordinates - Three Body System in One Dimension	59
C.1 Translative Terms	59
C.2 Hamiltonian - 3 Dimensions	61
D Continuity Equation and Flux Operator	63
D.1 Continuity Equation: Two Dimensions, Two Particles	63
D.2 Flux Operator Representations	64
E Accuracy of Strang-Marchuk Splitting	66

Introduction

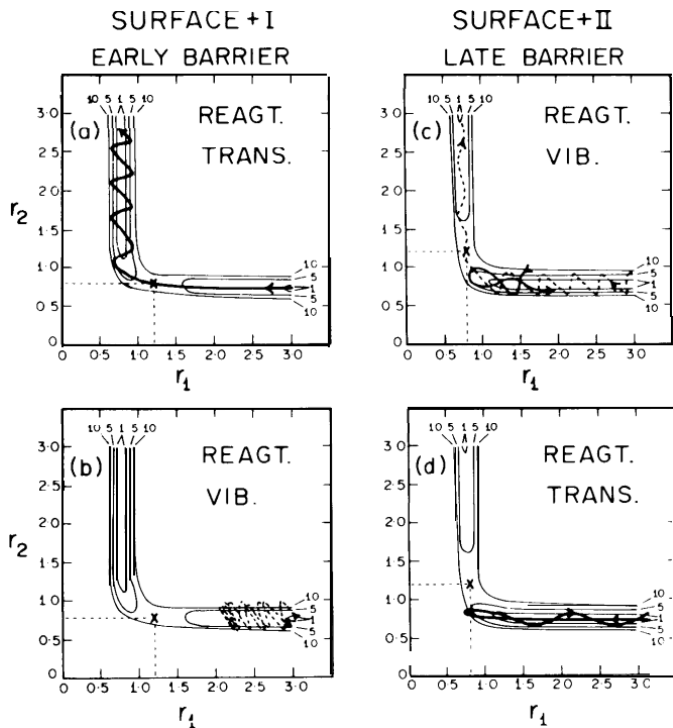


Figure 1: Specimen trajectories for early- and late-barrier for low and high vibrational/translative ratios, respectively (Reprint from Polanyi's Nobel lecture [22]).

early. ii) Reactant vibrational energy increases the reaction probability more than translative energy, when the reaction barrier is late. These rules can also be seen on Figure 1. This thesis investigates these rules by using the semi-empirical LEPS potential for three early- and late-barrier reactions. One thermoneutral reaction has been used to validate the methods used. Furthermore, the reaction probabilities of these reactions are compared to a recent paper, which restrict the Polanyi rules [26]. This thesis, however, will show that this restriction may only hold true for early-barrier reactions.

In 1971 John Charles Polanyi wrote an article concerning some concepts and trends in reaction dynamics, which resulted in him getting the Nobel prize in 1986 [22]. Based off previous experiments, quasiclassical simulations and classical Monte Carlo simulations, Polanyi comprised general trends for endothermic, thermoneutral⁸ and exothermic reactions as well as scattering angles with respect to the shape of the potential energy surface [23]. One of the trends he found, which are now referred to as the *Polanyi rules* by later papers, is provided by the following [24, 25]: i) Reactant translative energy increases the reaction probability more than vibrational energy, when the reaction barrier is

⁸A reaction is only thermoneutral, when $\Delta H_r = 0$. This is only true, when reactants and products are equal, which have small or no significance. Furthermore, endothermic and exothermic reactions are defined for $\Delta H_r \in]0, \infty[$ and $\Delta H_r \in]-\infty, 0[$, respectively. Obviously, one cannot study a reaction, whose ΔH_r goes to infinity. Polanyi therefore redefined thermoneutral to concern reactions for which $\Delta H_r \in]-30, 30[$ kcal mol⁻¹. In addition, his definition of exothermic reactions concerns reactions for which $\Delta H_r \in [-50, -30]$ kcal mol⁻¹. His definition of endothermic reactions concerns reactions for which $\Delta H_r \in [30, 50]$ kcal mol⁻¹. This paper uses the terminology, early-, late-barrier and thermoneutral. $R_{AB} > R_{BC}$ for early-barrier reactions, $R_{AB} < R_{BC}$ for late-barrier reactions and $R_{AB} \approx R_{BC}$ for central-barrier reactions. $\{R_{AB}, R_{BC}, R_{CA}\}$ is the set of relative coordinates defined in section 1.2.1. An example of an early-barrier reaction can be seen on Figure 1.3.

1. Reaction Dynamics

In this section, the reaction dynamics of the following reactions will be motivated:



In order to understand a reaction with respect to the rate constant, one must understand the following: The potential energy surface, the saddle point location coordinates of an potential energy surface, the wavefunction used and propagation as well as the rate constant. This chapter seeks to elaborate on the theory behind these for reactions (1.1a-d). Chapter 2 seeks to apply the methods described in this section computationally.

1.1 POTENTIAL ENERGY SURFACES

In this section, the choice of potential energy surface (PES) used in this thesis is motivated. Some historical background is provided in order to understand the Morse, London-Eyring-Polanyi (LEP) and London-Eyring-Polanyi-Sato (LEPS) potential. A special case for which the LEPS potential collapses into the Morse potential is mentioned. This is further utilized in section 1.2.2. This motivates the use of the LEPS potential in the following sections.

1.1.1 MORSE POTENTIAL

In this section, the Morse potential eigenstates and -values are reiterated. The Morse solution will be used in later sections for the wave propagation along with a Gaussian wavepacket. This resembles the Harmonic oscillator solution. Hence this section ends with a comparison between both.

In 1929, Philip M. Morse proposed a solution to the time-independent Schrödinger equation provided by eq. (0.21) describing a diatomic molecule under the Born-Oppenheimer approximation [11, 27]:

$$\nabla^2 \psi_{lmn}^{\text{Morse}}(R, \phi, \theta) + \frac{2\mu}{\hbar^2} \left[E_n^{\text{Morse}} - \frac{e^2 Z_1 Z_2}{R} + V_e(R) \right] \psi_{lmn}^{\text{Morse}}(R, \phi, \theta) = 0 \quad (1.2)$$

with $\mu = \frac{m_1 m_2}{m_1 + m_2}$ being the reduced mass for a diatomic system [kg], R is the distance between the nuclear positions [\AA], Z_1 and Z_2 the nuclear charges for atom 1 and 2 and e is the elementary charge [C]. $\frac{e^2 Z_1 Z_2}{R}$ is the coulombic interaction and $V_e(R)$ is the

electronic energy between two fixed nuclei in a fixed space separated by the distance, R . E_n is the allowed energy levels. Morse proposed an approximation to the last two potential energy terms in eq. (1.2) provided by:

$$\begin{aligned} V^{\text{Morse}}(R) &= \frac{e^2 Z_1 Z_2}{R} - V_e(R) \\ &\approx D_e \exp(-2\alpha(R - R_0)) - 2D_e \exp(-\alpha(R - R_0)) \end{aligned} \quad (1.3)$$

with R_0 being the equilibrium distance [Å], D_e being the minimum of the potential at $R = R_0$ [eV] and α is a fitting parameter¹ [Å⁻¹]. Morse argued that this potential was physically motivated using the following fourfold arguments: 1) $V^{\text{Morse}}(R)$ converges asymptotically towards a finite value for $R \rightarrow \infty$, 2) $V^{\text{Morse}}(R)$ has one and only one minimum, which is found at $R = R_0$, 3) $V^{\text{Morse}}(R = 0) \gg 0$ even though it should be mentioned that an even better potential would satisfy $V(R \rightarrow 0) \rightarrow \infty$ and 4) the energy levels ought to be determined exactly to be a finite polynomial. 1-3) are satisfied from eq. (1.3). Substituting eq. (1.3) into eq. (1.2) yields the following solution using separation of variables:

$$\psi_{lmn}^{\text{Morse}}(R, \phi, \theta) = N \cdot \Phi_m(\phi) \cdot \Theta_{lm}(\theta) \cdot \frac{\chi_n(R)}{R} \quad (1.4)$$

$$\Phi_m(\phi) = \exp(im\phi) \quad (1.5)$$

$$\Theta_{lm}(\theta) = \sin^m(\theta) \cdot P_l^m(\cos(\theta)) \quad (1.6)$$

$$\chi_n(R) = \exp\left(-\frac{y(R)}{R}\right) \cdot L_n^{2\beta}(y(R)) \cdot y^\beta(R) \quad (1.7)$$

where $l, m \in \mathbb{N}_0$ are the rotational and magnetic quantum numbers, respectively, P_l^m is the Legendre polynomium, which in the Rodrigues formulation is: $P_l(x) = \frac{1}{2^l l!} \frac{d^l}{dx^l} (x^2 - 1)^l$ [29], N is the normalization factor and the remaining functions and parameters are provided by:

$$y = \lambda \cdot \exp(-\alpha(R - R_0)) \quad (1.8)$$

$$\beta = \frac{\lambda - 2n - 1}{2} \quad (1.9)$$

$$L_n^{2\beta}(y(R)) = \frac{y^{-2\beta}(R)}{n!} \left(\frac{d}{dy(R)} - 1 \right)^n y^{n-2\beta}(R) \quad (1.10)$$

$$\lambda = \frac{(8\mu D_e)^{\frac{1}{2}}}{\alpha \hbar} \quad (1.11)$$

¹ α is also called the Morse parameter [28].

where $n \in \mathbb{N}_0$ is the vibrational quantum number and eq. (1.10) is the generalized Laguerre polynomial, which is written in the Rodrigues formulation [29].

This thesis purely concerns collinear systems, hence only vibrational states are concerned and the angles are zero. Hence $\{\phi, \theta, l, m\} = \{0, 0, 0, 0\}$. Substituting into eq. (1.5) and eq. (1.6) yields $\{\Phi, \Theta\} = \{1, 1\}$. Using $N^2 \int_{\mathbb{R}^+} R^2 |\psi(R)|^2 dR = 1$, it can be shown that the normalization factor becomes:

$$N = \left(\frac{2\alpha\beta\Gamma(n+1)}{\Gamma(\lambda-n)} \right)^{\frac{1}{2}} \quad (1.12)$$

with $\Gamma(x) = \int_{\mathbb{R}_0^+} t^{x-1} \exp(-t) dt$ being the Gamma function². Hence the wave function is:

$$\psi_n^{\text{Morse}}(R) = N \cdot \frac{\chi_n(R)}{R} = \left(\frac{2\alpha\beta\Gamma(n+1)}{\Gamma(\lambda-n)} \right)^{\frac{1}{2}} \exp\left(-\frac{y(R)}{R}\right) L_n^{2\beta}(y(R)) y^\beta(R) \quad (1.13)$$

and the found energy levels are provided by:

$$E_n^{\text{Morse}} = -D_e + \left(\frac{2D_e}{\mu} \right)^{\frac{1}{2}} \alpha\hbar \left(n + \frac{1}{2} \right) - \frac{1}{2\mu} \left(\alpha\hbar \left(n + \frac{1}{2} \right) \right)^2 \quad (1.14)$$

which is a finite second order polynomial with respect to $\alpha\hbar \left(n + \frac{1}{2} \right)$. Hence 4) is also satisfied.

The solution can easily be compared to the Harmonic oscillator. The derivation for the Harmonic oscillator can be found in many books and only the potential, the solution and energy levels will be provided in the relevance of the Morse potential [10, 11, 20, 28]. The potential can be rewritten using Morse values $\{D_e, \alpha, R_0\}$ to give the following (see section B for derivation):

$$V^{\text{Harmonic}}(R) = D_e \alpha^2 (R - R_0)^2 \quad (1.15)$$

²The formal definition of the Gamma function, $\Gamma(x)$, takes the restriction that $x \in \mathbb{C}$ and $\Re(x) > 0$. This is redundant here since the Gamma function only shows up in eq. (1.12). For $\Gamma(n+1)$, it follows that $n+1$ is always positive and for $\Gamma(\lambda-n)$, it must be stated that $\lambda > n$. An example of this is $\lambda \approx 35$ [unitless] for H₂, which has 15 vibrational states in the ground state [30]. The molecule has therefore dissociated long before $n > \lambda$ becomes a problem.

and the wave function solution is provided by:

$$\psi_n^{\text{Harmonic}}(R) = N \cdot \frac{\chi_n(R)}{R} = \frac{1}{(2^n n!)^{\frac{1}{2}}} \left(\frac{\alpha (2D_e \mu)^{\frac{1}{2}}}{\pi \hbar} \right)^{\frac{1}{4}} \cdot \exp \left(-\frac{\alpha}{\hbar} \left(\frac{\mu D_e}{2} \right)^{\frac{1}{2}} (R - R_0)^2 \right) \cdot H_n \left((R - R_0) \left[2\mu D_e \left(\frac{\alpha}{\hbar} \right)^2 \right]^{\frac{1}{4}} \right) \quad (1.16)$$

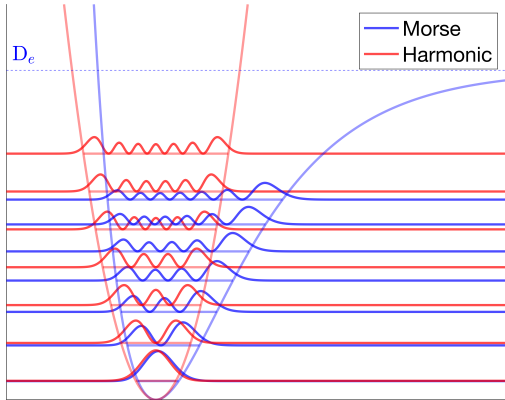


Figure 1.1: Energy levels for Morse and Harmonic oscillator potentials along with energy levels for both and their analytical solutions for $\{n\}_{n=0}^6$. Energy levels and potentials have lower opacity than the probability densities for clarity. All probabilities are calculated by squaring the eigenstates. Morse potential, eigenstates and eigenvalues, respectively (blue): eqs. (1.3), (1.13) and (1.14). Harmonic potential, eigenstates and eigenvalues, respectively (red): eqs. (1.15), (1.16) and (1.17).

this happens, the system is vibrationally unbounded, since the system exceeds the well depth and will dissociate. As an example, H_2 has 10 bound states [31]. This thesis considers total energies being $\approx 0.5 D_e$ initialized in vibrational state $n = 0$ or $n = 1$. Therefore, the problem of the diatomic molecules dissociating instead of reacting were not considered.

with H_n being the Hermite polynomial, whose Rodrigues formulation is: $H_n(x) = (-1)^n \exp(x^2) \frac{d^n}{dx^n} (\exp(x^2))$. Thus, the energy levels are provided by:

$$E_n^{\text{Harmonic}} = -D_e + \alpha \hbar \left(\frac{2D_e}{\mu} \right)^{\frac{1}{2}} \cdot \left(n + \frac{1}{2} \right) , \quad n \in \mathbb{N}_0 \quad (1.17)$$

Eqs. (1.3), (1.13) squared, (1.14), (1.15), (1.16) squared and (1.17) have been plotted on Figure 1.1. And it can be seen that the Morse potential eigenstates and -values resemble the Harmonic potential eigenstates and -values for small n . Furthermore, it can be seen that the eigenstates and -values deviate for greater n and are smaller for the Morse potential solutions than the Harmonic potential solution. This is due to eqs. (1.14) and (1.17) only differing by a term being negative for the Morse potential. As a final remark, it should be mentioned that the Morse eigenvalue might exceed the well depth, D_e , for some $n \in \mathbb{N}_0$. When

1.1.2 LONDON-EYRING-POLANYI (LEP) POTENTIAL

This subsection introduces the London-Eyring-Polanyi (LEP) potential. The LEP potential motivated the development of the LEPS potential, which is introduced in section 1.1.3 and has been used in this thesis. The LEP potential was proposed by H. Pelzer and E. P. Wigner in 1932 and is provided by [32]:

$$V^{\text{LEP}}(R_{AB}, R_{BC}) = D_e + V_0 - \left\{ \left(V_{AB}^{\text{Morse}} \right)^2 + \left(V_{BC}^{\text{Morse}} \right)^2 + \left(V_{CA}^{\text{Morse}} \right)^2 - V_{AB}^{\text{Morse}} V_{BC}^{\text{Morse}} - V_{BC}^{\text{Morse}} V_{CA}^{\text{Morse}} - V_{CA}^{\text{Morse}} V_{AB}^{\text{Morse}} \right\}^{1/2} \quad (1.18)$$

where D_e is the Morse potential well depth [eV], V_0 is the zero point energy [eV] and V_{ij}^{Morse} is the Morse potential, which was provided in eq. (1.3) with ij denoting the diatomic system in question. For a collinear reaction, using $R_{CA} = R_{AB} + R_{BC}$ decreases the dimensionality. In contrast to the Morse potential, there is no analytical solution, but it did, however, approximate a potential surface for a three-atomic system. A lot of criticism arose from eq. (1.18), most of which pointed to the semi-empirical nature of the equation [33]. This thesis uses no ab initio calculation and will therefore not intervene in this discussion. However, two other points were brought up: i) there are saddle points and ii) one can spot a basin-like contour for large R_{AB} and R_{BC} . These are unphysical and not present in the more accurate ab initio calculations. An example of the LEP potential is provided in Figure 1.2. Point i) and ii) were brought up by S. Sato, in 1955, who proposed a new potential energy surface, namely the LEPS potential, which resembled the ab initio calculations more [34].

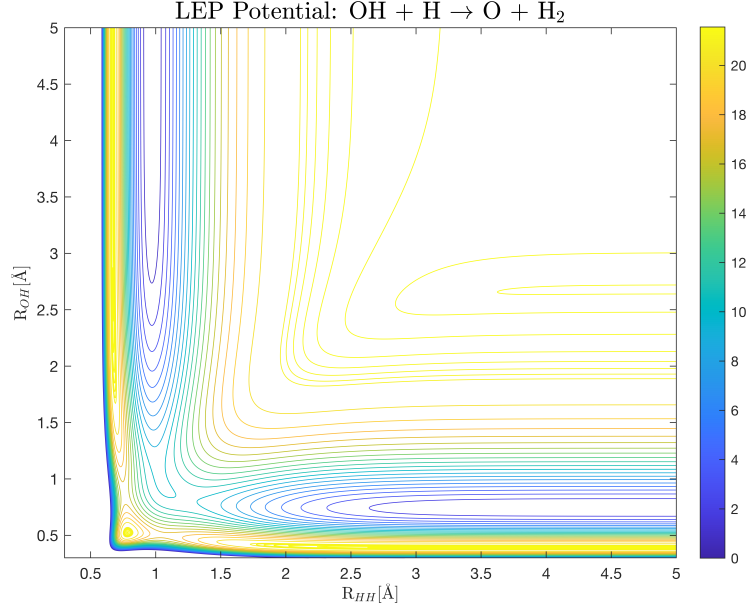


Figure 1.2: Eq. (1.18) using the reversed (1.1b) reaction as an example. $R_{AC} = R_{AB} + R_{BC}$ was used to decrease the dimensionality. The Morse parameters are provided in Table B.1.

1.1.3 LONDON-EYRING-POLANYI-SATO (LEPS) POTENTIAL

The London-Eyring-Polanyi-Sato potential was provided in 1955 by S. Sato [34, 35]:

$$V^{\text{LEPS}}(R_{\text{AB}}, R_{\text{BC}}) = \frac{Q_{\text{AB}}}{1 + S_{\text{AB}}^2} + \frac{Q_{\text{BC}}}{1 + S_{\text{BC}}^2} + \frac{Q_{\text{CA}}}{1 + S_{\text{CA}}^2} - \left\{ \frac{1}{2} \left[(\beta_{\text{AB}} - \beta_{\text{BC}})^2 + (\beta_{\text{BC}} - \beta_{\text{CA}})^2 + (\beta_{\text{CA}} - \beta_{\text{AB}})^2 \right] \right\}^{1/2} \quad (1.19)$$

where Q_{ij} , β_{ij} are the Coulomb and exchange integrals, respectively, and S_{ij} are the Sato parameters, which are fitted to resemble the true energy surface³ (see section 1.3). Similarly to the LEP potential for a collinear reaction, $R_{\text{CA}} = R_{\text{AB}} + R_{\text{BC}}$ is used to decrease dimensionality.

Sato argued that the Couloumb integral term and the exchange intergral term could be calculated using the Morse potential approximation for bonding energy state and a new antibonding energy state function:

$$E_{\text{bonding}, ij} = \frac{Q_{ij} + \beta_{ij}}{1 + S_{ij}^2} = D_{e,ij} [\exp(-2\alpha_{ij}(R_{ij} - R_{0,ij})) - 2 \exp(-\alpha_{ij}(R_{ij} - R_{0,ij}))]$$

$$E_{\text{antibonding}, ij} = \frac{Q_{ij} - \beta_{ij}}{1 - S_{ij}^2} = \frac{D_{e,ij}}{2} [\exp(-2\alpha_{ij}(R_{ij} - R_{0,ij})) + 2 \exp(-\alpha_{ij}(R_{ij} - R_{0,ij}))]$$

$$\Rightarrow \frac{Q_{ij}}{1 + S_{ij}^2} = \frac{1}{2} \left(E_{\text{bonding}, ij} + \frac{1 - S_{ij}^2}{1 + S_{ij}^2} E_{\text{antibonding}, ij} \right), \quad (1.20)$$

$$\frac{\beta_{ij}}{1 + S_{ij}^2} = \frac{1}{2} \left(E_{\text{bonding}, ij} - \frac{1 - S_{ij}^2}{1 + S_{ij}^2} E_{\text{antibonding}, ij} \right) \quad (1.21)$$

with D_e being Morse potential well depth [eV], R_{ij} being the distance between atom i and j [\AA], α_{ij} being a Morse parameter [\AA^{-1}] and $R_{0,ij}$ being the Morse potential equilibrium bond distance for which $\left(\frac{dE_{\text{bonding}, ij}}{dR_{ij}}\right)_{R_{ij}=R_{0,ij}} = 0$ holds true [\AA]. Figure 1.3 shows the LEPS potential for the same reaction as Figure 1.2. It showcases that the LEPS potential only has one saddle point and no basin for large R_{AB} and R_{BC} as stated in section 1.1.2. Similarly to the LEP potential, there is no analytical solution to the LEPS potential. Finally, the set: $\{R_{\text{AB}}, R_{\text{BC}}\} = \lim_{R_1 \rightarrow \infty} \{R_{\text{AB}}, R_{\text{BC}}\}$ is simply mentioned. After some algebra, one finds that $\lim_{R_{\text{AB}} \rightarrow \infty} V^{\text{LEPS}}(R_{\text{AB}}, R_{\text{BC}}) = V^{\text{Morse}}(R_{\text{BC}})$. This is used to motivate the choice of wavefunction in section 1.2 and also tuning the vibrational states.

³Prof. Sato called S_{ij} an overlap integral in his article from 1955, but it has since been renamed the *Sato parameter*. This was done, since multiple LEPS potentials were fitted using some negative Sato parameters, which is impossible for an overlap integral. This thesis refers to S_{ij}^2 as the Sato parameter, since it also uses some negative Sato parameters.

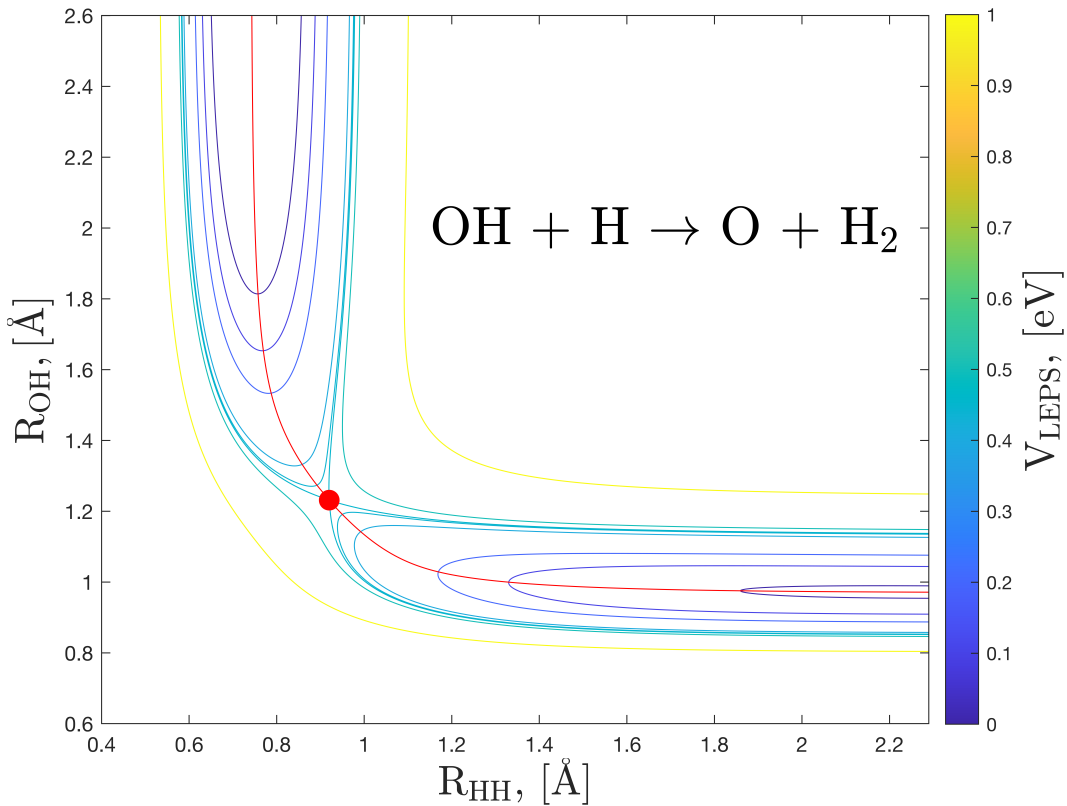


Figure 1.3: Eq. (1.19) using the reversed (1.1b) reaction as an example. $R_{AC} = R_{AB} + R_{BC}$ was used to decrease the dimensionality. Red dot represents the saddle point. The red line represents the minimum energy path, which is mentioned in section 1.4.2. The Morse parameters are provided in Table B.1 and the Sato parameters used are: $\{S_{AB}; S_{BC}; S_{CA}\} = \{0.4; 0.15; -0.455\}$.

1.2 HAMILTONIAN AND WAVEFUNCTION

This section motivates the choice of coordinates for the Hamiltonian and wavefunction, namely Jacobi coordinates. Furthermore, the wave function is explicitly written. Finally, the potential and wavefunction is illustrated in the new coordinates.

1.2.1 THE HAMILTONIAN

Before introducing the Hamiltonian, some coordinate transformations are made to reduce the dimensionality. So far, relative coordinates have been used (see section 1.1) without any introduction. This thesis considers reactions provided by $A + BC \rightarrow AB + C$, (see reactions (1.1a-d)) in a collinear configuration, meaning the atoms can only move along a one-dimensional line. The atomic position denotes the location of each atom on the line. The transformation from atomic positions to relative coordinates is provided

by:

$$R_{AB} = r_B - r_A, \quad R_{BC} = r_C - r_B, \quad R_{CA} = r_C - r_A \quad (1.22)$$

In order to reduce the dimensionality of the system, the center of mass frame coordinates is used. The transformation from atomic position to Jacobi coordinates: $\{r_A, r_B, r_C\} \rightarrow \{R_1, R_2, R_{CM}\}$ is provided by the following:

$$\begin{aligned} R_1 &= \frac{m_B r_B + m_C r_C}{m_B + m_C} - r_A, & R_2 &= r_C - r_B, \\ R_{CM} &= \sum_{i \in \{A, B, C\}} \frac{m_i}{M} r_i, & M &= \sum_{i \in \{A, B, C\}} m_i \end{aligned} \quad (1.23)$$

and finally, the transformation from relative coordinates to Jacobi coordinates:

$\{R_{AB}, R_{BC}, R_{CA}\} \rightarrow \{r_A, r_B, r_C\} \rightarrow \{R_1, R_2, R_{CM}\}$ can be found using eqs. (1.22) and (1.23):

$$R_{AB} = R_1 - \frac{m_C}{m_B + m_C} R_2, \quad R_{BC} = R_2, \quad R_{CA} = R_1 - \frac{m_C}{m_B + m_C} R_2 + R_2 \quad (1.24)$$

The Hamiltonian was provided by eq. (0.21) and is provided by the following for a three-atomic system and LEPS potential:

$$\hat{H} = -\frac{\hbar^2}{2} \sum_{i \in \{A, B, C\}}^3 \frac{1}{m_i} \nabla_i^2 + V^{\text{LEPS}}(R_{AB}, R_{BC}) \quad (1.25)$$

where ∇_i^2 is the Laplace operators: $\left\{ \frac{d^2}{dr_A^2}, \frac{d^2}{dr_B^2}, \frac{d^2}{dr_C^2} \right\}$ and V^{LEPS} is the LEPS potential explained in section 1.1.3 and provided by eq. (1.19). Using eq. (1.24), the LEPS potential is $V^{\text{LEPS}}(R_1 - \frac{\mu_{CA}}{\mu_{BC} + \mu_{CA}} R_2, R_2)$ in Jacobi coordinates. Furthermore, the following is derived in section C.1:

$$\hat{H} = -\frac{\hbar^2}{2} \sum_{k=1}^2 \frac{1}{M_k} \frac{\partial^2}{\partial R_k^2} + V^{\text{LEPS}} \left(R_1 - \frac{m_C}{m_B + m_C} R_2, R_2 \right) \quad (1.26)$$

with

$$\frac{1}{M_k} = \begin{cases} \frac{M}{m_A(m_B + m_C)} & \text{if } k = 1 \\ \frac{m_B + m_C}{m_B m_C} & \text{if } k = 2 \end{cases} \quad (1.27)$$

1.2.2 THE WAVEFUNCTION

It was postulated in the preface, eq. (0.14), that the state of the system is completely specified by the wave function, $|\Psi\rangle$. It was mentioned in section 1.1.3 that $\lim_{R_1 \rightarrow \infty} V^{\text{LEPS}}(R_1, R_2) = V^{\text{Morse}}(R_2)$. For large R_1 , it follows that R_1 and R_2 are uncoupled. Since the potential resembles that of a Morse potential for large R_1 , the initial wavefunction in the R_2 direction takes the form of eq. (1.13), $\psi_n^{\text{Morse}}(R_2)$. The wavefunction in the R_1 direction is chosen to be that of a Gaussian wave packet:

$$\psi(R_1) = \exp\left(-\frac{1}{2}\left(\frac{R_1 - R_{1,0}}{\sigma}\right)^2\right) \exp(-i k_0 (R_1 - R_{1,0})) \quad (1.28)$$

where $R_{1,0}$ is the initial center of the gaussian in the R_1 direction, σ is the standard deviation, which will be motivated in section 2.3.1, and k_0 is provided by $k_0 = \sqrt{\frac{2\langle T_0 \rangle}{M_2}}$ with M_k provided by eq. (1.27). The final initial wavefunction becomes:

$$\Psi(R_1, R_2) = \psi(R_1) \cdot \psi_n^{\text{Morse}}(R_2) \quad (1.29)$$

and the wavefunction provided by eq. (1.29) along with the LEPS potential in Jacobi coordinates can be seen on Figure 1.4.

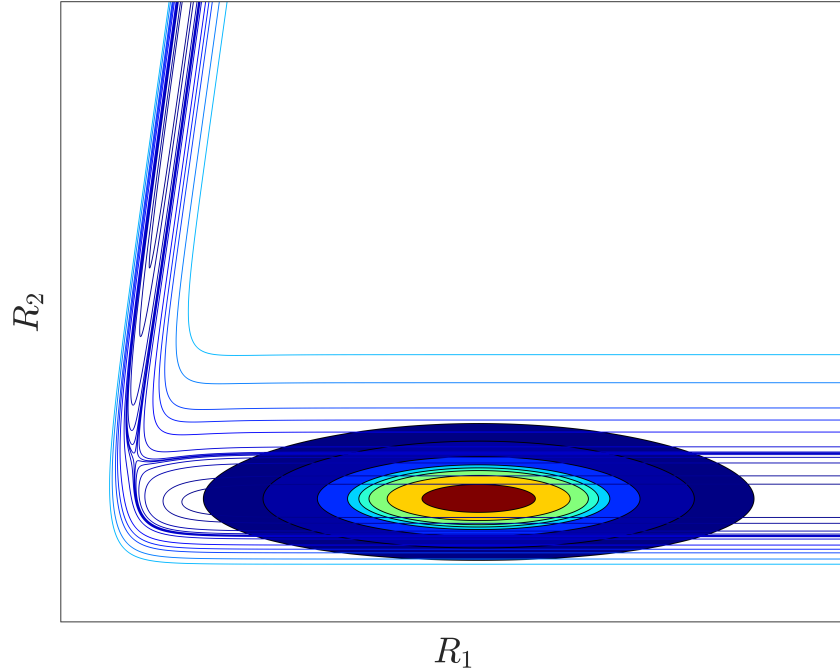


Figure 1.4: Sketch of the LEPS potential in Jacobi coordinates along with the wavefunction provided by eq. (1.29).

1.3 LEPS ENERGY BARRIERS

It was mentioned in section 1.1.3 that the Sato parameters were fitted to resemble the true potential energy surface. However, there is no analytical way to find the true Potential Energy Surface. Therefore, the Sato parameters were fitted to more precise ab initio methods found in the literature. This section provides the methods used to calculate the classical barrier height and the saddle point coordinates of reactions (1.1a-d). Furthermore, the classical barrier height and the saddle point coordinates used in this thesis are provided in Table 1.1. Finally, the plots are provided in Figure 1.5.

H + H₂ → H₂+ H reaction: The transition state location was found by Liu, B. using configuration interaction (CI) calculations with one-particle, symmetry-adapted Slater-type basis functions (SLT) for each hydrogen atom [36].

O + H₂ → OH + H reaction: The transition state location was found by Walch and Dunning using large scale polarization configuration interaction (POL-CI) calculations with (4s3p2d/3s1p) basis. For small basis sets, they either did not include a polarization function, (9s5p/4s)/(3s2p/2s), or referred to literature, (9s5pld/4s1p)/(3s2pld/2s1p) [37]. For larger basis sets, they optimized the exponents of the polarization functions using generalized valence bond (GVB) wavefunctions [38].

F + H₂ → HF+ H reaction: The transition state location was found by Bauschlicher Jr. et al. using multireference configuration interaction (MR-CI) with an active space of (322) including Davidson correction (+ Q) using the (5s5p3d2/1g/4s3p2d) basis [39]. Stark, Klaus and Werner further investigated the barrier height using MRCl(62/2) + Q as well as the AVQZ/VQZ basis [40].

F + HCl → HF + Cl reaction: The transition state barrier location was found by profs. Aoto, Y. A. and Köhn, A. using internally contracted multireference coupled-cluster for singlets, doublets and triples (icMRCCSD(T)) method with the aVTZ and aVQZ basis [41].

Table 1.1 reports the saddle point (also called transition state) location from the above mentioned references along with the fitted values from the literature. It is immediately obvious that the classical barriers and saddle point coordinates used in this thesis are not equal to the literature values. This is due to the fact that the LEPS potential is an approximation rather than a true potential energy surface. It is not guaranteed that a set of Sato parameters exists such that it yields the ab initio calculated potential energy surfaces. Therefore, the following prioritization was used: First, the Sato parameters were fitted in such a way that the late-barrier reactions ($R_{BC}^\ddagger > R_{AB}^\ddagger$) and early-barrier reactions ($R_{BC}^\ddagger < R_{AB}^\ddagger$) were in accordance with the literature. After early- or late-barrier reactions were ensured, the Sato-parameters were fitted further to resemble the classical barrier height of the literature. The fitted potentials used in this thesis for reactions (1.1a-d) along with the Sato parameters can be seen in Figure 1.5. The reversed reactions were found by using the following formula: $\{S_{1,\text{reversed}}, S_{2,\text{reversed}}, S_{3,\text{reversed}}\} = \{S_2, S_1, S_3\}$.

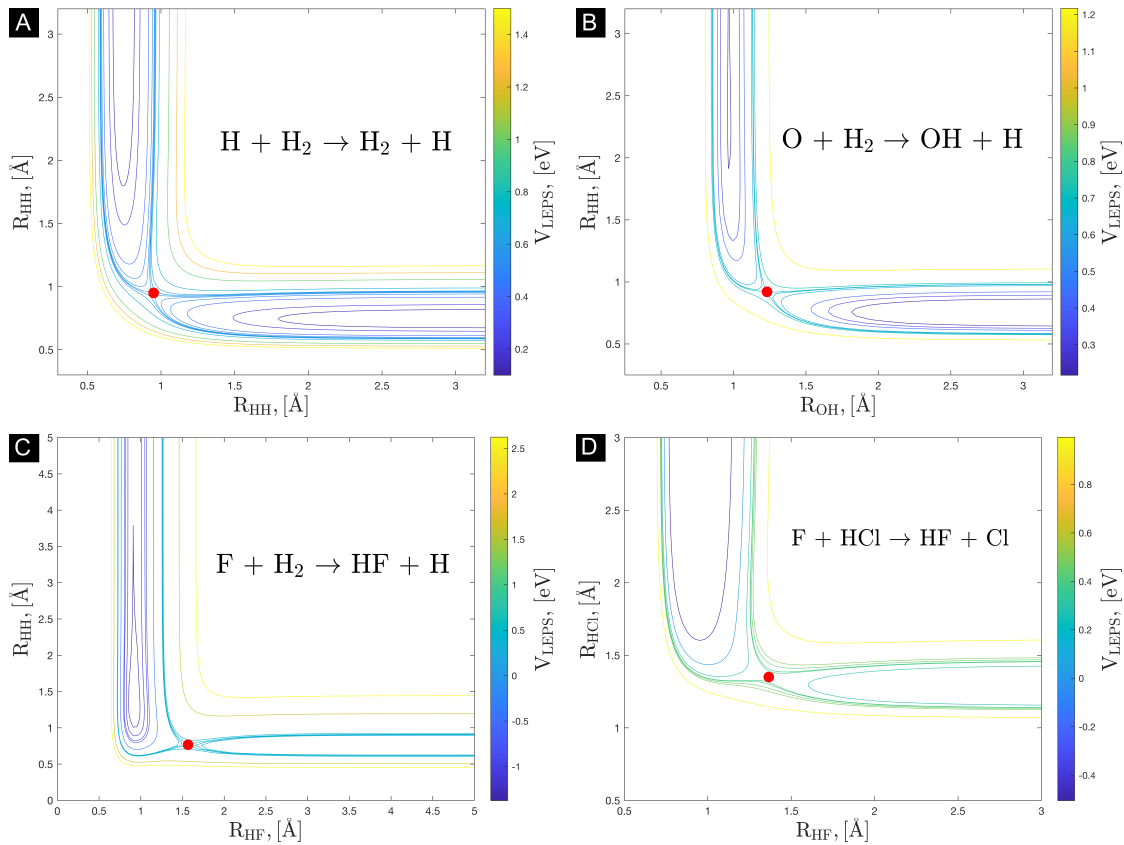


Figure 1.5: LEPS potentials for reactions (1.1a-d) written in relative coordinates for figures A-D respectively. The barrier locations and classical barrier heights are provided in Table 1.1. After fitting, the Sato parameters are provided by: A) $\{S_1; S_2; S_3\} = \{0.1; 0.1; 0.1\}$, B) $\{S_1; S_2; S_3\} = \{0.15; 0.4; -0.455\}$, C) $\{S_1; S_2; S_3\} = \{-0.132; 0.32; 0.6\}$ and D) $\{S_1; S_2; S_3\} = \{0.02; 0.004; -0.01\}$.

Table 1.1: Saddle point coordinates, R_{AB}^\ddagger and R_{BC}^\ddagger , and classical barrier heights, E_{cl} , were fitted according to literature values. Columns 2-4 denote the values saddle point energy barriers and locations used and columns 5-8 denote the literature values along with the angle of the incoming atom. Reaction coordinates and classical barrier height for reaction (1.1a) was found using the following source: [36]. Reaction coordinates and classical barrier height for reaction (1.1b) was found using the following sources: [37, 38]. Reaction coordinates and classical barrier height for reaction (1.1c) was found using the following sources: [39, 40]. Reaction (1.1d) was found using [41].

Reaction: $A + BC \rightarrow AB + C$	This thesis			Literature			
	R_{AB}^\ddagger [Å]	R_{BC}^\ddagger [Å]	E_{cl} [eV]	R_{AB}^\ddagger [Å]	R_{BC}^\ddagger [Å]	E_{cl} [eV]	θ [°]
$H + H_2 \rightarrow H_2 + H$	0.944	0.944	0.573	0.930	0.930	0.425	180
$O + H_2 \rightarrow OH + H$	1.23	0.92	0.667	1.23	0.92	0.205	180
$H + OH \rightarrow H_2 + O$	0.92	1.23	0.450	N/A	N/A	N/A	N/A
$F + H_2 \rightarrow HF + H$	1.57	0.767	0.363	1.56	0.767	0.0794	180
$H + HF \rightarrow H_2 + F$	0.767	1.57	1.73	N/A	N/A	N/A	N/A
$F + HCl \rightarrow HF + Cl$	1.37	1.35	0.380	1.545	1.315	0.0689	111.2
$Cl + HF \rightarrow HCl + F$	1.35	1.37	1.89	N/A	N/A	N/A	N/A

1.4 NORMAL MODES

This section describes, showcases and provides the normal frequencies of the activated complex for reactions (1.1a-d). The full derivation of the normal mode coordinates and frequencies can be found in section A. In order to calculate the rate constant using Transition State Theory (TST), the partition function associated with saddle point coordinate is uncoupled from the translational, vibrational, rotational and electronic partition function, when the normal mode basis is used. This decreases the degrees of freedom and can be seen in section 1.5, eq. (1.33).

1.4.1 SECOND DERIVATIVE TEST

In order to find the location of the reaction barriers, the second derivative test was used, after which the Sato parameters were tuned further. Hence, a classical barrier height, E_{cl} , and saddle point coordinates, R_{AB}^\ddagger and R_{BC}^\ddagger , resembling literature values could be achieved [42, 43].

The pseudocode for the second derivative test is provided by Algorithm 1. Finding the harmonic frequencies at the saddle point is derived in section A.

Algorithm 1 Finding saddle points

Require: $r_1, r_2 \in \mathbb{R}^+, V_0 \in \mathbb{R}$

- 1: **function** SADDLEPOINTS($V(r_1, r_2), V_0$)
- 2: $f(r_1, r_2) \leftarrow V(r_1, r_2) - V_0$ \triangleright Define the function to be analyzed
- 3: $\{\mathbf{r}_{1,\text{crit}}, \mathbf{r}_{2,\text{crit}}\} \leftarrow \text{solve} \left(\left\{ \frac{\partial f(r_1, r_2)}{\partial r_1}, \frac{\partial f(r_1, r_2)}{\partial r_2} \right\} = \{0, 0\} \right)$ \triangleright 2nd derivative test
- 4: $D \leftarrow 0$ \triangleright Placeholder value
- 5: **while** $D < 0 \parallel i > |\mathbf{r}_{1,\text{crit}}|$ **do**
- 6: $D \leftarrow \frac{\partial^2 f(r_1, r_2)}{\partial r_1^2} \Big|_{\{r_1, r_2\}=\{r_{1,\text{crit},i}, r_{2,\text{crit},i}\}} \cdot \frac{\partial^2 f(r_1, r_2)}{\partial r_2^2} \Big|_{\{r_1, r_2\}=\{r_{1,\text{crit},i}, r_{2,\text{crit},i}\}}$
- 7: $- \left(\frac{\partial^2 f(r_1, r_2)}{\partial r_1 \partial r_2} \Big|_{\mathbf{x}=\mathbf{a}} \right)^2$ \triangleright Calculate determinant of Hessian matrix
- 8: **if** $D < 0$ **then**
- 9: **return** $f(r_{1,\text{crit},i}, r_{2,\text{crit},i})$
- 10: **end if**
- 11: **end while**
- 12: **return** "No saddle point was found" \triangleright Terminate program, if no saddle points
- 13: **end function**

The formal mathematical criteria for using the second derivative test is provided by the following:

Critical point definition : Let $f \subseteq C^n$, where $2 \leq n \in \mathbb{N}$ and $f(\mathbf{x}) : X \subset \mathbb{R}^n \rightarrow \mathbb{R}$, be defined on a disk with the center, \mathbf{a} , such that $\nabla f(\mathbf{a}) = \mathbf{0}$, then \mathbf{a} is a critical point. Furthermore, let the Hessian be defined by $\mathbf{H} f(\mathbf{x}) = \nabla \otimes \nabla^\top f(\mathbf{x})$, then the following applies⁴:

1. If $\det(\mathbf{H} f(\mathbf{a})) > 0$ and $\frac{\partial^2 f(\mathbf{x})}{\partial x_1^2} \Big|_{\mathbf{x}=\mathbf{a}} > 0$, then $f(\mathbf{a})$ is a local minimum.
2. If $\det(\mathbf{H} f(\mathbf{a})) > 0$ and $\frac{\partial^2 f(\mathbf{a})}{\partial x_1^2} \Big|_{\mathbf{x}=\mathbf{a}} < 0$, then $f(\mathbf{a})$ is a local maximum.
3. if $\det(\mathbf{H} f(\mathbf{a})) < 0$, then \mathbf{a} is a saddle point.

1.4.2 NORMAL MODE FREQUENCIES AND REPRESENTATIONS

This section shows the normal mode coordinates corresponding to the \mathbf{L} matrix from section A, see Figure 1.6, and the normal mode frequencies corresponding to ν , see Table 1.2. The *orthogonal* label refers to the normal mode eigenvector being orthogonal to the minimum energy path of the LEPS potential, which was visualized in section 1.1.3, in Figure 1.3. The *parallel* label refers to the normal mode eigenvector being parallel to the minimum energy path of the LEPS potential. The *translation* label refers to the normal mode eigenvector coordinates having the same sign, which results in translational motion and the vibrational frequency being zero.

⁴The following three conditions and conclusions define the second derivative test.

Table 1.2: Normal mode frequencies found using the second derivative test for the LEPS potentials.

Activated complex	$\tilde{\nu}_{\text{orthogonal}} [\text{cm}^{-1}]$	$\tilde{\nu}_{\text{Translational}} [\text{cm}^{-1}]$	$\tilde{\nu}_{\text{parallel}} [\text{cm}^{-1}]$
H · · H · · H	2079.9	0	2302.9 i
O · · H · · H	1732.9	0	2044.9 i
F · · H · · H	3541.8	0	920.5 i
F · · H · · Cl	815.0	0	1032.0 i

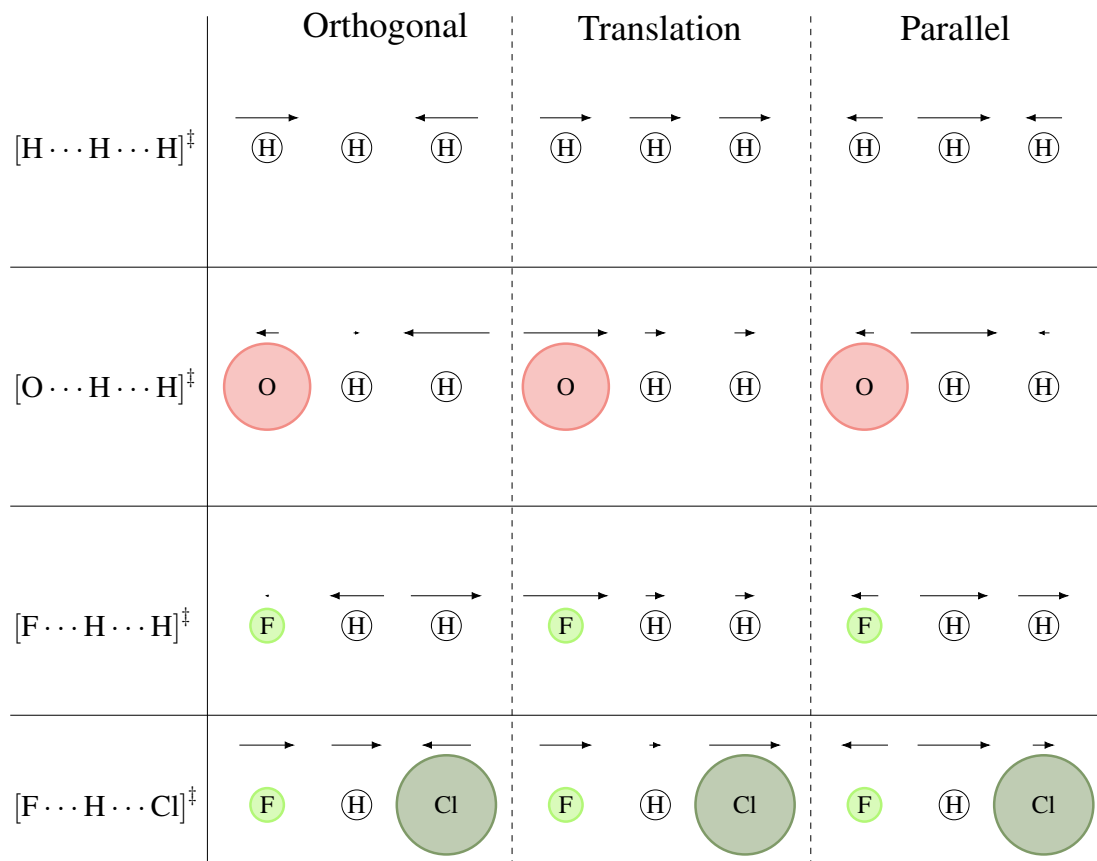


Figure 1.6: Normal mode representations: the sizes of the atoms are chosen such that the relative atomic radii of the atoms match each other. The length of the normal mode arrow representations fit accordingly to the calculated values: $\frac{R_O}{R_H} = 2.87$; $\frac{R_F}{R_H} = 1.13$; $\frac{R_{Cl}}{R_H} = 3.30$ [44–46].

1.5 TRANSITION STATE THEORY - RATE CONSTANT

In the following section, the rate constant will be derived for the bimolecular exchange reactions 1.1a-d using Transition State Theory. The main source for the derivation is *Theories of molecular reaction dynamics: the microscopic foundation of chemical kinetics* by Henriksen, Niels E. and Hansen, Flemming Y. [47]. The rate constants will then be calculated using the Transition state derived rate constant.

Transition State Theory (TST) was first described in 1935 by Eyring, H., who investigated activated complexes of three- and four-atomic reactions [48]. Transition state is an approximate approach to account for the reaction dynamics of a chemical reaction. Under TST, the nuclear configurations between reactants and products follow the minimum path obtained in section 1.1.3. Following this minimum path, a saddle point is eventually reached at the barrier location, which can be found using the second derivative test described in section 1.4.1. At this saddle point, it is assumed that the normal mode coordinates and the associated frequencies, ω_i , are known.

A bimolecular exchange reaction is defined as [49]:



Where A, B, C denote atoms, k is the reaction rate constant for the equilibrium reaction. $[.]^\ddagger$ denotes the activated complex.

The equilibrium constant for gas-phase reactions at equilibrium is provided by the following:

$$K_c(T) = \frac{[A \cdots B \cdots C]^\ddagger}{[A][BC]} = \frac{Q_{(AB)^\ddagger}/V}{(Q_A/V)(Q_{BC}/V)} \exp\left(-\frac{E_0}{k_B T}\right) \quad (1.31)$$

where $Q_{(AB)^\ddagger}$, Q_A and Q_{BC} denote the partition functions for the activated complex and reactants, respectively. T denotes the temperature [K], V denotes the volume [m^3] and k_B denotes Boltzmann's constant [$J K^{-1}$].

At the saddle point region with only one vibrational mode in the reaction direction, E_0 is provided by:

$$E_0 = E_{cl,0} + E_{ortho} - E_{reactant,0} = E_{cl} + \frac{h\nu_{ortho,0}^\ddagger}{2} - E_0^{\text{morse}} \quad (1.32)$$

where E_{cl} is the difference in energy between the saddle point height and reactant potential well, which is also called the classical barrier height [J]. ν^\ddagger is the vibrational frequencies associated with the electronic ground state solution of the harmonic oscillator for the saddle point [s^{-1}] (see. section A) and $E_{reactant}$ is the energy of the reactant molecules, which were found using the Morse potential approximation (see section 1.1.1). Note that changing the direction of the reaction for reactions, where the reac-

tants and products are not the same, namely reactions 1.1b-d, will change both E_{cl} and ν . From eq. (1.32), it can be seen that E_0 will also change. Therefore, flipping the reactions will change the reaction rate constant using TST. The parameters used are provided in Table 1.3.

In the normal-mode basis which was described in section 1.4, the reaction coordinate of the expansion point is separable from the degrees of freedom associated with the activated complex. The expansion point was chosen to be at the saddle point reaction coordinate, see section A. The movement of the reaction coordinate through the saddle point region can be treated as that of a free particle. Hence, the quantum mechanical solution to the particle in a box, is used. Furthermore, since the activated complex is collinear, the one-dimensional box solution is used. There are neither electronic, vibrational or rotational contributions from the reaction coordinate partition function. Hence the following applies for sufficiently high $k_B T$:

$$Q_{(AB)^{\ddagger}} = \left(\frac{2\pi \mu k_B T L^2}{h^2} \right)^{\frac{1}{2}} Q_{(AB)^{\ddagger}}^{\ddagger} \quad (1.33)$$

where $\mu = \frac{m_A(m_B+m_C)}{m_A+m_B+m_C}$ is the reduced mass [kg], L is the length of the box associated to the activated complex [Å] and h is Planck's constant [J s].

Substituting eq. (1.33) into eq. (1.31), yields:

$$\frac{[A \cdots B \cdots C]^{\ddagger}}{[A][BC]} = \left(\frac{2\pi \mu k_B T L^2}{h^2} \right)^{\frac{1}{2}} \frac{Q_{(AB)^{\ddagger}}^{\ddagger}/V}{(Q_A/V)(Q_{BC}/V)} \exp\left(-\frac{E_0}{k_B T}\right) \quad (1.34)$$

It is assumed that when an activated complex has been formed, the dynamics of the reaction coordinate is always in the direction of the product side. Furthermore, the velocity distribution of the reaction is considered to follow the Maxwell-Boltzmann distribution of speeds [28]:

$$f(v_x) = \left(\frac{\mu}{2\pi k_B T} \right)^{\frac{1}{2}} \exp\left(-\frac{\mu v_x^2}{2 k_B T}\right) \implies \langle v_x \rangle_+ = \langle f|v_x|f \rangle_+ = \frac{\int_{\mathbb{R}^+} f^*(v_x) v_x f(v_x) dv_x}{\int_{\mathbb{R}} |f(v_x)|^2 dv_x} = \left(\frac{k_B T}{2\pi \mu} \right)^{\frac{1}{2}} \quad (1.35)$$

Since L is the distance of reaction coordinate, $\langle v_x \rangle_+$, is the average velocity of the reaction dynamics in the product direction. The rate of product formation is identified by multiplying the concentration of the activated complex per length of the activated

complex box such that:

$$r = [A \cdots B \cdots C]^\ddagger \frac{\langle v_x \rangle_+}{L} = [A \cdots B \cdots C]^\ddagger \left(\frac{k_B T}{2\pi \mu L^2} \right)^{\frac{1}{2}} \quad (1.36)$$

Denoting that the rate of reaction for reaction (1.30) is provided by $r = k[A][BC]$, eq. (1.36) becomes:

$$\begin{aligned} k[A][BC] &= [A \cdots B \cdots C]^\ddagger \left(\frac{k_B T}{2\pi \mu L^2} \right)^{\frac{1}{2}} \Rightarrow \\ k &= \frac{[A \cdots B \cdots C]^\ddagger}{[A][BC]} \left(\frac{k_B T}{2\pi \mu L^2} \right)^{\frac{1}{2}} \end{aligned} \quad (1.37)$$

Furthermore, substituting eq. (1.34) into eq. (1.37) yields:

$$\begin{aligned} k_{TST}(T) &= \left(\frac{k_B T}{2\pi \mu L^2} \right)^{\frac{1}{2}} \left(\frac{2\pi \mu k_B T L^2}{h^2} \right)^{\frac{1}{2}} \frac{Q_{(AB)^\ddagger}/V}{(Q_A/V)(Q_{BC}/V)} \exp\left(-\frac{E_0}{k_B T}\right) \\ &= \frac{k_B T}{h} \frac{Q_{(AB)^\ddagger}/V}{(Q_A/V)(Q_{BC}/V)} \exp\left(-\frac{E_0}{k_B T}\right) \end{aligned} \quad (1.38)$$

where the label TST denotes that Transition State Theory was used.

The partition function, $\frac{Q_{(AB)^\ddagger}/V}{(Q_A/V)(Q_{BC}/V)}$, can be separated into 4 groups of degrees of freedom: Translational (trans), vibrational (vib), rotational (rot) and electronic (elec). These are also uncoupled such that the ratio of molecular partition function can be written as the product of the these:

$$\begin{aligned} \frac{Q_{(AB)^\ddagger}/V}{(Q_A/V)(Q_{BC}/V)} &= \left(\frac{Q_{(AB)^\ddagger}/V}{(Q_A/V)(Q_{BC}/V)} \right)_{\text{trans}} \left(\frac{Q_{(AB)^\ddagger}}{(Q_A)(Q_{BC})} \right)_{\text{vib}} \\ &\quad \times \left(\frac{Q_{(AB)^\ddagger}}{(Q_A)(Q_{BC})} \right)_{\text{rot}} \left(\frac{Q_{(AB)^\ddagger}}{(Q_A)(Q_{BC})} \right)_{\text{elec}} \end{aligned} \quad (1.39)$$

The one dimensional translational partition function is provided by:

$$\begin{aligned} \left(\frac{Q_{(AB)^\ddagger}/V}{(Q_A/V)(Q_{BC}/V)} \right)_{\text{Trans}} &= \left(\frac{Q_{(AB)^\ddagger}/L}{(Q_A/L)(Q_{BC}/L)} \right)_{\text{Trans}} \\ &= \left(\frac{h^2}{2\pi k_B T} \right)^{\frac{1}{2}} \left(\frac{m_{[ABC]^\ddagger}}{m_A m_{BC}} \right)^{\frac{1}{2}} = \left(\frac{h^2}{2\pi \mu k_B T} \right)^{\frac{1}{2}} \end{aligned} \quad (1.40)$$

The vibrational partition function is provided by:

$$\left(\frac{Q_{(AB)^{\ddagger}}}{(Q_A)(Q_{BC})} \right)_{\text{vib}} = \frac{1 - \exp\left(-\frac{h\nu}{k_B T}\right)}{1 - \exp\left(-\frac{h\nu^{\ddagger}}{k_B T}\right)} \quad (1.41)$$

where ν is the vibrational ground state frequency of the Morse potential, ν [cm⁻¹]. Since the activated complex is a one dimensional problem, the rotational partition becomes an identity operator. Since the activated complex is in the electronic ground state, the electronic partition function is approximately equal to the degeneracy of the ground, ω_0 , which here is set equal to unity:

$$\left(\frac{Q_{(AB)^{\ddagger}}}{(Q_A)(Q_{BC})} \right)_{\text{rot}} = 1, \quad \left(\frac{Q_{(AB)^{\ddagger}}}{(Q_A)(Q_{BC})} \right)_{\text{elec}} \approx \omega_0 \approx 1 \quad (1.42)$$

Hence, the ratio of molecular partition function can be found by substituting eqs. (1.40), (1.41) and (1.42) into eq. (1.38):

$$\frac{Q_{(AB)^{\ddagger}}/V}{(Q_A/V)(Q_{BC}/V)} = \left(\frac{h^2}{2\pi \mu k_B T} \right)^{\frac{1}{2}} \frac{1 - \exp\left(-\frac{h\nu}{k_B T}\right)}{1 - \exp\left(-\frac{h\nu^{\ddagger}}{k_B T}\right)} \quad (1.43)$$

And the final rate constant becomes:

$$k_{\text{TST}}(T) = \left(\frac{k_B T}{2\pi \mu} \right)^{\frac{1}{2}} \frac{1 - \exp\left(-\frac{h\nu}{k_B T}\right)}{1 - \exp\left(-\frac{h\nu^{\ddagger}}{k_B T}\right)} \exp\left(-\frac{E_0}{k_B T}\right) \quad (1.44)$$

which was to be derived.

In order to plot eq. (1.44), the harmonic vibrational frequency, ν , of the reactants are calculated along with the reduced masses using Table B.1, $\nu = \tilde{\nu} c$ and $\mu = \frac{m_A(m_B + m_C)}{m_A + m_B + m_C}$. Similarly, the saddle point frequency for the motion orthogonal to the minimum energy path, $\nu_{\text{orthogonal}}^{\ddagger}$, is calculated using Table 1.2. The difference in zero-point energies between the activated complex and the reactants, E_0 is calculated using (1.32). The values are listed in Table 1.3:

Table 1.3: Parameters used to plot eq. (1.44) for reactions (1.1a-d). μ denotes the reduced mass. $\nu_{\text{orthogonal}}^{\ddagger}$ denotes the normal mode frequency orthogonal to the minimum energy path. E_{cl} denotes the classical barrier height. E_0 is the difference in energy between the difference in ground state energy between the saddle point and reactant reaction coordinates relative to the well depth of the reactants. E_0 was found using eq. (1.32).

Reaction	μ [m_e]	$\nu_{\text{orthogonal}}^{\ddagger}$ [cm^{-1}]	E_{cl} [eV]	E_0 [eV]
$\text{H}_2 + \text{H} \rightarrow \text{H} + \text{H}_2$	918.6	2080	0.573	0.433
$\text{H} + \text{OH} \rightarrow \text{H}_2 + \text{O}$	1728	1733	0.450	0.329
$\text{O} + \text{H}_2 \rightarrow \text{OH} + \text{H}$	918.6	1733	0.667	0.505
$\text{H} + \text{HF} \rightarrow \text{H}_2 + \text{F}$	1744	3542	1.73	1.70
$\text{F} + \text{H}_2 \rightarrow \text{HF} + \text{H}$	918.6	3542	0.363	0.313
$\text{F} + \text{HCl} \rightarrow \text{HF} + \text{Cl}$	1786	815.0	0.380	0.248
$\text{Cl} + \text{HF} \rightarrow \text{HCl} + \text{F}$	1744	815.0	1.89	1.69

The rate constant provided by eq. (1.44) is plotted for reactions (1.1a-d) and the reversed reactions for reactions (1.1b-d) in Figure 1.7 using Tables 1.3 and B.1. The rate constant for reaction (1.1d) increases faster than the rest of the reactions. This is primarily due to the low E_0 , see Table 1.3. Additionally, from eq. (1.44), it can be seen that TST ignores the barrier location. This is also true in Figure 1.7, since the shape of the rate constant does not depend on the reaction being of type early- or late-barrier. Finally, it can be seen that the rate constant

does not decrease, which is also a result of the TST approximation, which was stated in eq. (1.35): the dynamics is always in the product direction after formation of the activated complex. The validity of this approximation is discussed in section 3.4.

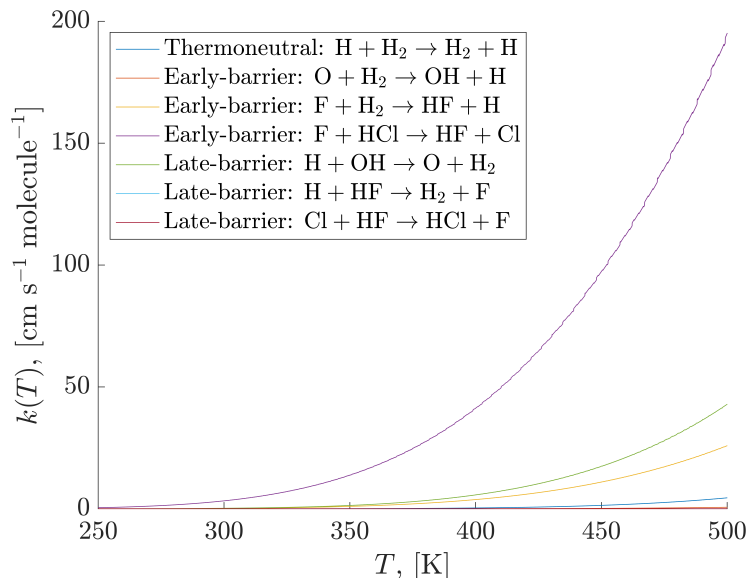


Figure 1.7: The TST-derived rate constant [$\text{cm s}^{-1} \text{ molecule}^{-1}$] as a function of temperature [K] for reactions (1.1a-d) along with the reversed reactions for reactions (1.1b-d). The parameters used can be found in Table 1.3 and ν was found using the Morse potential-derived zero-point frequency from Table B.1.

2. Numerical Methods

It was mentioned in section 1 that there exists no analytical solution to the time-independent Schrödinger equation using the LEPS potential. This also holds true for the time-dependent Schrödinger equation. Therefore, one must use numerical methods in order to describe the dynamics of the system. This chapter describes the numerical grid and motivates the use of the Strang-Marchuk algortihm. Furthermore, the output of the reactions is the reaction probability. This thesis uses the reactive flux method to calculate the reaction probability [50]. This method is validated by the dividing line method. Finally, test cases were run to motivate the choice of standard deviation for the initial wavefunction, the stepsize and the grid spacing.

2.1 SPLITTING-OPERATOR METHOD

In order for a simulation to move forward in time, time steps must be involved. A lot of work has been put into the field of time propagation in order to improve computational efficiency. In this thesis, computational efficiency is measured by 3 conditions: *Accuracy*, *stability* and *consistency*. *Accuracy* is measured as the numerical deviation from the exact solution. *Stability* is measured as the growth in local error. A method is *consistent*, if the method becomes exact, when the time step goes to 0. Together, *Stability* and *consistency* imply convergence [51].

One of these methods is the *splitting-operator method* (also called the *split step method* or the *operator splitting method*). The splitting-operator method simply describes the separation, or *splitting*, of differential operators into smaller parts, which are more easily solved. In this section, the accuracy, stability and consistency of the Strang-Marchuk algorithm will be derived. The operators, conventionally called \hat{A} and \hat{B} in computational science, have been replaced with $-\frac{i}{\hbar}\hat{T}$ and $-\frac{i}{\hbar}\hat{V}$, to illustrate the direct application to the time-dependent Schrödinger equation, which concerns this thesis [52–54].

Let $\mathcal{L}^2(\mathbb{R}^n)$ be a Banach space and $\hat{T}, \hat{V} : \mathcal{L}^2(\mathbb{R}^n) \rightarrow \mathbb{R}$ be time-independent linear-bounded operators, then the following is a Cauchy problem:

$$\frac{d}{dt} |\Psi(t)\rangle = -\frac{i}{\hbar} (\hat{T} + \hat{V}) |\Psi(t)\rangle, \quad t \in [0; T], \quad |\Psi(t=0)\rangle = |\Psi(t_0)\rangle \quad (2.1)$$

which can be solved numerically using the following assumption:

Splitting-operator assumption: *Let a system be described by eq. (2.1), then the Cauchy solution is provided by $|\Psi(t)\rangle = \hat{U}_{\Delta t} |\Psi(t_0)\rangle$ for which the time propagator,*

$\hat{U}_{\Delta t}$, can be split up into two or more terms provided by:

$$\hat{U}_{\Delta t} = \prod_{i=1}^m \exp \left(-\frac{i}{\hbar} a_i \Delta t \hat{T} - \frac{i}{\hbar} b_i \Delta t \hat{V} \right) + \mathcal{O}(t^{m+1}) \quad (2.2)$$

where $\{a_i\}_{i=1}^m, \{b_i\}_{i=1}^m \in \mathbb{R}$ are sets of free parameters depending on the method used. This can be applied to the wavefunction N number of time steps, Δt , to yield a full propagation time:

$$|\Psi(t)\rangle = \hat{U}_{\Delta t}^N |\Psi(t_0)\rangle + \mathcal{O}(t^{m+1}) \quad (2.3)$$

where $\mathcal{O}(t^{m+1})$ is neglected.

2.1.1 THE STRANG-MARCHUK ALGORITHM

In the following, the Strang-Marchuk (also called Symmetric Strang) algorithm will be summarized, after which the order of accuracy is proved. Finally, stability and consistency has been left out [55]. Let $\hat{T}, \hat{V} : \mathcal{L}^2(\mathbb{R}^n) \rightarrow \mathbb{R}$, $t \in [0, \infty[$ and $\{a_1, a_2, b_1, b_2\} = \{0, 1, \frac{1}{2}, \frac{1}{2}\}$ for the following differential system:

$$\begin{aligned} \frac{d}{dt} |\Psi^*(t)\rangle &= -\frac{i\hat{V}}{\hbar} |\Psi(t)\rangle, \quad t \in [n\Delta t; (n + 1/2)\Delta t], \\ |\Psi(n\Delta t)\rangle &= |\Psi(t_0)\rangle \end{aligned} \quad (2.4a)$$

$$\begin{aligned} \frac{d}{dt} |\Phi(t)\rangle &= -\frac{i\hat{T}}{\hbar} |\Phi(t)\rangle, \quad t \in [n\Delta t; (n + 1)\Delta t], \\ |\Phi(n\Delta t)\rangle &= |\Psi((n + 1/2)\Delta t)\rangle \end{aligned} \quad (2.4b)$$

$$\begin{aligned} \frac{d}{dt} |\varphi(t)\rangle &= -\frac{i\hat{V}}{\hbar} |\varphi(t)\rangle, \quad t \in [(n + 1/2)\Delta t; (n + 1)\Delta t], \\ |\varphi((n + 1/2)\Delta t)\rangle &= |\Phi((n + 1)\Delta t)\rangle \end{aligned} \quad (2.4c)$$

hence, the Cauchy solution is found by substituting $\{a_i, b_i\}_{i=1}^2$ into eq. (2.2):

$$\begin{aligned} |\Psi_{\text{SM}}(t)\rangle &= \hat{U}_{\Delta t, \text{SM}}^N |\Psi(t_0)\rangle \\ &\approx \left(\exp \left(-\frac{i\Delta t}{2\hbar} \hat{V} \right) \exp \left(-\frac{i\Delta t}{\hbar} \hat{T} \right) \exp \left(-\frac{i\Delta t}{2\hbar} \hat{V} \right) \right)^N |\Psi(t_0)\rangle \end{aligned} \quad (2.5)$$

and the pseudocode is provided by Algorithm 2:

Algorithm 2 Strang-Marchuk algorithm

Require: $t_0, \Delta T, T \in \mathbb{R}^+, t_0 < t < T, |\Psi(t_0)\rangle \in \mathcal{L}^2(\mathbb{R}^n)$

- 1: **function** STRANG_MARCHUK($t_0, \Delta T, T, |\Psi(t_0)\rangle$)
- 2: $nT \leftarrow \lceil \frac{T-t_0}{\Delta T} \rceil$ ▷ Assign number of timesteps. Round up to nearest integer
- 3: $|\Psi\rangle \leftarrow zeros(nT)$ ▷ Assign empty array for each timestamp
- 4: $|\Psi_1\rangle \leftarrow |\Psi(t_0)\rangle$ ▷ Assign boundary condition to first element
- 5: **for** i to $nT - 1$ **do**
- 6: $|\Psi_i\rangle \leftarrow \exp\left(-\frac{i\hat{V}}{2\hbar}\Delta t\right) |\Psi_{i-1}\rangle$ ▷ Calculate first step of SM splitting
- 7: $|\Psi_i\rangle \leftarrow \exp\left(-\frac{i\hat{T}}{\hbar}\Delta t\right) |\Psi_i\rangle$ ▷ Calculate second step of SM splitting
- 8: $|\Psi_i\rangle \leftarrow \exp\left(-\frac{i\hat{V}}{2\hbar}\Delta t\right) |\Psi_i\rangle$ ▷ Calculate third and final step of SM splitting
- 9: **end for**
- 10: **end function**

In order to showcase the order of accuracy of the Strang-Marchuk algorithm, the exact eq. (2.2) is Taylor expanded to second order and subtracted from the Taylor expanded Strang time propagator as mentioned in the original paper by G. Strang [55]. From eq. (2.2), it can be seen that $\frac{d}{dt} |\Psi(t)\rangle = -\frac{i}{\hbar} (\hat{T} + \hat{V}) |\Psi(t)\rangle$ and therefore $\frac{d^2}{dt^2} |\Psi(t)\rangle = -\frac{1}{\hbar^2} (\hat{T} + \hat{V})^2 |\Psi(t)\rangle$. Taylor expanding eq. (2.2) with respect to Δt at expansion point $|\Psi(t_0)\rangle$ yields:

$$\begin{aligned} |\Psi_{\text{SOM}}^{(2)}(t)\rangle &= |\Psi(t_0)\rangle - \frac{i\Delta t}{\hbar} (\hat{T} + \hat{V}) |\Psi(t_0)\rangle \\ &\quad - \frac{\Delta t^2}{2!\hbar^2} (\hat{T} + \hat{V})^2 |\Psi(t_0)\rangle + \mathcal{O}(\Delta t^3) \end{aligned} \quad (2.6)$$

where the superscript (2) means that only terms up to 2nd order are explicitly shown. Taylor expanding eq. (2.4a) with respect to $\Delta t/2$ at expansion point $|\Psi(t_0)\rangle$, eq. (2.4b) with respect to Δt at expansion point $|\Psi^{(2)}(\Delta t)\rangle$ and eq. (2.4c) with respect to $\Delta t/2$ at

expansion point $|\varphi_{\text{SM}}^{(2)}(\Delta t/2)\rangle$ yield the following:

$$\begin{aligned} |\Psi_{\text{SM}}^{(2)}(\Delta t/2)\rangle &= |\Psi(t_0)\rangle - \frac{\Delta t}{2} \frac{i\hat{V}}{\hbar} |\Psi(t_0)\rangle \\ &\quad - \frac{(\Delta t/2)^2}{2!} \frac{\hat{V}^2}{\hbar^2} |\Psi(t_0)\rangle + \mathcal{O}(\Delta t^3) \end{aligned} \quad (2.7)$$

$$\begin{aligned} |\Phi_{\text{SM}}^{(2)}(\Delta t)\rangle &= |\Psi_{\text{SM}}^{(2)}(\Delta t/2)\rangle - \Delta t \frac{i\hat{T}}{\hbar} |\Psi_{\text{SM}}^{(2)}(\Delta t/2)\rangle \\ &\quad - \frac{\Delta t^2}{2!} \frac{\hat{T}^2}{\hbar^2} |\Psi_{\text{SM}}^{(2)}(\Delta t/2)\rangle + \mathcal{O}(\Delta t^3) \end{aligned} \quad (2.8)$$

$$\begin{aligned} |\varphi_{\text{SM}}^{(2)}(\Delta t/2)\rangle &= |\Phi_{\text{SM}}^{(2)}(\Delta t)\rangle - \frac{\Delta t}{2} \frac{i\hat{V}}{\hbar} |\Phi_{\text{SM}}^{(2)}(\Delta t)\rangle \\ &\quad - \frac{(\Delta t/2)^2}{2!} \frac{\hat{V}^2}{\hbar^2} |\Phi_{\text{SM}}^{(2)}(\Delta t)\rangle + \mathcal{O}(\Delta t^3) \end{aligned} \quad (2.9)$$

Substituting eq. (2.7) into eq. (2.8), after which eq. (2.8) is substituted into eq. (2.9) yields:

$$\begin{aligned} |\varphi_{\text{SM}}^{(2)}(\Delta t/2)\rangle &= |\Psi(t_0)\rangle - \frac{i\Delta t}{\hbar} (\hat{T} + \hat{V}) |\Psi(t_0)\rangle \\ &\quad - \frac{\Delta t^2}{2!\hbar^2} (\hat{T}^2 + \hat{T}\hat{V} + \hat{V}\hat{T} + \hat{V}^2) |\Psi(t_0)\rangle + \mathcal{O}(\Delta t^3) \end{aligned} \quad (2.10)$$

The steps to find eq. (2.10) consisted of lengthy basic algebraic steps, which can be seen in section E. Subtracting the Strang-Marchuk solution provided by eq. (2.10) from the exact solution provided by eq. (2.6) and using $(\hat{T} + \hat{V})^2 = \hat{T}^2 + \hat{T}\hat{V} + \hat{V}\hat{T} + \hat{V}^2$ yields:

$$|\varphi_{\text{SM}}^{(2)}(\Delta t/2)\rangle - |\Psi_{\text{SOM}}^{(2)}(\Delta t)\rangle = \mathcal{O}(\Delta t^3) \quad (2.11)$$

which means the Strang-Marchuk algorithm has second order accuracy.

The consistency of the algorithm will not be proved but is found by calculating the maximum slope of all differences between the exact solution and the Strang-Marchuk solution. This is also called the global truncation error [56]:

$$\lim_{\Delta t \rightarrow 0} \max_{n \in \mathbb{N}} \left\| \frac{|\Psi_{\text{SOM}}^{(2)}((n+1)\Delta t)\rangle - |\Psi_{\text{SOM}}^{(2)}(n\Delta t)\rangle}{\Delta t} \right. \\ \left. - \frac{|\varphi_{\text{SM}}^{(2)}((n+1)\Delta t/2)\rangle - |\varphi_{\text{SM}}^{(2)}(n\Delta t/2)\rangle}{\Delta t} \right\|_{\mathcal{L}^2(\mathbb{R}^n)} = \mathcal{O}(\Delta t^2) \quad (2.12)$$

and as noted in eq. (2.12), Strang-Marchuk splitting in the scheme of eq. (2.1) is consistent to second order. Finally, Strang proved in 1968 that the algorithm is stable, meaning that it fulfills the following [57]:

$$\|\hat{U}_{\Delta t, \text{SM}}^N\|_{\mathcal{L}^2(\mathbb{R}^n)} \leq C \quad (2.13)$$

where there exists a $C \in \mathbb{R}^+$ for all $0 \leq N \Delta t \leq T$.

While the arguments needed to prove eqs. (2.12) and (2.13) are beyond the scope of this thesis, the conclusion is very relevant. When stability and consistency is established, it follows that the algorithm converges [58]:

$$\lim_{\Delta t \rightarrow 0} \|\hat{U}_{\Delta t, \text{SM}}^N |\Psi(t_0)\rangle - |\Psi(t)\rangle\|_{\mathcal{L}^2(\mathbb{R}^n)} = 0 \quad (2.14)$$

for any $t \in [0, T]$. Hence, second order accuracy was proved and convergence was shown.

2.2 REACTIVE FLUX AND COMPLEX ABSORBING POTENTIALS

This section motivates and explains the use of Flux Analysis as introduced by A. Jäckle and H.-D. Meyer in 1996. The main advantage being a clever way of avoiding periodic boundary problems without increasing the grid size. Section 2.2.1 introduces the Complex Absorbing Potential (CAP). Section 2.2.2 describes the reactive flux method. Section 2.2.3 validates the Reactive Flux Method.

2.2.1 COMPLEX ABSORBING POTENTIAL (CAP)

Reflections and wraparounds at the grid boundaries during physical simulations is called a periodic boundary problem. This is unphysical. Nevertheless, these are well-known artefacts from numerical calculations. This motivated R. Kosloff and D. Kosloff in 1984 to introduce Complex Absorbing Potentials (CAPs) [59]. This section describes one CAP, which has been used for calculations in this thesis.

The CAP is defined from the Hamiltonian:

$$\hat{H}(\eta) = \hat{H} - i\eta\hat{W}(R_1, R_2) \quad (2.15)$$

where \hat{H} is the Hamiltonian for which the LEPS potential is provided by eq. (1.19), $i\eta\hat{W}$ is the CAP, η is the strength parameter and \hat{W} is the shape of the boundary absorption, typically denoted by a piece-wise monomial function. This thesis uses the definition of the CAP from G. Fabien et al. with both \hat{W} and η written as a product of 2 monomial

piece-wise functions [60]:

$$\hat{W}(R_1, R_2) = \theta(R_1 - R_c)\theta(R_2 - R_c)$$

where θ is the Heavyside function and R_c is the cutoff distance, which makes sure that the absorbing potential is only turned on near the cutoff region.

Substituting the Hamiltonian provided by eq. (2.15) into eq. (2.2) using the Strang–Marchuk method described in section 2.1.1 yields:

$$\begin{aligned} \exp\left(-\frac{i}{\hbar}\hat{H}(\eta)\right) &= \exp\left(-\frac{i}{\hbar}\hat{H}(\eta)\Delta t\right) = \exp\left(-\frac{i}{\hbar}(\hat{H} - i\eta\hat{W})\Delta t\right) \\ &= \exp\left(-\frac{i\hat{H}\Delta t}{2\hbar}\right) \exp\left(-\frac{\eta\hat{W}\Delta t}{\hbar}\right) \exp\left(-\frac{i\hat{H}\Delta t}{2\hbar}\right) + \mathcal{O}(\Delta t^3) \end{aligned} \quad (2.16)$$

However, using the CAP method, introduces new reflections and transmissions. These can be derived using a semiclassical argument, namely that the quantum mechanical wave function is varying its phase and amplitude slowly. This behaviour is referred to as a semiclassical expansion. Using this physical approximation leads to the mathematical Wentzel–Kramers–Brillouin (WKB) approximation, which states that a differential equation, in this case the Schrödinger equation, has a solution provided by a Poincaré type asymptotic expansions, which is typically exponential functions [61, 62]. From this, reflections and transmissions are introduced and further derived using scattering theory. The full derivations of these were made by U. V. Riss and H. -D. Meyer in 1996 [63]:

$$|\mathcal{R}|^2 = \left(\frac{n!}{2^{n+2}}\right)^2 \left(\frac{1}{2M}\right)^n \frac{\eta^2}{T^{n+2}} \quad (2.17)$$

$$|\mathcal{T}|^2 = \exp\left(-\frac{\eta\hat{W}(L)}{T} \cdot \frac{k \cdot L}{n+1}\right) \quad (2.18)$$

where $|\mathcal{R}|^2$ and $|\mathcal{T}|^2$ are the reflection and transmission coefficients, respectively [both unitless]. μ is the reduced mass [kg], n is quantum number [unitless], $k = \sqrt{2\mu T}/\hbar$ is the real wave number, L is the length of the absorber region [\AA] and T is the translational energy [eV]. The CAP region is chosen such that $|\mathcal{R}|^2 + |\mathcal{T}|^2 \ll 1$. From eq. (2.17), it can be seen that choosing η too big results in less transmissions but more reflections. Reflections cause the probability density to be bounced off the CAP and move towards the energy barrier. This is unphysical. From eq. (2.18), it can be seen that choosing η too small results in less reflection but more transmissions. This results in more probability propagating through the CAP region and eventually hitting the boundary of the defined grid. Then it is anyone's guess, where the value is stored. In the case of this thesis,

an example would be that the probability density hits the boundary of the grid, after which the density is introduced at the other end of the grid boundary or reflected. This is called numerical boundary error and is unphysical. In order to get the least amount of transmission and reflections, the sum of the two is differentiated with respect to η and set equal to 0:

$$\frac{d}{d\eta} \left(|\mathcal{R}|^2 + |\mathcal{T}|^2 \right) |_{\eta=\eta_{\text{op}}} = 0 \implies \eta_{\text{op}} = \frac{T(n+1)}{kLW(L)} W_{\text{Lambert},0} \left(\frac{2^{n+1} (kL)^{2n+2}}{n! (n+2)^2 i^{n-1}} \right) \quad (2.19)$$

where η_{op} is the optimal strength parameter found provided by eq. (2.19), W_{Lambert} is the Lambert W function, which in this thesis is defined for the principal branch: $W_0(z) \exp(W_0(z)) = z$ with $z \in \mathbb{C}$ (initially proposed by J. H. Lambert in 1758 and later L. Euler [64, 65]) and $W(L)$ is the CAP defined by eq. (2.16). While it is possible to calculate the translative energy, T , at the CAP region, T is assumed to be equal to the initial translational energy, T_{init} , in order to reduce the number of computations.

2.2.2 REACTIVE FLUX

In order to calculate the probability density, the continuity equation is used [50, 66, 67]:

$$\frac{d|\langle \Psi | \Psi \rangle|^2}{dt} = -\nabla \cdot j(R_1, R_2; t) \quad (2.20)$$

where $\nabla = \left(\frac{\partial}{\partial R_1}, \frac{\partial}{\partial R_2} \right)$ is the nabla operator in 2 dimensions and j is the probability density flux represented by:

$$j(R_1, R_2) = \Re(\Psi^* \hat{P} \Psi) \quad (2.21)$$

where $\hat{P} = -\frac{i\hbar}{m} \nabla$ is the momentum operator and \Re yields the real part $\Psi^* \hat{P} \Psi$. From the *Transformations, distributions and spaces* section, eq. (0.12b) and the *quantum mechanical operators* section, eq. (0.19), $\hat{P} \Psi$ can easily be calculated using inverse Fourier transformation:

$$\hat{P} \Psi = \mathcal{F}^{-1}(k\Phi) \quad (2.22)$$

The full derivations of eq. (2.20) and eq. (2.21) can be seen in sections D.1 and D.2, respectively. For this thesis, the flux is calculated, when the wave function propagates through a *Flux line*, which was chosen as a horizontal line in the product channel placed before the CAP region. Therefore, computations only happened for $R_2 > R_{2,\text{fluxline}}$.

Finally, the probability density is found by integrating (2.20) with respect time:

$$|\langle \Psi | \Psi \rangle|^2 = - \int_0^{t_{\text{final}}} (\nabla \cdot j(R_1, R_2; t)) dt \quad (2.23)$$

where $t \in [0, t_{\text{final}}]$. Eq. (2.23) is not directly applicable to computational systems, since these calculations need to be discrete and not continuous. This will be described in section 2.2.3.

After applying the flux, the wavefunction is absorbed using the CAP from section 2.2.1 in order to avoid double counting. On Figure 2.1, the flux line is illustrated as a dashed red line and the CAP is illustrated as the grey area. A Gaussian wave packet was used to illustrate the wave function propagating through the flux line.

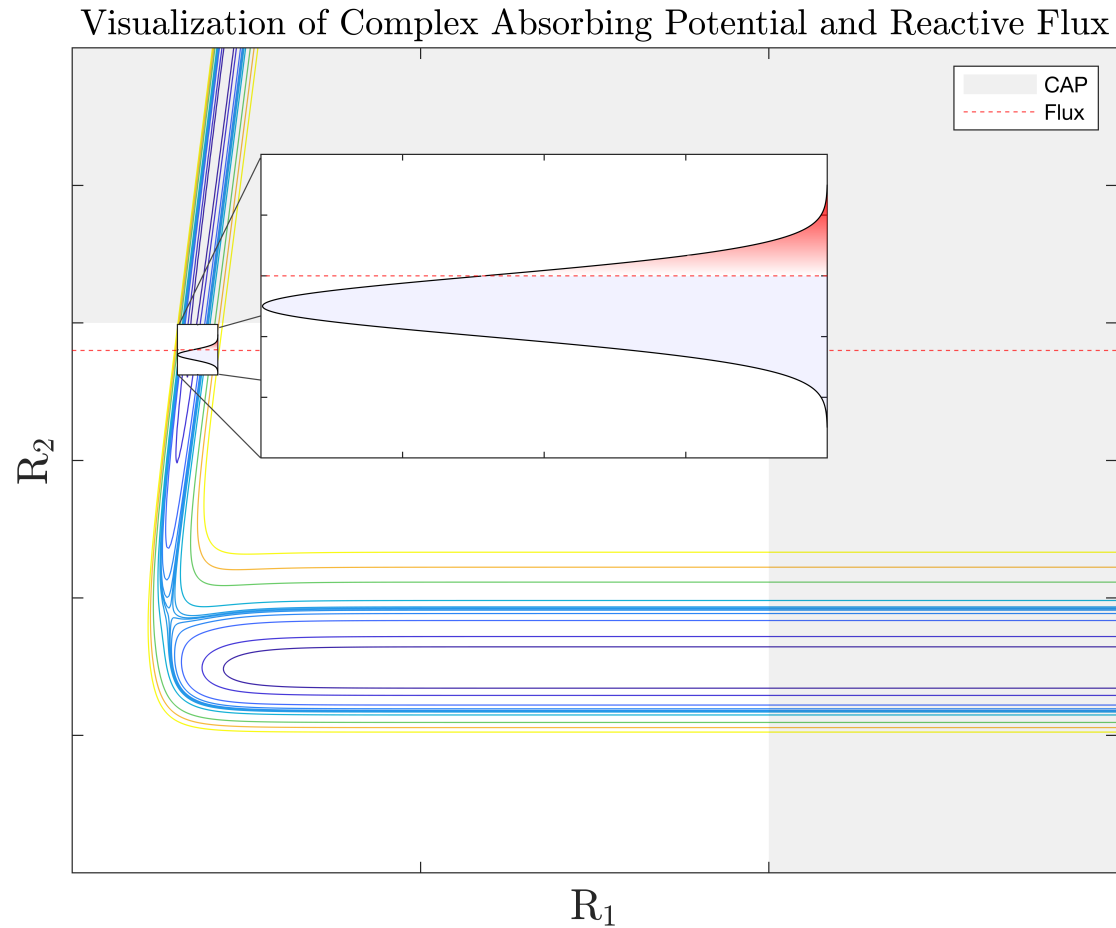


Figure 2.1: LEPS potential provided by eq. (1.19) using the reversed (1.1b) reaction potential as a sketch. $R_3 = R_1 + R_2$ was used to decrease the dimensionality. The horizontal red line represents the fluxline. A Gaussian wave packet represents the wavefunction passing the fluxline. The blue area of the wavefunction represents that the flux is not calculated before it passes the flux line. The red area of the wavefunction represents that the flux is calculated. The darker red region of the wavefunction represents bigger attribution to the flux while semi-transparent represents smaller attribution to the flux.

The pseudocode depicting the flux calculation along with the CAP incorporation is provided by:

Algorithm 3 CAP and Reactive Flux

Require: $t_0, \Delta T, T, R_{2,\text{Fluxline}} \in \mathbb{R}^+$, $t_0 < t < T, N_{R1} \in \mathbb{N}, |\Psi(R_1, R_2; t_0)\rangle \in \mathcal{L}^2(\mathbb{R}^n)$

- 1: **function** FLUX_AND_CAP($t_0, \Delta t, T, R_{\text{Fluxline}}, N_{R1}, |\Psi(t_0)\rangle$)
- 2: $nT \leftarrow \lceil \frac{T-t_0}{\Delta t} \rceil$ ▷ Assign number of timesteps. Round up to nearest integer
- 3: Flux $\leftarrow \text{zeros}(N_{R1}, nT)$ ▷ Assign empty array for each timestamp and R_1
- 4: $t \leftarrow t_0 : nT : T$
- 5: $|\Psi_1(R_1, R_2)\rangle \leftarrow |\Psi(R_1, R_2; t_0)\rangle$ ▷ Assign boundary condition to first element
- 6: **for** i to $nT - 1$ **do**
- 7: $|\Psi_i(R_1, R_2)\rangle \leftarrow \exp\left(-\frac{i\hat{V}}{2\hbar}\Delta t\right) |\Psi_{i-1}(R_1, R_2)\rangle$ ▷ Potential step
- 8: Flux $_i \leftarrow \text{trapz}\left[\left(\mathcal{F}^{-1}(|\Psi_{i-1}(R_1, R_{2,\text{Fluxline}})|)\right) \mathcal{F}^{-1}\left(\frac{\hat{P}_2}{\mu_2} |\Psi_{i-1}(R_1, R_{2,\text{Fluxline}})\rangle\right)\right]$
- 9: $|\Psi_i(R_1, R_2)\rangle \leftarrow \exp\left(-\frac{i\hat{T}}{\hbar}\Delta t\right) |\Psi_{i-1}(R_1, R_2)\rangle$ ▷ Translative step
- 10: $|\Psi_i(R_1, R_2)\rangle \leftarrow \exp\left(-\frac{i\hat{V}}{2\hbar}\Delta t\right) \mathcal{F}^{-1} |\Psi_{i-1}(R_1, R_2)\rangle$ ▷ Potential step
- 11: $|\Psi_i(R_1, R_2)\rangle \leftarrow \exp\left(-\frac{\eta\hat{W}}{\hbar}\Delta t\right) |\Psi_{i-1}(R_1, R_2)\rangle$ ▷ CAP
- 12: $|\Psi_i(R_1, R_2)\rangle \leftarrow \exp\left(-\frac{i\hat{V}}{2\hbar}\Delta t\right) |\Psi_{i-1}(R_1, R_2)\rangle$ ▷ Potential step
- 13: $|\Psi_i(R_1, R_2)\rangle \leftarrow \exp\left(-\frac{i\hat{T}}{\hbar}\Delta t\right) \mathcal{F} |\Psi_{i-1}(R_1, R_2)\rangle$ ▷ Translative step
- 14: $|\Psi_i(R_1, R_2)\rangle \leftarrow \exp\left(-\frac{i\hat{V}}{2\hbar}\Delta t\right) \mathcal{F}^{-1} |\Psi_{i-1}(R_1, R_2)\rangle$ ▷ Potential step
- 15: **end for**
- 16: **return** "Reaction probability = " $\text{trapz}[t, \text{Flux}]$
- 17: **end function**

The line "trapz [t, Flux]" from Algorithm 3 refers to the trapezoidal rule, which is explained in section 2.2.3.

2.2.3 CUMULATIVE FLUX METHOD AND TRAPEZOIDAL RULE

This section verifies the reactive flux probability calculations by comparing to the calculated integral of the reacted probability directly. It was mentioned in section 2.2.2 that eq. (2.23) is directly applicable to discrete systems. In order to calculate integrals numerically, one has to resort to using sums. One of the methods to calculating the integral using sums is the trapezoidal rule¹. This section introduces the direct calculation of the norm, which also needs to calculate the integral using the trapezoidal method. The trapezoidal rule is a numerical technique to calculate the integral numerically [68]. The reason for not choosing the trapezoidal rule over the reactive flux method is clarified at

¹The trapezoidal rule is also called the trapezoid rule or the trapezium rule

the end of this section.

The new method will be called the Dividing Line Method, which soon will be obvious. It was established in section 1.1.3 that the LEPS potential only has one saddle point. These were provided in section 1.3 in Table 1.1 and can be seen in Figure 1.5 for reactions (1.1a-d). Let a line pass from the grid corner of the LEPS, $[\min(R_1); \min(R_2)]$, through the saddle point, $[R_1^\ddagger; R_2^\ddagger]$. Then the line is provided by:

$$R_{2,\text{DL}}(R_{1,\text{DL}}) = \frac{R_2^\ddagger - \min(R_2)}{R_1^\ddagger - \min(R_1)} (R_{1,\text{DL}} - \min(R_1)) + \min(R_2) \quad (2.24)$$

where $[R_1, R_2] \in \{m \Delta R_1; n \Delta R_2\}_{m,n \in \mathbb{N}_0}$ is the set of equidistant grid points and $[R_{1,\text{DL}}, R_{2,\text{DL}}]$ is the coordinates forming the dividing line. Therefore eq. (2.24) defines the dividing line and motivates it's name. Eq. (2.24) is showcased on Figure 2.2A). The trapezoidal rule is provided by the following:

$$\int_{\min(R_2)}^{\max(R_2)} \int_{\min(R_1)}^{\max(R_1)} P(R_1, R_2; t_{\text{final}}) dR_1 dR_2 \approx \sum_{n,m \in \mathbb{N}_0} \frac{P((m+1)\Delta R_1, (n+1)\Delta R_2; t_{\text{final}}) + P(m\Delta R_1, n\Delta R_2; t_{\text{final}})}{2} \Delta R_1 \Delta R_2 \quad (2.25)$$

where $P = \Psi^* \Psi$. t_{final} is used due to the norm being calculated after the reaction has taken place. Assume that all density, whose coordinates satisfies $R_2 > R_{2,\text{DL}}(n \Delta R_1)$, be reacted probability density, the reacted probability density can now be differed from non-reacted probability density, which along with eq. (2.24) and (2.25) yields:

$$N_{\text{product}}(n, m) = \begin{cases} \text{eq. (2.25),} & \text{if } R_2 > R_{2,\text{DL}}(n \Delta R_1) \\ 0, & \text{otherwise} \end{cases} \quad (2.26)$$

Finally, the question of why the trapezoidal rule is not used to calculate the reaction probability is obvious in the following two cases. i) Suppose one uses the trapezoidal method along with the CAP mentioned in section 2.2.1, then the integral and therefore the norm in the product channel is absorbed, which leads to a lower norm. This is unphysical. ii) One may argue that one can turn off the CAP in the product channel. Doing this will result in reintroducing the periodic boundary problem, which was mentioned in section 2.2.1. In this case, one would have to increase the grid boundary in the R_2 direction, which in turn increases the grid space or increase the amount of grid points. This leads to more computational power. The reactive flux method does not have to deal with problems i) and ii), hence this was used.

From Figure 2.2B), it can be seen that the reactive flux method and the dividing line method converges towards the same reaction probability. It can also be seen that the dividing line method overestimates the reaction probability. This is due to the fact that some of the wavefunction crosses the barrier, after which it recrosses the barrier and

goes back into the reactant channel. The fluxline used for the reactive flux method is placed late into the product channel such that recrossing is negligible.

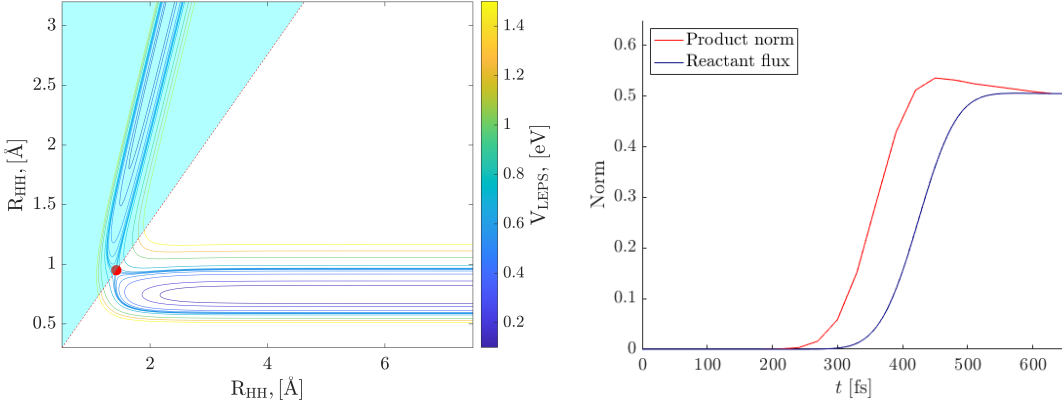


Figure 2.2: A) Sketch of the dividing line method using reaction (1.1a). The red line is the dividing line provided by eq. (2.24). The cyan-shaded area denotes the area, which is assumed to be reacted probability corresponding to the first case in eq. (2.26). The non-shaded area is assumed to be non-reacted probability corresponding to the second case in eq. (2.26). B) Sketch of the reaction probability plotted using the dividing line method (red) and the reactive flux method (blue). The grid spacing used was $[0.2576; 0.2576] a_0$. The time is $t \in [0; 650]$. The timestep used was $\Delta t = 0.01 \text{ fs}$.

2.3 TEST CASES

This section introduces the test cases used to validate and support the selection of parameters. As noted in the *introduction*, it was mentioned that thermoneutral reactions had limited significance. Nevertheless, reliance on one such reaction, namely reaction (1.1a), is based on its well-established presence in the literature. This choice is informed by a comprehensive understanding of this reaction, contributing to a validation of methods and parameter choices. Importantly, for efficiency, the same set of parameters is applied to reactions (1.1b-d). Section 2.3.1 proposes a standard deviation, σ , for the wavefunction provided in eq. (1.28) based off the coefficient of variance for the energy. Section 2.3.2 uses a convergence test to estimate a good stepsize and a good grid spacing.

2.3.1 STANDARD DEVIATION OF GAUSSIAN WAVE PACKET

As mentioned in section 1.2.2, the standard deviation of the Gaussian wave packet in the R_1 direction, will be motivated in this section. In order to motivate the choice of the standard deviation, the coefficient of variation for the energy measured in percentage is

used [69]:

$$\text{CV}_E = 100\% \frac{\sigma_E}{\langle E \rangle} \quad (2.27)$$

where $\langle E \rangle$ is the energy mean, which can be found from the Hamiltonian:

$$\langle E \rangle = \langle \hat{H} \rangle = \langle \hat{T} + \hat{V} \rangle = \langle \hat{T} \rangle + \langle \hat{V} \rangle = \langle \Psi | \hat{T} | \Psi \rangle + \langle \Psi | \hat{V} | \Psi \rangle \quad (2.28)$$

please note that linearity of inner products were used (see eq. (0.6a)). σ_E is the standard deviation of the energy provided by:

$$\sigma_E = \sqrt{\langle \hat{H}^2 \rangle - \langle \hat{H} \rangle^2} \quad (2.29)$$

$\langle \hat{H} \rangle^2$ is found by squaring eq. (2.28). $\langle \hat{H}^2 \rangle$ is provided by:

$$\begin{aligned} \langle \hat{H}^2 \rangle &= \langle \Psi | \hat{H}^2 | \Psi \rangle = \langle \Psi | (\hat{T} + \hat{V})^2 | \Psi \rangle \\ &= \langle \Psi | \hat{T}^2 + T\hat{V} + \hat{V}\hat{T} + \hat{V}^2 | \Psi \rangle \\ &= \langle \Psi | \hat{T}^2 | \Psi \rangle + \langle \Psi | \hat{T}\hat{V} | \Psi \rangle + \langle \Psi | \hat{V}\hat{T} | \Psi \rangle + \langle \Psi | \hat{V}^2 | \Psi \rangle \end{aligned} \quad (2.30)$$

and in turn, there are only 6 terms left to calculate:

$$\begin{aligned} \langle \Phi | \hat{T} | \Phi \rangle &= \int_{k_1, \min}^{k_1, \max} \int_{k_2, \min}^{k_2, \max} \Phi^*(k_1, k_2; t) \left(\frac{P_1^2}{2M_1} + \frac{P_2^2}{2M_2} \right) \Phi(k_1, k_2; t) dk_2 dk_1 \\ \langle \Psi | \hat{V} | \Psi \rangle &= \int_{R_1, \min}^{R_1, \max} \int_{R_2, \min}^{R_2, \max} \Psi^*(R_1, R_2; t) V^{\text{LEPS}} \Psi(R_1, R_2; t) dR_2 dR_1 \\ \langle \Psi | \hat{V}^2 | \Psi \rangle &= \int_{R_1, \min}^{R_1, \max} \int_{R_2, \min}^{R_2, \max} \Psi^*(R_1, R_2; t) (V^{\text{LEPS}})^2 \Psi(R_1, R_2; t) dR_2 dR_1 \\ \langle \Phi | \hat{T}^2 | \Phi \rangle &= \int_{k_1, \min}^{k_1, \max} \int_{k_2, \min}^{k_2, \max} \Phi^*(k_1, k_2; t) \left(\frac{P_1^2}{2M_1} + \frac{P_2^2}{2M_2} \right) \Phi(k_1, k_2; t) dk_2 dk_1 \\ \langle \Psi | \hat{T}\hat{V} | \Psi \rangle &= \int_{R_1, \min}^{R_1, \max} \int_{R_2, \min}^{R_2, \max} \Psi^*(R_1, R_2; t) \\ &\quad \mathcal{F}^{-1} \left[\left(\frac{P_1^2}{2M_1} + \frac{P_2^2}{2M_2} \right) \mathcal{F} [V^{\text{LEPS}} \Psi(R_1, R_2; t)] \right] dR_2 dR_1 \\ \langle \Psi | \hat{V}\hat{T} | \Psi \rangle &= \int_{R_1, \min}^{R_1, \max} \int_{R_2, \min}^{R_2, \max} \Psi^*(R_1, R_2; t) V^{\text{LEPS}} \\ &\quad \mathcal{F}^{-1} \left[\left(\frac{P_1^2}{2M_1} + \frac{P_2^2}{2M_2} \right) \mathcal{F} [\Psi(R_1, R_2; t)] \right] dR_2 dR_1 \end{aligned}$$

where the Fourier and inverse Fourier transformations between momentum space and position space can be seen in eqs. (0.12a) and (0.12b). In order to find a suitable standard deviation of the Gaussian wave packet, a coefficient of variation of 1% was chosen. From Figure 2.3, it can be seen that the coefficient of variance stagnates around 1% in the interval $t \in [0; 150]$ fs, after which it diverges. From visual inspection of the wavefunction, the wavefunction interacted with the LEPS potential barrier after 200 fs. Hence, the standard deviation of the energy, σ_E , must differ from average energy, $\langle E \rangle$, at the transition state location. This may due to some of the probability density being reflected from LEPS potential, causing deviation between the $\langle \hat{H}^2 \rangle$ and $\langle H \rangle^2$, see eq. (2.29). This remained the case for different standard deviation. Therefore, the standard deviation is based off of the coefficient of variance for small t . As can be seen in Figure 2.3, $CV_E \approx 1\%$ holds true for $\sigma_E = 15 a_0$. Furthermore, some deviation in CV_E was visible, if the initial wavefunction was placed too close to the reaction barrier or too close to the grid boundary. After the standard deviation of $\sigma = 15 a_0$ was established, the initial location of the wavefunction was chosen to be $[R_{1,0}; R_{2,0}] = [42 \text{ \AA}; R_{eq}^{\text{Morse}}]$, where R_{eq}^{Morse} depends on the diatomic reactant molecule and can be seen in Table B.1. Furthermore, a grid of $R_1 \in [0.2; 70] \text{ \AA}$ and $R_2 \in [0.2; 3] \text{ \AA}$.

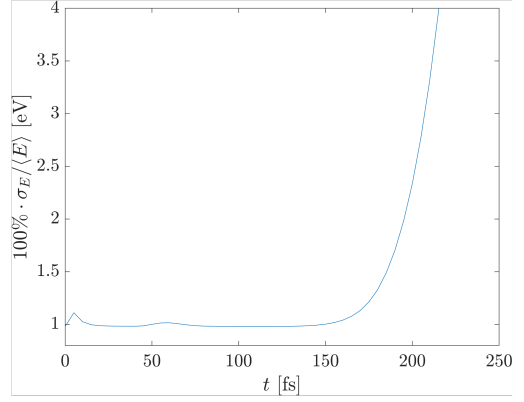


Figure 2.3: Eq. (2.27) as function of time, $t \in [0, 300]$ fs at time steps $\Delta t = 0.02$ fs, initial translational energy of $T_{init} = 0.4$ eV, standard deviation of $\sigma = 15 a_0$ and grid spacing of $[0.0322; 0.0103] a_0$ for reaction (1.1a): $H + H_2 \rightarrow H_2 + H$.

2.3.2 CHOICE OF STEPSIZE, Δt AND GRID SPACING

In order to propagate the wavefunction, a proper stepsize has to be chosen along with a proper grid spacing. This section uses a convergence test, with the reactive flux method described in section 2.2.2 as output measurement to find the stepsize, Δt , and grid spacing.

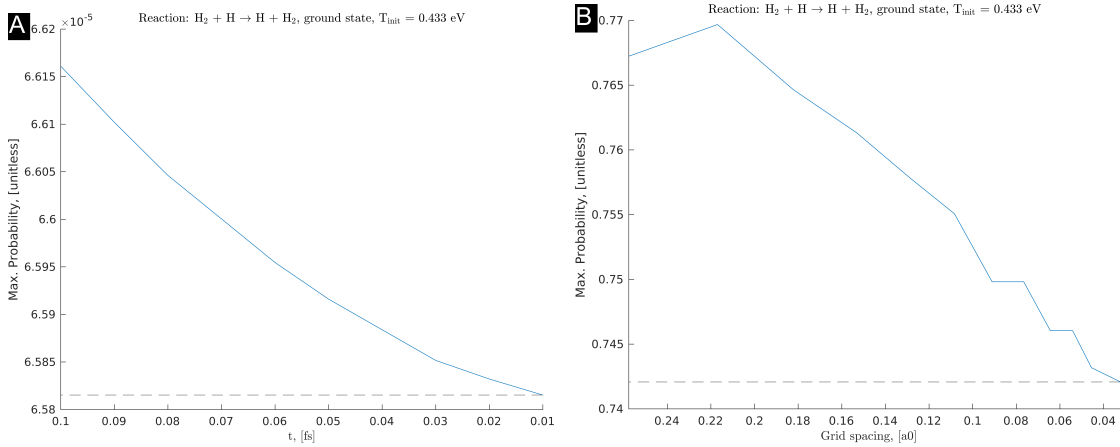


Figure 2.4: Reaction probabilities using the reactive flux method cumulative flux method at converged cumulative reaction probabilities as a function of A) stepsize, Δt and B) grid spacing, $[a_0]$, respectively. All data points used reaction (1.1a), the standard deviation of the Gaussian wave packet, $\sigma = 15 a_0$, see section 2.3.1, initial location of $[R_{1,0}; R_{2,0}] = [42 \text{ \AA}; R_{HH}^{\text{Morse}}]$ and an initial translational energy of $T_{\text{init}} = 0.433 \text{ eV}$. For A), a grid spacing of $0.0322 a_0$ was consistently used. For B), a timestep of 0.01 fs was consistently used.

From Figure 2.4A), it can be seen that decreasing the stepsize, Δt , in the interval $\Delta t \in [0.01; 0.1] \text{ fs}$ had an insignificant impact of $\approx 0.03 \cdot 10^{-5}$ in reaction probability. Hence, a timestep of $\Delta t = 0.01 \text{ fs}$ was used throughout section 3. From Figure 2.4B), it can be seen that decreasing the grid spacing in the interval $[0.2576; 0.0322] a_0$ decreases the reaction probability of about $2 \cdot 10^{-2}$. From the trajectory of Figure 2.4B), the reaction probability is expected to decrease even further, but due to the extended simulation times, a grid spacing of $0.0322 a_0$ was chosen. As a final note, it ought be noted that this section treats at timestep and grid spacing separately. However, this may not be the case and simulations, which vary stepsize and grid spacing ought to be run².

²To pursue the idea of running simulations, which combine the stepsize, Δt , and the grid spacing, efficiency ought to prioritized. Multiple methods and algorithms exist, which increase the amount of information from the least amount of data. One of these methods is the full factorial design, which takes the span of the number of variables, in this case the stepsize and grid spacing, after which it provides the initial timesteps and grid spacings, which ought to be used to get the most amount of information. An example of the full factorial design of simulations can be seen in the following article: [70].

3. Results and Discussion

This section provides the reaction probabilities, mentioned in section 2.2.2, as a function of the initial translational energy. The reaction probabilities were found by visual inspection of the cumulative reaction probabilities using eq. (2.23) and the trapezoidal rule described in section 2.2.3. If the cumulative reaction probabilities converged at $t = t_{\text{final}}$, then the data point was denoted. Otherwise, it was deleted. This is because that depicting non-converged reaction probabilities is not a true reaction probability, since some probability density is still crossing the fluxline and maybe even the reaction barrier. The ratios $\frac{P_{n=0} T_{\text{Init}}}{P_{n=1} (T_{\text{Init}} - E_1)}$ were also provided, where $E_1 = E_1^{\text{Morse}} - E_0^{\text{Morse}}$. Similarly, $E_2 = E_2^{\text{Morse}} - E_0^{\text{Morse}}$. The Morse potential in question is that of the diatomic reactant, e.g. for reaction (1.1d) initiated in the first excited vibrational state: $E_1^{\text{HCl}} = E_1^{\text{Morse, HCl}} - E_0^{\text{Morse, HCl}}$. Similarly, for the reversed reaction starting in the second excited vibrational state (1.1b): $E_2^{\text{OH}} = E_2^{\text{Morse, OH}} - E_0^{\text{Morse, OH}}$. The quantum tunnel effect is shortly described here:

The tunnel effect is an effect in quantum mechanics, which describes the transmission of a wavefunction through a potential, whose value is greater than the sum of the translational and potential energy of the in-going wavefunction¹. Overall, it can be said for the one-dimensional case that the transmission increases for greater initial translational energy and $\lim_{\frac{T_{\text{Init}}}{V_0} \rightarrow \infty} \approx 1$ with V_0 being the barrier height and T_{Init} being the initial translational energy [11, 72]. Furthermore, the transmission probabilities increase greatly around $\frac{T_{\text{Init}}}{V_0} \approx 1$. Specifically, the reaction probability is equal to 1/2, when $E = T_{\text{Init}} - E_n$ for the Eckart potential: $V(x) = \frac{A \exp(ax)}{1 + \exp(ax)} + \frac{B \exp(ax)}{(1 + \exp(ax))^2}$ with $a, B \in \mathbb{R}^+$

and $A \in \mathbb{R}_0^-$. This also holds true for the parabolic potential: $V(x) = V_0 + \frac{1}{2} x^2 \left. \frac{dV(x)}{dx^2} \right|_{x=0}$ [47]. The following sections are in two dimensions, where recrossing is possible. Hence, the reaction probability is expected to be lower than the one-dimensional case. From this, it is expected in the following sections that the reaction probabilities similarly increase around E_0 , when the diatomic reactant is initialized in the vibrational ground state. Due to the excited 1st and 2nd vibrational states being higher in energy, these are expected to be higher in reaction probability for smaller translational energies.

¹One of the earliest papers (received 1927) was by Von L. Mandelstam and M. Leontowitseh: [71]. If the reader pursues to read the article, the following ought to be noted: i) the authors used an infinite potential and did not use the δ distribution potential terminology, since this notation came out the same year, ii) the authors did not use the transmission and tunneling terminology, rather they independently solved the Schrödinger equation and iii) this thesis compares the probability density, but they provide the wavefunction solution. While E_0 is not infinite, one can easily convince themselves that quantum tunneling exists for finite potentials, if it is true for infinite potentials

Figure 3.1 shows a successfull reaction, which has converged. This is simply done by visually inspecting the graph plotting the cumulative flux described in section 2.2.2 as function of time, t . If the cumulative flux stagnates at t_{final} , the cumulative flux is converged and the data point consisting of the translative energy along with the cumulative flux at the final time step, $P(t_{\text{final}})$, is noted in a .txt file. The values are then plotted together and can be seen in the following sections. From section 2.3, the standard deviation of the Gaussian wave packet, the initial wave function location, the grid spacing and the timestep were argued to be the following: 15 a_0 , $[42 \text{ \AA}; R_{eq}^{\text{Morse}}]$, 0.0322 a_0 and 0.01 fs . R_{eq}^{Morse} is the equilibrium distance of Morse potential for the diatomic reactant provided by Table B.1. These values remained the same throughout this chapter for all reactions.

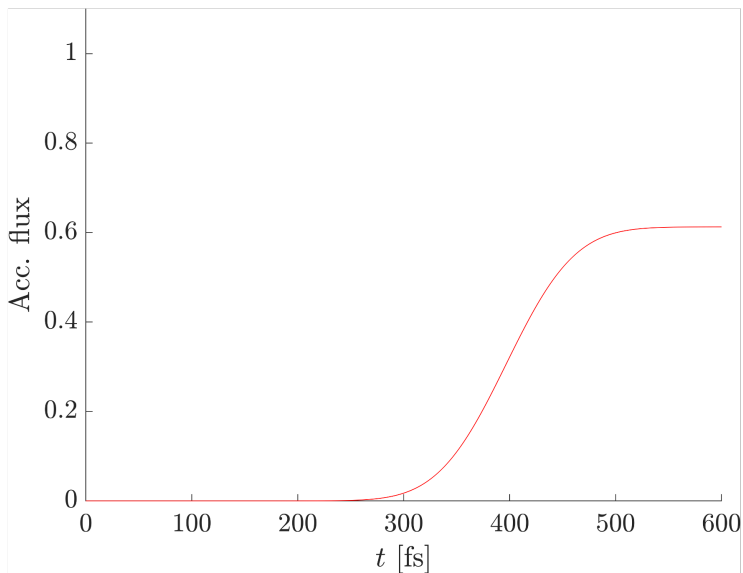


Figure 3.1: Example of a converged cumulative flux [unitless] as a function of time, t , [fs]. The method used is the reactive flux method described in section 2.2.2. Reaction (1.1a): $H + H_2 \rightarrow H_2 + H$, with an initial translative energy of 0.4 eV. The following timestep, grid spacing and standard deviation were used: $\Delta t = 0.01 \text{ fs}$, 0.0322 a_0 and $\sigma = 15 \text{ a}_0$. The simulation was run for $t \in [0; 600] \text{ fs}$.

location, the grid spacing and the timestep were argued to be the following: 15 a_0 , $[42 \text{ \AA}; R_{eq}^{\text{Morse}}]$, 0.0322 a_0 and 0.01 fs . R_{eq}^{Morse} is the equilibrium distance of Morse potential for the diatomic reactant provided by Table B.1. These values remained the same throughout this chapter for all reactions.

3.1 THERMONEUTRAL REACTION, $H + H_2 \rightarrow H_2 + H$

This section provides reaction probabilities for reaction (1.1a) as well as the ratio $\frac{P_{n=0}T_{\text{Init}}}{P_{n=1}(T_{\text{Init}}-\Delta E_1)}$. Section 3.4 compares these plots with the cross section from the literature.

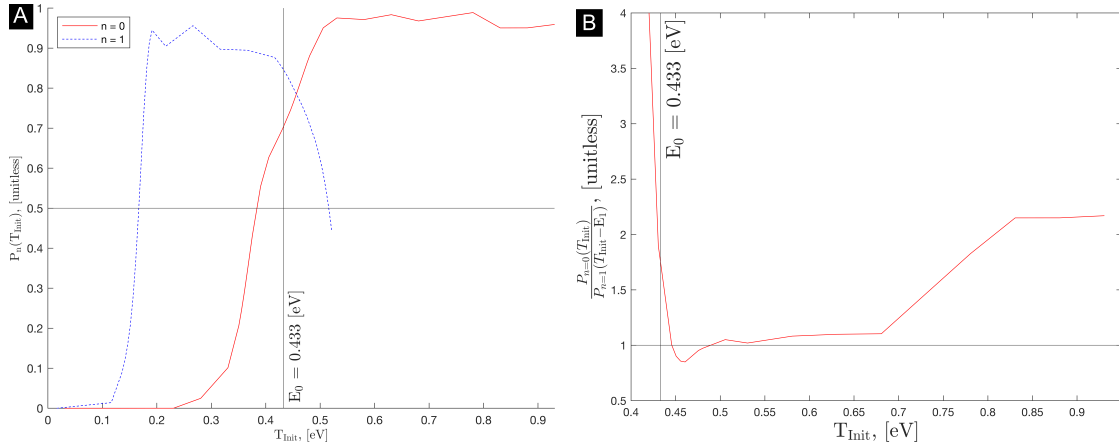


Figure 3.2: A) Reaction probabilities, $P_n(T_{\text{Init}})$, [unitless] for reaction (1.1a): $H + H_2 \rightarrow H_2 + H$, as a function of initial translational energy, T_{Init} , [eV] for initial vibrational ground states, $n = 0$, (red circles) and 1st excited vibrational states, $n = 1$, (blue squares), respectively. E_0 [eV] is plotted from Table 1.3. B) Ratio $\frac{P_{n=0}(T_{\text{Init}})}{P_{n=1}(T_{\text{Init}}-E_1)}$ [unitless] for reaction (1.1a) as function of initial translational energy.

Figure 3.2A) shows that the tunnel effect happens earlier, when the diatomic molecule starts in its excited state, $n = 1$ than in its ground state, $n = 0$. The reaction probability for the initial vibrational ground state reaction exceeds 0.5 at $T_{\text{Init}} < E_0$. This will not be the case for any other reactions in sections 3.2 and 3.3. This may be due to the narrow parabolic curve in the direction parallel to the minimum energy path. Recall from Table 1.2 that the reaction (1.1a) had the greatest $\tilde{\nu}_{\text{parallel}}$ of 2302.9 i cm^{-1} . This results in a smaller distance, which the reaction coordinate needs to travel through in order to pass into the product channel. In Figure 3.2B), it can be seen that the ratio is great for small translational energy. This is in contradiction to the Polanyi rules for small translational energies. For greater translational energies, the reaction probability stagnates at ≈ 1 . This is expected for a thermoneutral reaction, since these neither favour distributing the total energy of the system to vibrational nor translatable energies.

3.2 EARLY-BARRIER REACTIONS

This section provides reaction probabilities for reactions (1.1b-d) as well as the ratio $\frac{P_{n=0}T_{\text{Init}}}{P_{n=1}(T_{\text{Init}}-\Delta E_1)}$. Section 3.4 compares these plots with the cross section from the literature.

3.2.1 $\text{O} + \text{H}_2 \rightarrow \text{OH} + \text{H}$

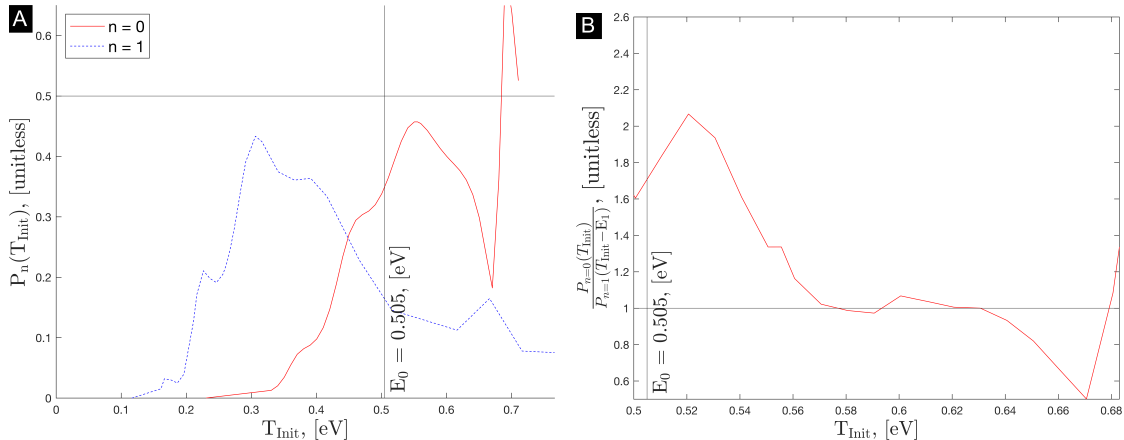


Figure 3.3: A) Reaction probabilities, $P_n(T_{\text{Init}})$, [unitless] for reaction (1.1b): $\text{O} + \text{H}_2 \rightarrow \text{OH} + \text{H}$, as a function of initial translational energy, T_{Init} , [eV] for initial vibrational ground states, $n = 0$, (red circles) and 1st excited vibrational states, $n = 1$, (blue squares), respectively. E_0 [eV] from Table 1.3 is plotted as well. B) Ratio $\frac{P_{n=0}(T_{\text{Init}})}{P_{n=1}(T_{\text{Init}} - E_1)}$ [unitless] for reaction (1.1b) as function of Initial translational energy, T_{Init} , [eV].

Similarly to Figure 3.2A), Figure 3.3A) shows that the tunnel effect happens earlier, when the diatomic molecule starts in its excited state, $n = 1$, than in its ground state, $n = 0$. Contrary to section 3.2, Figure 3.3A) does not exceed a reaction probability of 0.5. This is also in contradiction to the transmission described in the beginning of the chapter. This can be due to the fact the the considered system is two-dimensional. Some probability may therefore cross the reaction barrier, after which it recrosses back into the reactant channel. This also explains the downtrending curve for greater translational energy. The reactive flux method from section 2.2.2 neither denies nor confirms this. Furthermore, it can be seen in Figure 3.3B) that the ratio is great for small translational energies. While this is consistent with the Polanyi rules for early-barrier reactions, the great ratio at small translational energies is also present throughout section 3.3, which describes the late-barrier reactions. Hence, this may be an artefact. For greater translational energies, it stagnates at 1 but stays greater than 1. The ratio being greater than 1 for early-barrier reactions is in accordance with the Polanyi rules. These state that distributing the total energy of the system, in favour of translational energy over

vibrational energy, increases reaction probability for early-barrier reactions.

3.2.2 $F + H_2 \rightarrow HF + H$

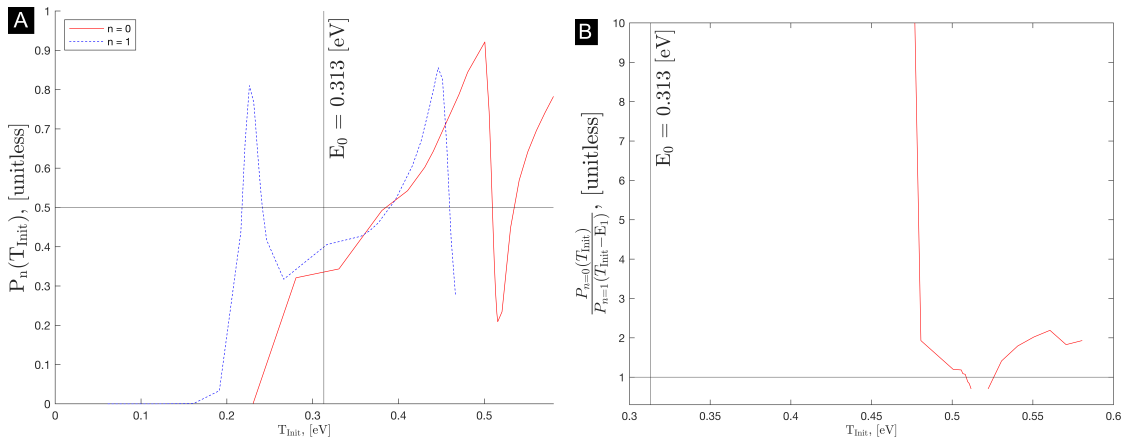


Figure 3.4: A) Reaction probabilities [unitless] for reaction (1.1c): $F + H_2 \rightarrow HF + H$, as a function of initial translational energy [eV] for initial vibrational ground states, $n = 0$, (red circles) and 1st excited vibrational states, $n = 1$, (blue squares), respectively. E_0 [eV] is plotted from Table 1.3. B) Ratio $\frac{P_{n=0}(T_{\text{init}})}{P_{n=1}(T_{\text{init}}-E_1)}$ for reaction (1.1c) as function of initial translational energy.

Similarly to Figure 3.3A), Figure 3.4A) shows that the tunnel effect happens earlier, when the diatomic molecule starts in its excited state, $n = 1$, than in its ground state, $n = 0$. In contrary to Figure 3.2A), Figure 3.4A) passes the reaction probability of 0.5 at $T_{\text{Init}} > E_0$. Recall from Table 1.2 that reaction (1.1c) had the lowest $\tilde{\nu}_{\text{parallel}}$ of 920.5 i. This results in a broader parabolic curve in the direction of the minimum energy path. Hence, the reaction coordinate needs to travel further in order to pass into the product channel. This results in less tunnel effect and is in accordance with the one-dimensional case. Furthermore, in contrary to Figure 3.3A), Figure 3.4A) does exceed a reaction probability of 0.5, after which the reaction probability decrease almost instantly for $n = 1$. For $n = 0$, however, the reaction probability decreases at $T_{\text{Init}} \approx 0.5$ eV and increases at $T_{\text{Init}} \approx 0.55$ eV. One could investigate, whether the same tendency would repeat at greater initial translational energies for $n = 1$. Similarly to section 3.2.1, the decrease in reaction probability may be due to recrossing. It can be seen in Figure 3.4B) that the ratio is much greater for small translational energies than it was in Figure 3.3B). This may be due to reaction (1.1c) being a much earlier barrier, $[R_{HF}^{\ddagger}; R_{HH}^{\ddagger}] = [1.57; 0.767]$ Å, than eq. (1.1b), $[R_{OH}^{\ddagger}; R_{HH}^{\ddagger}] = [1.23; 0.92]$ (values taken from Table 1.1). For greater translative energies, $\frac{P_{n=0}(T_{\text{Init}})}{P_{n=1}(T_{\text{Init}}-E_1)}$ stays above 1. This is again consistent with the Polanyi rules for early-barrier reactions, which state that translative

energy over vibrational energy enhances reaction probability more effectively for early-barrier reactions.

3.2.3 $\text{F} + \text{HCl} \rightarrow \text{HF} + \text{Cl}$

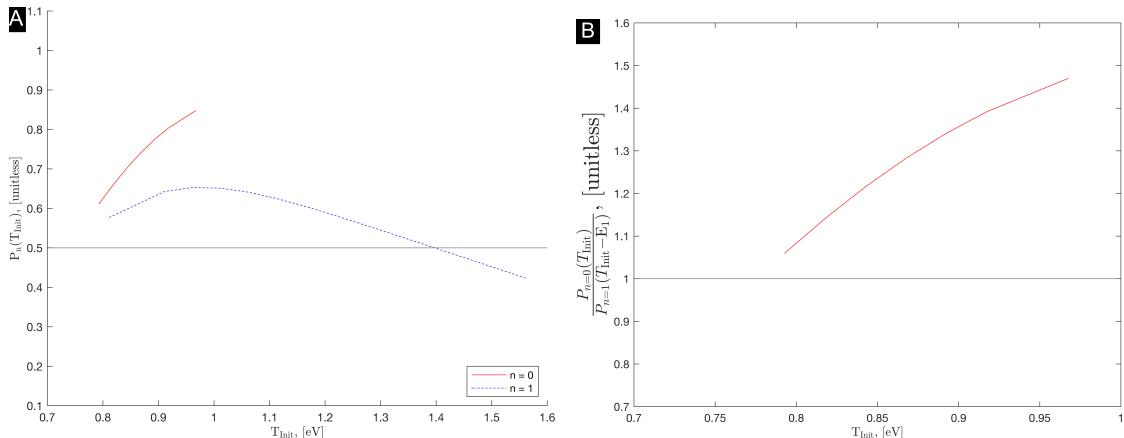


Figure 3.5: A) Reaction probabilities [unitless] for reaction (1.1d) as a function of initial translational energy [eV] for initial vibrational ground states, $n = 0$, (red circles) and 1st excited vibrational states, $n = 1$, (blue squares), respectively. E_0 [eV] is plotted from Table 1.3. B) Ratio $\frac{P_{n=0}(T_{\text{init}})}{P_{n=1}(T_{\text{init}})}$ for reaction (1.1d) as function of initial translational energy.

Similarly to Figure 3.3A) and Figure 3.4A), Figure 3.5A) shows that the tunnel effect happens earlier, when the diatomic molecule starts in its excited state, $n = 1$, than in its ground state, $n = 0$. Similarly to Figure 3.3A), Figure 3.5A) does not exceed a reaction probability of 0.5 for $n = 0$. This could be due to the few amount of data points and one ought to expand on this by increasing the translative energy for $n = 0$. For $n = 1$, however, the reaction probability exceeds 0.5 at $T_{\text{Init}} \approx 0.7$ eV. In Figure 3.4B), it can be seen that small initial translative energies contradict the Polanyi, since reaction vibrational energy is more effective in increasing the reaction probability. At greater initial translative energies, $T_{\text{Init}} > 0.6$ eV, translative energy is favoured. Hence, the Polanyi rules hold true for greater initial translative energies. Finally, it ought to be mentioned that no data points were yielded at small initial translative energies, $T_{\text{Init}} < 0.4$ eV, due to the system being too heavy. This resulted in the wavefunction moving at a slower pace than reactions (1.1b) and (1.1c), which led to non-converged results. One could increase the final time of the system to yield results at smaller translative energies.

3.3 LATE-BARRIER REACTIONS

This section provides reaction probabilities for the reversed reactions (1.1b-d) as well as the ratio $\frac{P_{n=0}T_{\text{Init}}}{P_{n=1}(T_{\text{Init}} - \Delta E_1)}$. Section 3.4 compares these plots with the cross section from the literature. Due to sections 3.7 and 3.3.3 yielding small reaction probabilities, $P < 0.01$, for both the vibrational ground state and the 1st excited vibrational state, another 2nd excited vibrational state was further investigated for the reversed reactions (1.1c) and (1.1d).

3.3.1 OH + H → O + H₂

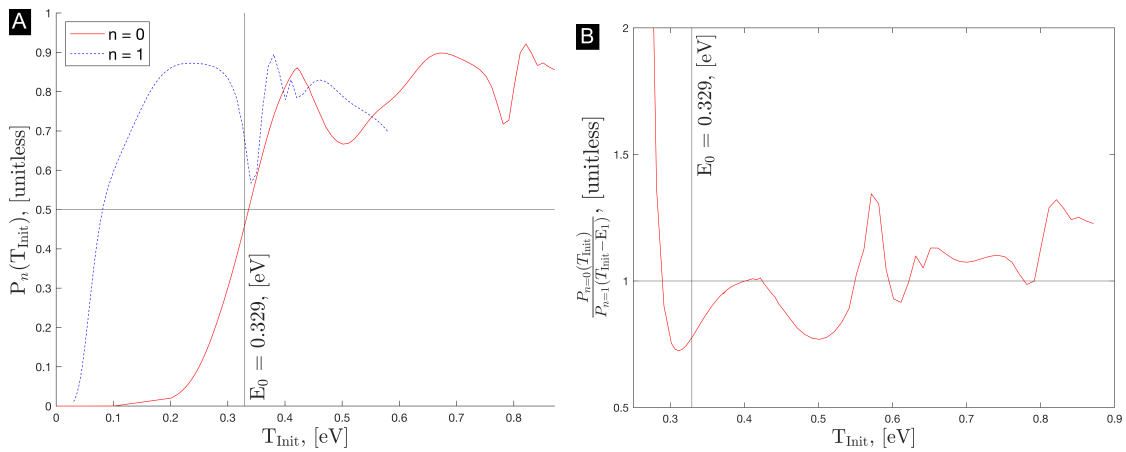


Figure 3.6: A) Reaction probabilities [unitless] for the reversed reaction (1.1b): H + OH → O + H₂ as a function of initial translational energy [eV] for initial vibrational ground states, n = 0, (red circles) and 1st excited vibrational states, n = 1, (blue squares), respectively. E₀ [eV] is plotted as well. B) Ratio $\frac{P_{n=0}(T_{\text{Init}})}{P_{n=1}(T_{\text{Init}} - E_1)}$ for the reversed reaction (1.1b) as function of Initial translational energy, T_{Init}, [eV].

Similarly to sections 3.1 and 3.2, Figure 3.6A) shows that the tunnel effect happens earlier, when the diatomic molecule starts in its excited state, $n = 1$, than in its ground state, $n = 0$. Contrary to section 3.2, the reaction probability, when the wavefunction is initiated in the first excited vibrational state is shifted more to the left. Furthermore, a reaction probability of 0.5 can already be achieved at $T_{\text{Init}} = 0.1$ eV for the 1st excited state and at $T_{\text{Init}} = 0.4$ eV. Reaction (1.1b) from section 3.3 could not achieve a reaction probability of 0.5. Finally, with respect to Figure 3.6A), the ground state passes through a reaction probability of 0.5 at $T_{\text{Init}} \approx E_0$, which is similar to the one-dimensional case. In Figure 3.3B), the ratio is much greater than 1 for small initial translative energies, $T_{\text{Init}} < 0.3$ eV. For late-barrier reactions, this is in contradiction with the Polanyi rules, which state the opposite: reaction probability favours vibrational energy for late-barrier

reactions. The ratio fulfills the Polanyi rules in the interval $0.3 \text{ eV} < T_{\text{Init}} < 0.52 \text{ eV}$. After this, the ratio exceeds 1 again, which is in contradiction with the Polanyi rules. Hence, there seems to be an subinterval for the reversed reaction (1.1b). Such a subinterval was not necessary for the thermoneutral reaction nor the early-barrier reactions from sections 3.1 and 3.2.

3.3.2 $\text{HF} + \text{H} \rightarrow \text{F} + \text{H}_2$

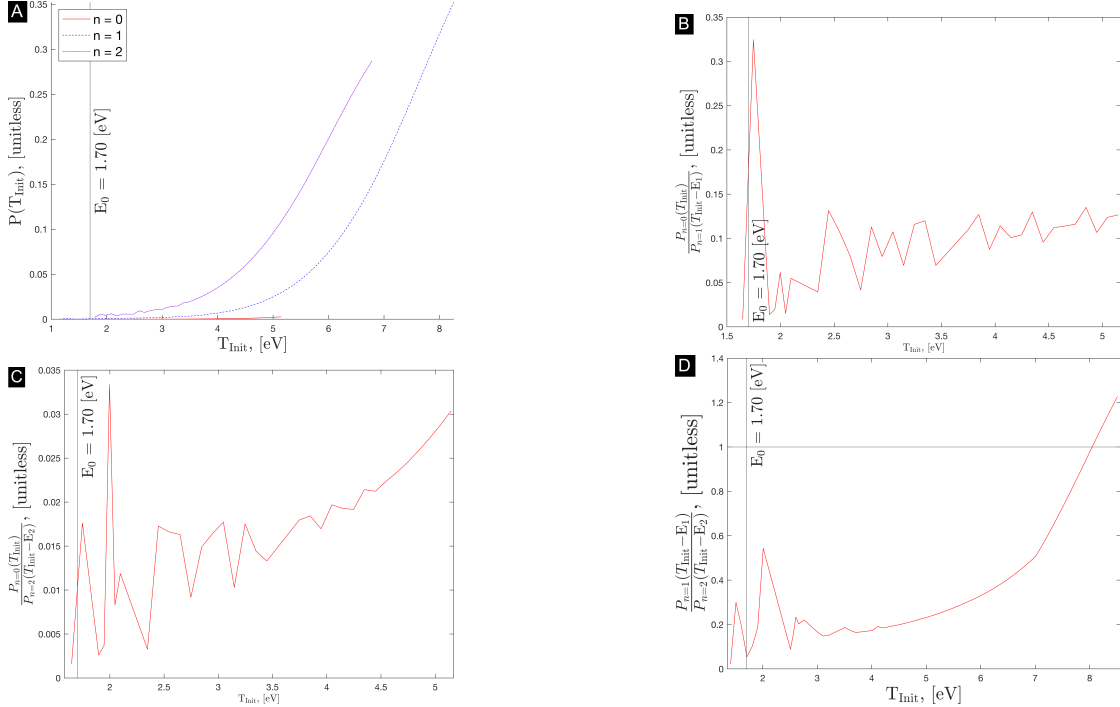


Figure 3.7: A) Reaction probabilities [unitless] for the reversed reaction (1.1c): $\text{HF} + \text{H} \rightarrow \text{F} + \text{H}_2$ as function of initial translational energy [eV] for initial vibrational ground states, $n = 0$, (red circles), 1st excited vibrational states, $n = 1$, (blue squares) and 2nd excited vibrational states, $n = 2$, (purple triangles), respectively. E_0 [eV] is plotted as well. B) Ratio $\frac{P_{n=0}(T_{\text{Init}})}{P_{n=1}(T_{\text{Init}} - E_1)}$ for the reversed reaction (1.1c) as function of initial translational energy, T_{Init} , [eV]. C) Ratio $\frac{P_{n=0}(T_{\text{Init}})}{P_{n=2}(T_{\text{Init}} - E_2)}$ for the reversed reaction (1.1c) as function of initial translational energy, T_{Init} , [eV]. D) Ratio $\frac{P_{n=1}(T_{\text{Init}} - E_1)}{P_{n=2}(T_{\text{Init}} - E_2)}$ for the reversed reaction (1.1c) as function of initial translational energy, T_{Init} , [eV].

In contrary to the rest of the reactions, small reaction probabilities of $P < 0.01$ was yielded even at great initial translative energy, $T_{\text{Init}} \approx 4 \text{ eV}$. Hence, the 2nd excited vibrational state was investigated. In contrary to the rest of the reactions, the reaction probability remained low, $P < 0.03$, even at great kinetic energies. Nevertheless, it

can be seen on Figures 3.7B-C) that reaction probability favours vibrational energy over translative energy. This is in accordance with the Polanyi rules, since this is a late-barrier reaction. Recall that the barrier coordinates, which can be seen in Table 1.2 are provided by $[R_{\text{HH}}^{\ddagger}; R_{\text{HF}}^{\ddagger}] = [0.767; 1.57] \text{ \AA}$. 3.7D) shows that initializing the wavefunction in the 2nd vibrational state enhances the reaction probability greater than for the 1st excited vibrational state in the interval $0.1 \text{ eV} < T_{\text{Init}} < 5 \text{ eV}$. However, similarly to Figure 3.6B), the ratio exceeds 1 for great translative energies, $T_{\text{Init}} > 5 \text{ eV}$. Hence, the Polanyi rules are again fulfilled in a subinterval of translative energies for some chosen initial vibrational states rather than for all translative energies.

3.3.3 $\text{HF} + \text{Cl} \rightarrow \text{F} + \text{HCl}$

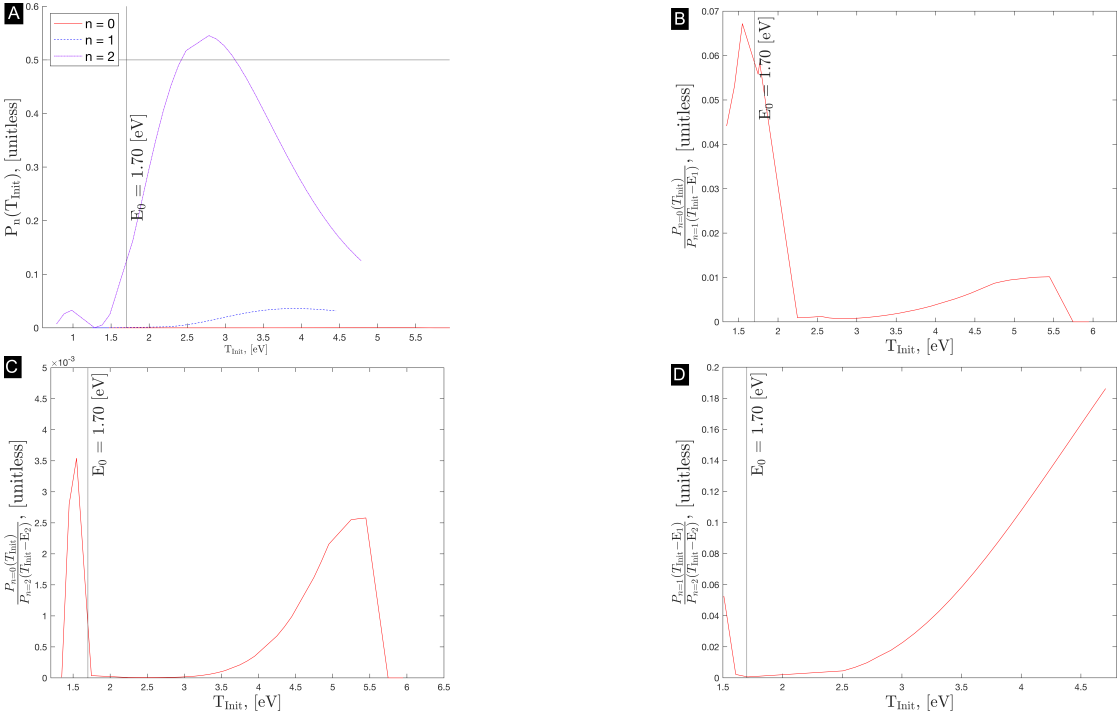
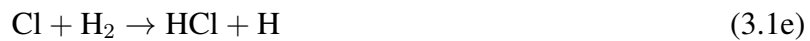


Figure 3.8: A) Reaction probabilities [unitless] for the reversed reaction (1.1d): $\text{HF} + \text{Cl} \rightarrow \text{F} + \text{HCl}$ as function of initial translational energy [eV] for initial vibrational ground states, $n = 0$, (red circles), 1st excited vibrational states, $n = 1$, (blue squares) and 2nd excited vibrational states, $n = 2$, (purple triangles), respectively. E_0 [eV] is plotted as well. B) Ratio $\frac{P_{n=0}(T_{\text{Init}})}{P_{n=1}(T_{\text{Init}} - E_1)}$ for the reversed reaction (1.1d) as function of initial translational energy, T_{Init} , [eV]. C) Ratio $\frac{P_{n=0}(T_{\text{Init}})}{P_{n=2}(T_{\text{Init}} - E_2)}$ for the reversed reaction (1.1d) as function of initial translational energy, T_{Init} , [eV]. D) Ratio $\frac{P_{n=1}(T_{\text{Init}} - E_1)}{P_{n=2}(T_{\text{Init}} - E_2)}$ for the reversed reaction (1.1d) as function of initial translational energy, T_{Init} , [eV].

Similarly to section 3.3.2, this section investigates the reaction probability with initialized vibrational states $n \in \{0,1,2\}$. This was done, since reaction probabilities remained small, $P < 0.05$, for $n = 0$ and $n = 1$. Looking at Figure 3.8A), it can easily be seen that exciting the initial vibrational state effectively increases the reaction probability. The 2nd vibrational propagations were the only ones to exceed a reaction probability of 0.5. Figure 3.8B) shows that using $n = 1$ results in more reaction probability than $n = 0$. Figures 3.8C-D) show that using vibrational state $n = 2$ results in more reaction probability compared to $n = 1$ and $n = 0$ for all T_{Init} . These conclusions are in accordance with the Polanyi rules, which state that vibrational energy enhances reaction probability more effectively than translative energy for late-barrier reactions. In contrary to the late-barrier sections 3.3.1 and 3.3.2, there is no need to introduce subintervals of T_{Init} , for which the Polanyi rules do not hold true.

3.4 DISCUSSION

This section discusses and compares this thesis' results with the results of the article: *Relative efficacy of vibrational vs. translational excitation in promoting atom-diatom reactivity: Rigorous examination of Polanyi's rules and proposition of sudden vector projection (SVP) model* by Bin Jiang and Hua Guo [26]². They considered the following reactions:



where reactions (3.1a-b) are central-barrier, reactions (3.1c-d) are early-barriers and reaction (3.1e) is a late barrier reaction. The n in reaction (3.1a) denotes the hydrogen isotope. They investigated the reaction cross section using already calculated Potential Energy Surfaces (PESs). Reactions (3.1c-d) used the (BKMP2) PES, reactions (3.1c) and (3.1e) used the (LWA)-5 PES and eq. (3.1d) used the (DHTSN) PES. They got the results reprinted in Figure 3.9. They state for Figure 3.9A) representing reactions (3.1a-b) that vibrational energy is less efficient than translational energy for small total energies. For greater total energies, the opposite is true. This is in agreement with the results proposed in this thesis in section 3.1. For Figure 3.9B), they state that the cross section favours translational energies for small total energies. Again, the reverse is true for greater total energies. A similar note was made for the same reaction in section 3.2.2 for small translative energies. However, this thesis found that reaction probability favour both translational and vibrational energy for great initial translational energies. For Figure 3.9C), they state that vibrational energy over translational energy for great total values, Total energy > 0.9 eV. This is accordance with this thesis' findings in section 3.2.3. For Figure 3.9D), they state that there also exists a cross-over point for (3.1e), which was much earlier than the rest of the reactions due to the late-barrier nature of the PES. For total energy < 0.3 eV, the cross section favours translative energy over vibrational energy. The reverse was true for greater total energies. While this finding was in accordance with the reaction from section 3.3.1, this rules seems hardly to be the case. The reaction probabilities in sections 3.3.2 and 3.3.3 very much favoured greater vibrational states than translative energy. Furthermore, 3.3.2 drew the opposite conclusion than when $n = 2$ and $n = 1$ were considered. Hence, rules similar to the Polanyi rules ought to also take greater states into account rather than only $n = 0$ and

²They used the terminology, early-, central- and late-barriers. This thesis uses the early- and late-barrier as well as thermoneutral reaction terminology.

$n = 1$.

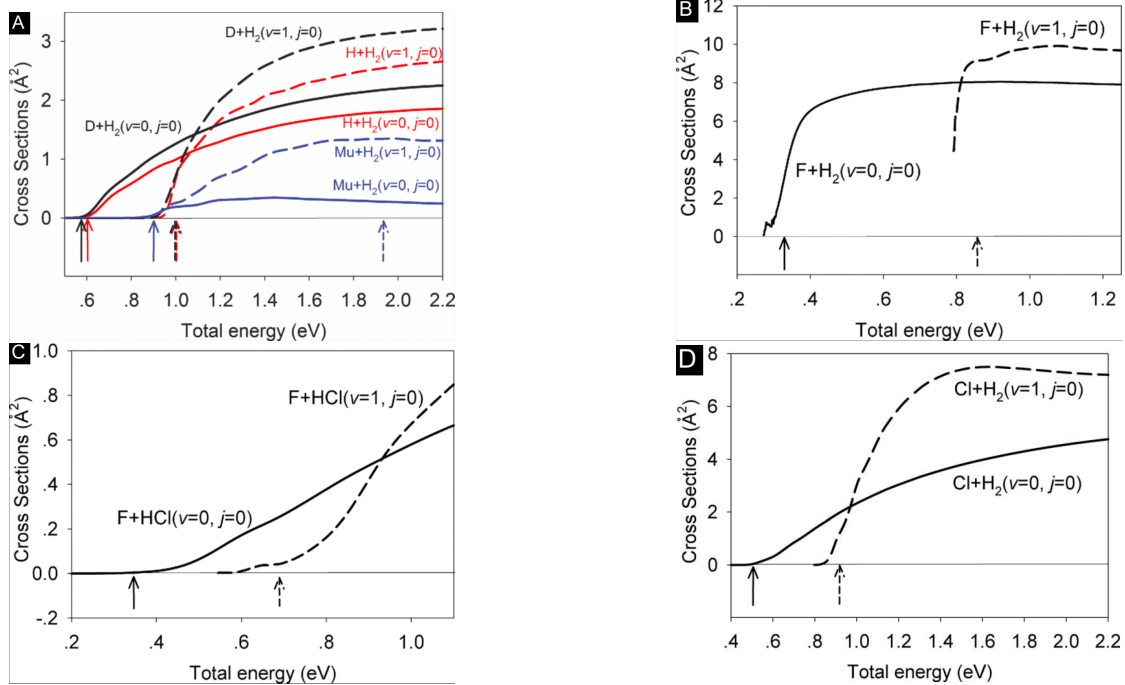


Figure 3.9: Reprints of cross section [\AA^2] as a function total energy [eV] from [26] (their FIG. 2., FIG. 4, FIG. 5 and FIG 3, respectively). A) Reactions (3.1a-b), B) Reactions (3.1c), C) Reaction (3.1d) and D) Reaction (3.1e).

In section 1.5, Figure 1.7, it was mentioned that the rate constant only increases for greater temperatures. As it was shown throughout section 3, all reactions showed decreasing reaction probabilities for greater translational energies regardless of the initial vibrational state. This is also the case for the cross section as mentioned by Bin Jiang and Hua Guo. One can regard temperature as the average translational energy of the system scaled up to a macroscopic measurement [28]. While this definition is not entirely true, it suffices to the extend of this thesis. Drawing this parallel between the translational energy and temperature, it can be concluded that the TST approximation differs from the true rate constant for greater initial translational energies.

Conclusion

The investigation into the chemical reaction probabilities of reactions (1.1a-d) in relation to the Polanyi rules revealed that the rules held true early-barrier reactions. These were in agreement with findings of Bin Jiang and Hua Guo, who investigated the cross section for similar reactions in 2013 [26]. These generally claimed that favouring translative energy over vibrational energy for smaller total energies would favour the cross section. This thesis, however, showed that this is not true for late-barrier reactions. For late-barrier reactions, there is a greater dependency on greater initial states, even for small total energies.

Additionally, the lack of recrossing at great total energies raised questions about the applicability of Transition State Theory in these conditions. It was found that the Transition State Theory deviates for great energies.

Bibliography

- [1] O. Christensen, *Functions, Spaces, and Expansions: Mathematical Tools in Physics and Engineering*. Birkhäuser Verlag, 2010th ed., June 2010.
- [2] E. Kreyszig, *Introductory Functional Analysis with Applications*. John Wiley & Sons, Limited, 1st ed., February 1989.
- [3] V. Hansen and P. Hjorth, *Fundamental Concepts in Modern Analysis, An Introduction to Nonlinear Analysis*. Singapore: World Scientific Publishing Company, 2nd edition ed., June 2019.
- [4] L. Hörmander, *Analysis of Linear Partial Differential Operators II*. Springer Berlin Heidelberg, 2005th ed., November 2007.
- [5] P. A. M. Dirac and R. H. Fowler, “The physical interpretation of the quantum dynamics,” *Proceedings of the Royal Society of London. Series A, Containing Papers of a Mathematical and Physical Character*, vol. 113, no. 765, pp. 621–641, 1927.
- [6] A. M. Kabe and B. H. Sako, *Structural Dynamics Fundamentals and Advanced Applications*. Academic Press, 1st ed., July 2020.
- [7] R. A. Brewster and J. D. Franson, “Generalized delta functions and their use in quantum optics,” *Journal of Mathematical Physics*, vol. 59, January 2018.
- [8] T. M. Apostol, *Mathematical analysis*. Addison-Wesley series in mathematics, Addison-Wesley, 2nd ed., January 1974.
- [9] Y. M. Berezansky, Z. G. Sheftel, and G. F. Us, *Measures in the Products of Spaces. Fubini Theorem*, vol. I, pp. 133–145. Basel: Birkhäuser Basel, 1996.
- [10] L. E. Ballentine, *Quantum Mechanics: a Modern Development: 2nd Edition*. World Scientific Publishing Co., 2nd edition ed., 2014.
- [11] D. A. McQuarrie, *Quantum Chemistry*. University Science Books, 2nd ed., August 2007.
- [12] V. Moretti, *Spectral Theory and Quantum Mechanics*, vol. 110. Springer International Publishing, 2nd ed., February 2017.
- [13] J. von Neumann, *Mathematical foundations of quantum mechanics*. Princeton, NJ: Princeton University Press, February 2018.
- [14] A. Galindo and P. Pascual, *The Postulates of Quantum Mechanics*, pp. 33–87. Berlin, Heidelberg: Springer Berlin Heidelberg, 1990.

- [15] E. Schrödinger, “An undulatory theory of the mechanics of atoms and molecules,” *Phys. Rev.*, vol. 28, pp. 1049–1070, December 1926.
- [16] L. E. Ballentine, “Can the statistical postulate of quantum theory be derived?—a critique of the many-universes interpretation,” *Foundations of Physics*, vol. 3, no. 2, pp. 229–240, 1973.
- [17] M. Born, “Zur quantenmechanik der stoßvorgänge,” *Eur. Phys. J. A*, vol. 37, pp. 863–867, Dec. 1926.
- [18] M. Born, “On the Quantum Mechanics of Collision Processes,” *Zeitschrift für Physik*, vol. 37, pp. 863–868, June 1926. The German title of this Max Born article is: Die Quantenmechanik der Stoßvorgänge. Terry Bollinger translated the article to English on 2021-08-28.
- [19] I. Levine, *Quantum Chemistry*. New York: Pearson Education, 7th ed., February 2013.
- [20] D. J. Griffiths, *Introduction to Quantum Mechanics (2nd Edition)*. Pearson Prentice Hall, 2nd ed., April 2004.
- [21] W. Magnus and W. Schoenmaker, *Quantum Mechanics*, pp. 35–51. Berlin, Heidelberg: Springer Berlin Heidelberg, 1st ed., 2012.
- [22] J. C. Polanyi, “Some concepts in reaction dynamics,” *Science*, vol. 236, no. 4802, pp. 680–690, 1987.
- [23] P. Kuntz, E. Nemeth, J. Polanyi, S. Rosner, and C. Young, “Energy distribution among products of exothermic reactions. ii. repulsive, mixed, and attractive energy release,” *The Journal of Chemical Physics*, vol. 44, no. 3, pp. 1168–1184, 1966.
- [24] S. Yan, Y.-T. Wu, and K. Liu, “Tracking the energy flow along the reaction path,” *Proceedings of the National Academy of Sciences*, vol. 105, no. 35, pp. 12667–12672, 2008.
- [25] Z. Zhang, Y. Zhou, D. H. Zhang, G. Czakó, and J. M. Bowman, “Theoretical study of the validity of the polanyi rules for the late-barrier Cl+CH₃ reaction,” *The Journal of Physical Chemistry Letters*, vol. 3, no. 23, pp. 3416–3419, 2012.
- [26] B. Jiang and H. Guo, “Relative efficacy of vibrational vs. translational excitation in promoting atom-diatom reactivity: Rigorous examination of Polanyi’s rules and proposition of sudden vector projection (SVP) model,” *The Journal of Chemical Physics*, vol. 138, p. 234104, 06 2013.
- [27] P. M. Morse, “Diatomic molecules according to the wave mechanics. ii. vibrational levels,” *Phys. Rev.*, vol. 34, pp. 57–64, July 1929.

- [28] P. Atkins, J. De Paula, and J. Keeler, *Atkins' Physical Chemistry*. Oxford University Press, 11th ed., 2017.
- [29] D. Zwillinger, *CRC standard mathematical tables and formulae, 32nd edition*. Advances in Applied Mathematics, Boca Raton, FL: CRC Press, 32nd ed., June 2011.
- [30] J. Poll and G. Karl, “On the vibrational frequencies of the hydrogen molecule,” *Canadian Journal of Physics*, vol. 44, no. 7, pp. 1467–1477, 1966.
- [31] R. Pingak, A. Johannes, F. Nitti, and M. Ndii, “A theoretical study on vibrational energies of molecular hydrogen and its isotopes using a semi-classical approximation,” *Indonesian Journal of Chemistry*, vol. 21, pp. 725–739, April 2021.
- [32] H. Pelzer and E. Wigner, “Über die geschwindigkeitskonstante von austauschreaktionen,” *Part I: Physical Chemistry. Part II: Solid State Physics*, pp. 69–95, 1997.
- [33] M. J. Nye, “Working tools for theoretical chemistry: Polanyi, eyring, and debates over the “semiempirical method”,” *Journal of Computational Chemistry*, vol. 28, no. 1, pp. 98–108, 2007.
- [34] S. Sato, “A new method of drawing the potential energy surface,” *Bulletin of the Chemical Society of Japan*, vol. 28, pp. 450–453, July 1955.
- [35] S. Sato, “On a New Method of Drawing the Potential Energy Surface,” *The Journal of Chemical Physics*, vol. 23, pp. 592–593, December 1955.
- [36] B. Liu, “Ab initio potential energy surface for linear H_3 ,” *The Journal of Chemical Physics*, vol. 58, pp. 1925–1937, August 2003.
- [37] F. W. Bobrowicz and W. A. Goddard, *The Self-Consistent Field Equations for Generalized Valence Bond and Open-Shell Hartree—Fock Wave Functions*, pp. 79–127. Boston, MA: Springer US, 1977.
- [38] S. P. Walch, T. H. Dunning Jr, R. C. Raffenetti, and F. W. Bobrowicz, “A theoretical study of the potential energy surface for $O(^3P)+H_2$,” *The Journal of Chemical Physics*, vol. 72, pp. 406–415, July 1980.
- [39] J. Bauschlicher, Charles W., S. P. Walch, S. R. Langhoff, P. R. Taylor, and R. L. Jaffe, “Theoretical studies of the potential surface for the $F+H_2 \rightarrow HF+H$ reaction,” *The Journal of Chemical Physics*, vol. 88, pp. 1743–1751, 02 1988.
- [40] K. Stark and H. Werner, “An accurate multireference configuration interaction calculation of the potential energy surface for the $F+H_2 \rightarrow HF+H$ reaction,” *The Journal of Chemical Physics*, vol. 104, pp. 6515–6530, 05 1996.

- [41] Y. Aoto and A. Köhn, “Revisiting the F+HCl→ HF+Cl reaction using a multireference coupled-cluster method,” *Physical Chemistry Chemical Physics*, vol. 18, no. 44, pp. 30241–30253, 2016.
- [42] J. Stewart, D. K. Clegg, and S. Watson, *Multivariable calculus*. Cengage Learning, 9th ed., January 2012.
- [43] S. J. Colley, *Vector calculus*. Pearson Education, 4th ed., September 2011.
- [44] E. Clementi, D. L. Raimondi, and W. P. Reinhardt, “Atomic Screening Constants from SCF Functions. II. Atoms with 37 to 86 Electrons,” *The Journal of Chemical Physics*, vol. 47, pp. 1300–1307, May 2004.
- [45] M. Mantina, A. C. Chamberlin, R. Valero, C. J. Cramer, and D. G. Truhlar, “Consistent van der waals radii for the whole main group,” *The Journal of Physical Chemistry A*, vol. 113, no. 19, pp. 5806–5812, 2009. PMID: 19382751.
- [46] J. C. Slater, “Atomic Radii in Crystals,” *The Journal of Chemical Physics*, vol. 41, pp. 3199–3204, July 2004.
- [47] N. E. Henriksen and F. Y. Hansen, *Theories of molecular reaction dynamics: the microscopic foundation of chemical kinetics*. Oxford University Press, second ed., 2018.
- [48] H. Eyring, “The Activated Complex in Chemical Reactions,” *The Journal of Chemical Physics*, vol. 3, pp. 107–115, 11 1935.
- [49] S. Edelstein, *Modeling of Bimolecular Reactions*, pp. 1–3. New York, NY: Springer New York, 2013.
- [50] T. Horiba, S. Shirai, and H. Hirai, “Missing-rung problem in vibrational ladder climbing,” *Phys. Rev. A*, vol. 105, p. 013117, January 2022.
- [51] R. Glowinski, S. J. Osher, and W. Yin, *Splitting Methods in Communication, Imaging, Science, and Engineering*. Springer Publishing Company, Incorporated, 1st ed., 2018.
- [52] B. Li, X. Tang, and G. Yang, “Time-step optimization method to improve calculation efficiency and feasibility validation reliance,” *Engineering Optimization*, vol. 51, pp. 1324–1335, 2019.
- [53] H. Cao, X. Qian, Z. Chen, and H. Zhu, “Enhanced particle swarm optimization for size and shape optimization of truss structures,” *Engineering Optimization*, vol. 49, no. 11, pp. 1939–1956, 2017.

- [54] G. Tanoğlu and Y. Yazıcı, *Operator splitting methods for differential equations*. PhD thesis, The Graduate School of Engineering and Izmir Institute of Technology, Gülbahçe, İzmir Yüksek Teknoloji Enstitüsü, 35433 Urla/İzmir, May 2010.
- [55] G. Strang, “On the construction and comparison of difference schemes,” *SIAM Journal on Numerical Analysis*, vol. 5, no. 3, pp. 506–517, 1968.
- [56] A. Bertozzi and C.-B. Schönlieb, “Unconditionally stable schemes for higher order inpainting,” *Communications in Mathematical Sciences*, vol. 9, no. 2, pp. 413–457, 2011.
- [57] E. Isaacson and H. Keller, *Analysis of Numerical Methods*. Dover Books on Mathematics, Dover Publications, 1994.
- [58] L. N. Trefethen, *Ordinary differential equations*, pp. 8–78. Ithaca, N.Y. : Cornell University Dept. of Computer Science and Center for Applied Mathematics, 1996. accessed January 15, 2024.
- [59] R. Kosloff and D. Kosloff, “Absorbing boundaries for wave propagation problems,” *Journal of Computational Physics*, vol. 63, no. 2, pp. 363–376, 1986.
- [60] F. Gatti, B. Lasorne, H.-D. Meyer, and A. Nauts, *Introduction to Numerical Methods*, pp. 201–285. Cham: Springer International Publishing, 2017.
- [61] B. M. Karnakov and V. P. Krainov, *WKB Approximation in Atomic Physics*. Springer Science & Business Media, 1 ed., August 2012.
- [62] N. Bleistein and R. Handelsman, *Asymptotic Expansions of Integrals*. Dover Books on Mathematics Series, Dover Publications, 1986.
- [63] U. V. Riss and H. Meyer, “Investigation on the reflection and transmission properties of complex absorbing potentials,” *The Journal of Chemical Physics*, vol. 105, pp. 1409–1419, July 1996.
- [64] J. H. Lambert, “Observationes variae in mathesin puram,” *Acta Helvetica*, vol. 3, no. 1, pp. 128–168, 1758.
- [65] L. Euler, “De serie lambertina plurimisque eius insignibus proprietatibus,” *Acta Academiae scientiarum imperialis petropolitanae*, pp. 29–51, 1783.
- [66] A. Jäckle and H. Meyer, “Time-dependent calculation of reactive flux employing complex absorbing potentials: General aspects and application within the multi-configuration time-dependent Hartree wave approach,” *The Journal of Chemical Physics*, vol. 105, pp. 6778–6786, October 1996.

- [67] W. H. Miller, S. D. Schwartz, and J. W. Tromp, “Quantum mechanical rate constants for bimolecular reactions,” *The Journal of Chemical Physics*, vol. 79, pp. 4889–4898, November 1983.
- [68] A. F. Abdulhameed and Q. A. Memon, “An improved trapezoidal rule for numerical integration,” *Journal of Physics: Conference Series*, vol. 2090, p. 012104, November 2021.
- [69] H. Abdi, “Coefficient of variation,” *Encyclopedia of research design*, vol. 1, no. 5, 2010.
- [70] S. Y. Huolong Liu and M. Li, “Three-dimensional computational fluid dynamics (cfd) study of the gas–particle circulation pattern within a fluidized bed granulator: By full factorial design of fluidization velocity and particle size,” *Drying Technology*, vol. 35, no. 9, pp. 1043–1058, 2017.
- [71] L. Mandelstam and M. Leontowitsch, “Zur theorie der schrödingerschen gleichung,” *Zeitschrift für Physik*, vol. 47, no. 1-2, pp. 131–136, 1928.
- [72] R. S. F. Peter W. Atkins, *Molecular Quantum Mechanics*. Oxford University Press, 5th ed., 2011.
- [73] W. M. Haynes, *CRC handbook of chemistry and physics*. CRC Handbook of Chemistry and Physics, CRC press, 95th ed., 2014.
- [74] W. Hua, “Four-parameter exactly solvable potential for diatomic molecules,” *Phys. Rev. A*, vol. 42, pp. 2524–2529, September 1990.
- [75] H. M. Hulbert and J. O. Hirschfelder, “Potential energy functions for diatomic molecules,” *The Journal of Chemical Physics*, vol. 9, no. 1, pp. 61–69, 1941.
- [76] E. Fidiani, “Modeling of diatomic molecule using the Morse potential and the Verlet algorithm,” *AIP Conference Proceedings*, vol. 1719, p. 030001, March 2016.
- [77] W. SUN, “The energy-consistent method for the potential energy curves and the vibrational eigenfunctions of stable diatomic states,” *Molecular Physics*, vol. 92, no. 1, pp. 105–108, 1997.
- [78] R. Ortega, A. Loría, P. J. Nicklasson, and H. Sira-Ramírez, *Euler-Lagrange systems*, pp. 15–37. London: Springer London, 1998.
- [79] P. A. Tipler and G. Mosca, *Physics for scientists and engineers, extended version, 2020 media update*. W. H. Freeman, 6th ed., August 2007.

A. Normal Mode Analysis

This section derives the normal mode coordinates and eigenvalues of the saddle points for potential energy surfaces (PES). Let the potential energy be provided such that $V(q_1; q_2) : \mathbb{R}^n \rightarrow \mathbb{R}$. When written in cartesian coordinates, the distance can be translated using the following transformation: $q_i \mapsto r'_i$, $r'_i = q_i + q_{i,sd}$, where sd denotes the saddle point displacement. Taylor expanding to 2nd order and choosing the expansion point at the saddle point such that $\sum_{i=\{1,2\}} \left(\frac{\partial V}{\partial r'_i} \right)_{r'_{i,sd}} = 0$ yields (see section 1.4.1, second derivative test):

$$\begin{aligned} V^{(2)}(r_1; r_2) &= V(r_{1,sd}; r_{2,sd}) + \frac{1}{2!} \sum_{i,j} \left(\frac{\partial^2 V}{\partial r_i \partial r_j} \right)_{r'_{i,sd}=0} r_i r_j \\ &= V(r_{1,sd}; r_{2,sd}) + \frac{1}{2} (\mathbf{r}')^\top \mathbf{V}' \mathbf{r}' \end{aligned}$$

Let mass weighted coordinates be provided by $r'_i \mapsto r_i$, $r_i = r'_i m_i^{1/2}$, where m_i is the mass of atom i . Then the potential takes the form:

$$V^{(2)}(r_1; r_2) = V(r_{1,sd}; r_{2,sd}) + \frac{1}{2} \mathbf{r}'^\top \mathbf{F} \mathbf{r} \quad (\text{A.1})$$

with $\mathbf{F} = (m_i m_j)^{-\frac{1}{2}} \mathbf{V}'$. Equation (A.1) is to be diagonalized. However, for this to happen, \mathbf{F} has to be diagonal, which is by no means necessarily true. Hence, the following is introduced: $\mathbf{r} \mapsto \mathbf{Q}$, $\mathbf{r} = \mathbf{L}\mathbf{Q}$. $\mathbf{L} \in \mathbb{C}^{n \times n}$ such that $\mathbf{L}^\top \mathbf{F} \mathbf{L}$ is diagonal and \mathbf{Q} is the normal mode coordinates.

Rewriting the second order potential yields:

$$V^{(2)}(r_1; r_2) = V(r_{1,sd}; r_{2,sd}) + \frac{1}{2} \mathbf{Q}^\top \mathbf{L}^\top \mathbf{F} \mathbf{L} \mathbf{Q}$$

Choosing \mathbf{L} such that $\mathbf{L}^\top \mathbf{F} \mathbf{L}$ is diagonalizable, that is there exists a set of eigenvalues, ω_j , with corresponding eigenvectors, \mathbf{L}_j so $\mathbf{F} \mathbf{L}_j = \omega_j^2 \mathbf{L}_j$. This is solved using $|\mathbf{F} - \omega \mathbf{I}| = 0$, where \mathbf{I} is the identity operator. Furthermore, since \mathbf{F} is symmetric, it follows that each column is mutually orthogonal and \mathbf{L} is an orthogonal matrix. Then $\mathbf{L}^{-1} = \mathbf{L}^\top$ and the following eigenproblem arises:

$$\mathbf{F} \mathbf{L} = \mathbf{L} \boldsymbol{\omega}^2 \implies \boldsymbol{\omega}^2 = \mathbf{L}^\top \mathbf{F} \mathbf{L}$$

Chapter A

which can be substituted such that

$$V^{(2)}(r_1; r_2) = V(r_{1,\text{sd}}, r_{2,\text{sd}}) + \frac{1}{2} \sum_{i=\{1,2\}} \omega_i^2 Q_i^2$$

which ends the derivation.

B. Morse Parameters

This chapter shows the derivation of the exponent Morse parameter, α , from the Harmonic potential. Furthermore, the Morse parameters are provided in Table B.1:

Table B.1: Equilibrium distance, R_0 , and vibrational zero-point frequency, ν_0 , were found in the 95th edition of CRC Handbook of physics and chemistry, section 9, page 102-107 [73]. α was found using eq. (B.3) [†]. Depth of Morse potential well, D_e , was found by converting values to eV from Prof. Hua, Wei [74]. ^{} Depth of Morse potential well, D_e , was found by converting values to eV from Profs. Hulbert, Hugh M. & Hirschfelder, Joseph O. [75]. [#] Depth of Morse potential well, D_e , was found from Prof. Fidiani, E. [76]. [†] Depth of Morse potential well, D_e , was found by converting to eV from Prof. Sun, W. [77].*

Molecule	R_0 [\AA]	μ [10^{-27} kg]	ν_0 [cm $^{-1}$]	α [\AA $^{-1}$]	D_e [eV]
Cl-F	1.628	20.54	783.5	2.288	2.667 [†]
F-H	0.9169	1.589	4 138	2.219	6.123 [‡]
H-Cl	1.27456	1.627	2 991	1.868	4.618 [#]
H-H	0.7414	0.8368	4 401	1.944	4.748 [‡]
H-O	0.9697	1.574	3 738	2.318	4.531 [*]

The potential for the Harmonic oscillator is

$$V^{\text{Harmonic}}(R) = \frac{k(R - R_0)^2}{2} \quad (\text{B.1})$$

where k is the force constant. The force constant is defined by $\left. \frac{d^2 V(R)}{dR^2} \right|_{R=R_0}$ [28]. For eq. (1.15), the differential quotient can be calculated by the 2nd quadratic formula or by using the chain rule: $\left. \frac{d^2 V^{\text{Harmonic}}(R)}{dR^2} \right|_{R=R_0} = \frac{k}{2} \frac{d^2}{dR^2} (R - R_0)^2 = k$. And for eq. (1.3), using the chain rule twice yields

$$\begin{aligned} k &= \left. \frac{d^2 V^{\text{Morse}}(R)}{dR^2} \right|_{R=R_0} = 4\alpha^2 D_e \exp(-2\alpha(R - R_0)) \\ &\quad - 2\alpha^2 D_e \exp(-\alpha(R - R_0)) \Big|_{R=R_0} = 4\alpha^2 D_e - 2\alpha^2 D_e = 2\alpha^2 D_e \end{aligned} \quad (\text{B.2})$$

In order to calculate the exponent parameter, α , eq. (B.2) is substituted into the following definition of the vibrational frequency [28]:

$$\nu = \left(\frac{k}{\mu} \right)^{1/2} = \left(\frac{2\alpha^2 D_e}{\mu} \right)^{1/2} = \alpha \left(\frac{2D_e}{\mu} \right)^{1/2} \implies \alpha = \nu \left(\frac{\mu}{2D_e} \right)^{1/2} \quad (\text{B.3})$$

Chapter B

which was to be shown. Furthermore, eq. (B.2) can be substituted into the harmonic potential provided by eq. (B.1) to yield eq. (1.15). Th

C. Jacobi Coordinates - Three Body System in One Dimension

In this chapter, the translative energy is derived using Jacobi coordinates, after which the Hamiltonian is explicitly written using the Jacobi coordinates. The main source for this derivation is *Theories of molecular reaction dynamics: the microscopic foundation of chemical kinetics* by Henriksen, Niels E. and Hansen, Flemming Y. [47].

C.1 TRANSLATIVE TERMS

Let $\mathbf{x} = \{x_i\}_{i=1}^3$ and $\dot{\mathbf{x}} = \{\dot{x}_i\}_{i=1}^3 = \{\frac{dx_i}{dt}\}_{i=1}^3$ be the set of coordinates and velocities respectively. Then the collinear 1 dimensional three body Langrangian is defined by the Euler-Lagrange equations in cartesian coordinates [78]:

$$\frac{d}{dt} \left(\frac{\partial L}{\partial \dot{x}_i} \right) = \left(\frac{\partial L}{\partial x_i} \right), \quad i = 1, 2, 3 \quad (\text{C.1})$$

from which it can be shown that $L(\mathbf{x}, \dot{\mathbf{x}}) = K(\dot{\mathbf{x}}) - V(\mathbf{x})$ by direct substitution into eq. (C.1) using $F = \frac{\partial V}{\partial x_i}$ and Newton's 2nd law on the right hand side [79]. One can also show this using the cartesian coordinates along with the momentum coordinates. The momentum coordinates are provided by:

$$p_i = \frac{\partial L}{\partial \dot{x}_i} \quad (\text{C.2})$$

In order to evaluate p_i , using eq. (C.2), \dot{x}_i needs to be assessed. New coordinates are therefore introduced. The new coordinates are defined using the following linear transformations, which are illustrated on Figure C.1:

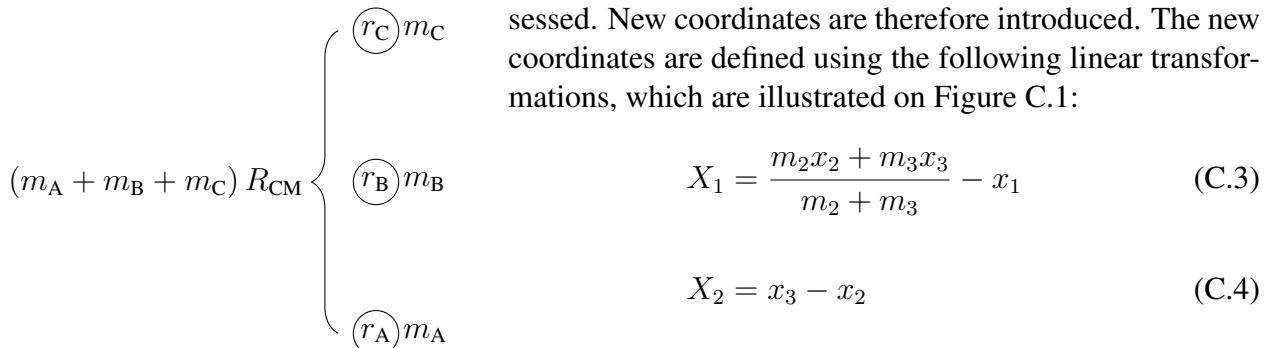


Figure C.1: Jacobi coordinate representation for triatomic systems.

$$X_1 = \frac{m_2 x_2 + m_3 x_3}{m_2 + m_3} - x_1 \quad (\text{C.3})$$

$$X_2 = x_3 - x_2 \quad (\text{C.4})$$

$$X_3 = \sum_{i=1}^3 \frac{m_i}{M} x_i, \quad M = \sum_{i=1}^3 m_i \quad (\text{C.5})$$

where X_1 corresponds to the distance between x_1 and the center-of-mass of x_2 and x_3 , X_2 corresponds to the distance between x_2 and x_3 and X_3 corresponds to the center-of-

mass movement for a 3 body system.

These coordinates are defined, such that there exists a change of coordinate matrix, \mathbf{A} , that fulfills the following:

$$\mathbf{x} \longrightarrow \mathbf{X} = \{X_i\}_{i=1}^3, \quad \mathbf{X} = \mathbf{Ax} \implies \dot{\mathbf{X}} = \mathbf{A}\dot{\mathbf{x}}$$

$$\mathbf{A} = \begin{pmatrix} -1 & \frac{m_2}{m_2+m_3} & \frac{m_3}{m_2+m_3} \\ 0 & -1 & 1 \\ \frac{m_1}{M} & \frac{m_2}{M} & \frac{m_3}{M} \end{pmatrix} \quad (\text{C.6})$$

where the matrix elements in eq. (C.6) was found using eqs. (B.11-B.13). Applying eq. (C.2) to eq. (C.6) yields:

$$p_i = \sum_{j=1}^3 \left(\frac{\partial L}{\partial \dot{X}_j} \right) \left(\frac{\partial \dot{X}_j}{\partial \dot{x}_i} \right) = \sum_{j=1}^3 P_j A_{ji} \implies \mathbf{p} = \mathbf{A}^\top \mathbf{P} \quad (\text{C.7})$$

For the three body problem consisting of masses $\{m_i\}_{i=1}^3$, an inverse diagonal square matrix \mathbf{m}^{-1} can be constructed from the 3 mass points using: $\mathbf{m}^{-1} = ((m_1, m_2, m_3) \cdot (m_1, m_2, m_3)^\top)^{-1/2}$. Using eq. (C.7), the translative energy is provided by the following:

$$T = \frac{1}{2} \mathbf{p}^\top \mathbf{m}^{-1} \mathbf{p} = \frac{1}{2} \mathbf{P}^\top \mathbf{A} \mathbf{m}^{-1} \mathbf{A}^\top \mathbf{P} \quad (\text{C.8})$$

Since eqs. (B.11-B.13) were chosen such that eq. (C.6) fulfills

$$\sum_{i=1}^3 A_{ki} = \delta_{k,3} \quad (\text{C.9})$$

it follows that eq. (C.8) can be separated into two terms consisting of the internal translative terms and the center-of-mass translative term, respectively, since $\delta_{k,3}$ assures that the sum of the first and second row is zero, while the sum of the third row is one. This row corresponds to X_3 , which was the center-of-mass coordinates. Hence, the center-of-mass coordinates can be separated according to the eq. (C.9) restriction.

Summing eq. (C.7) over all momenta and substituting eq. (C.9) yields:

$$\sum_{i=1}^3 p_i = \sum_{i=1}^3 \sum_{k=1}^3 P_k A_{ki} = \sum_{k=1}^3 P_k \delta_{k,3} = P_3 \quad (\text{C.10})$$

which is conjugate to X_3 .

And eq. (C.8) can be rewritten such that:

$$T = \sum_{k=1}^2 \sum_{l=1}^2 \left(\sum_{i=1}^3 \frac{A_{ki} A_{li}}{2m_i} \right) P_k P_l + \sum_{i=1}^3 \frac{1}{2m_i} \frac{m_i^2}{M^2} P_3^2 \quad (\text{C.11})$$

with the first and last terms being the internal translative energy and the translative energy from the center-of-mass frame, respectively. In order for eq. (C.11) to be diagonal, the following restrictions are provided:

$$\sum_{i=1}^3 \frac{A_{ki} A_{li}}{2m_i} = 0, \quad (k \neq l) \wedge (k, l \neq 3) \quad (\text{C.12})$$

Introducing the following compact notation using eq. (C.6):

$$\sum_{i=1}^3 \frac{A_{ki}^2}{2m_i} = \frac{1}{2M_k} = \begin{cases} \frac{M}{2m_1(m_2+m_3)} & \text{if } k = 1 \\ \frac{m_2+m_3}{2m_2 m_3} & \text{if } k = 2 \\ \frac{1}{2M} & \text{if } k = 3 \end{cases} \quad (\text{C.13})$$

where the $k = 3$ case is ignored due to the eq. (C.12) restriction, the translative energy can be rewritten by substituting eq. (C.13) into eq. (C.11):

$$T = \sum_{k=1}^2 \frac{P_k^2}{2M_k} + \frac{P_3^2}{2M} \quad (\text{C.14})$$

If the cartesian coordinates, \mathbf{X} , are chosen such that the conjugate momentum coordinates, \mathbf{P} , fulfill eq. (C.14) holds true, then \mathbf{X} are called Jacobi coordinates. This was to be shown.

C.2 HAMILTONIAN - 3 DIMENSIONS

The Hamiltonian is provided by eq. (0.21). The translational operator for a 3 body system in 1 dimension is then:

$$\hat{T} = -\frac{\hbar^2}{2} \sum_{i=1}^3 \frac{1}{m_i} \frac{\partial^2}{\partial x_i^2} \quad (\text{C.15})$$

Applying eq. (C.6) to eq. (C.15), using the chain rule and separating the center-of-mass term out yields [29]:

$$\hat{T}_{\text{int}} = -\frac{\hbar^2}{2} \sum_{k=1}^2 \sum_{l=1}^2 \left(\sum_{i=1}^3 \frac{A_{ki} A_{li}}{m_i} \right) \left(\frac{\partial}{\partial X_k} \frac{\partial}{\partial X_l} \right) \quad (\text{C.16})$$

This resembles eq. (C.11). Therefore, by introducing the same restriction as eq. (C.9), the internal term in the center-of-mass frame becomes:

$$\hat{T}_{\text{int}} = -\frac{\hbar^2}{2} \sum_{k=1}^2 \frac{1}{M_k} \frac{\partial^2}{\partial X_k^2} \quad (\text{C.17})$$

where M_k is defined by eq. (C.13). The Hamiltonian is found by substituting (C.17) into eq. (0.21):

$$\hat{H} = -\frac{\hbar^2}{2} \sum_{k=1}^2 \frac{1}{M_k} \frac{\partial^2}{\partial X_k^2} + V(\mathbf{X}) \quad (\text{C.18})$$

which was to be found.

D. Continuity Equation and Flux Operator

In this chapter, the continuity equation provided by:

$$\frac{dP}{dt} = -\nabla \cdot j \quad (\text{D.1})$$

will be derived in two dimensions for two particles. The following representations of the flux operator, j , will be derived:

$$j = -\frac{i\hbar}{2m} (\Psi^* \nabla \Psi - \Psi \nabla \Psi^*) = \frac{\hbar}{m} \Im(\Psi^* \nabla \Psi) = \Re(\Psi^* \hat{P} \Psi) \quad (\text{D.2})$$

D.1 CONTINUITY EQUATION: TWO DIMENSIONS, TWO PARTICLES

For two spatial dimensions, the probability density is provided by: $P(R_1, R_2; t) = |\Psi(R_1, R_2; t)|^2 = \Psi^*(R_1, R_2; t)\Psi(R_1, R_2; t)$ and for two particles, there are two mass points, μ_1 and μ_2 . Substituting into the left hand side of eq. (D.1) and using the time-dependent Schrödinger eq. provided by eq. (0.21) yields:

$$\begin{aligned} \frac{\partial P(R_1, R_2; t)}{\partial t} &= \frac{\partial}{\partial t} |\Psi(R_1, R_2; t)|^2 = \frac{\partial}{\partial t} [\Psi^*(R_1, R_2; t)\Psi(R_1, R_2; t)] \stackrel{\text{Product rule}}{=} \\ &\Psi^*(R_1, R_2; t) \frac{\partial \Psi(R_1, R_2; t)}{\partial t} + \Psi(R_1, R_2; t) \frac{\partial \Psi^*(R_1, R_2; t)}{\partial t} \stackrel{\text{TDSE}}{=} \\ &- \Psi^*(R_1, R_2; t) i \left[\frac{\hbar}{2} \left(-\frac{1}{\mu_1} \frac{\partial^2}{\partial R_1^2} - \frac{1}{\mu_2} \frac{\partial^2}{\partial R_2^2} \right) + \frac{V}{\hbar} \right] \Psi(R_1, R_2; t) \\ &+ \Psi(R_1, R_2; t) i \left[\frac{\hbar}{2} \left(-\frac{1}{\mu_1} \frac{\partial^2}{\partial R_1^2} - \frac{1}{\mu_2} \frac{\partial^2}{\partial R_2^2} \right) + \frac{V}{\hbar} \right] \Psi^*(R_1, R_2; t) = \\ &- \Psi^*(R_1, R_2; t) i \left[\frac{\hbar}{2} \left(-\frac{1}{\mu_1} \frac{\partial^2}{\partial R_1^2} - \frac{1}{\mu_2} \frac{\partial^2}{\partial R_2^2} \right) \right] \Psi(R_1, R_2; t) \\ &+ \Psi(R_1, R_2; t) i \left[\frac{\hbar}{2} \left(-\frac{1}{\mu_1} \frac{\partial^2}{\partial R_1^2} - \frac{1}{\mu_2} \frac{\partial^2}{\partial R_2^2} \right) \right] \Psi^*(R_1, R_2; t) \end{aligned} \quad (\text{D.3})$$

In two dimensions, $\nabla = \left(\frac{\partial}{\partial R_1}, \frac{\partial}{\partial R_2} \right)$, define $M = -\frac{1}{2} \begin{pmatrix} \frac{1}{\mu_1} & 0 \\ 0 & \frac{1}{\mu_2} \end{pmatrix}$, then $\nabla \cdot M \cdot \nabla = -\frac{1}{2\mu_1} \frac{\partial^2}{\partial R_1^2} - \frac{1}{2\mu_2} \frac{\partial^2}{\partial R_2^2}$ and eq. (D.3) can be written as the following:

$$\begin{aligned} & \frac{\partial P(R_1, R_2; t)}{\partial t} \\ &= (-i\hbar [\Psi^*(R_1, R_2, t) \nabla \cdot M \cdot \nabla \Psi(R_1, R_2, t) + \Psi(R_1, R_2, t) \nabla \cdot M \cdot \nabla \Psi^*(R_1, R_2, t)]) = \\ &= -\nabla \cdot (-i\hbar [\Psi^*(R_1, R_2, t) M \cdot \nabla \Psi(R_1, R_2, t) + \Psi(R_1, R_2, t) M \cdot \nabla \Psi^*(R_1, R_2, t)]) \stackrel{\text{Div def.}}{=} \\ &= -\text{div}(-i\hbar [\Psi^*(R_1, R_2, t) M \cdot \nabla \Psi(R_1, R_2, t) - \Psi(R_1, R_2, t) M \cdot \nabla \Psi^*(R_1, R_2, t)]) \\ &= -\text{div}(j(R_1, R_2, t)) \end{aligned}$$

where j is defined by: $j(R_1, R_2, t) = -i\hbar \Psi^*(R_1, R_2, t) M \cdot \nabla \Psi(R_1, R_2, t) + i\hbar \Psi(R_1, R_2, t) \cdot M \cdot \nabla \Psi^*(R_1, R_2, t)$. Hence the continuity relation has been derived. j is called the Probability Flux.

D.2 FLUX OPERATOR REPRESENTATIONS

Section D.1 yielded flux operators provided by $j = -\frac{i\hbar}{2m} (\Psi^* \nabla \Psi - \Psi \nabla \Psi^*)$. This section rewrites the flux operator using imaginary parts and real parts of complex numbers to yield eqs. (D.2). Since this section deals with algebraic manipulation of complex numbers, some identities are reiterated, even though these ought to be well known. The wavefunction, Ψ , consists of a real part and an imaginary part: $\Psi = \Psi_{Re} + i\Psi_{Im}$, where $i^2 = -1$. Taking the real and imaginary part yield the following: $\Re(\Psi) = \Psi_{Re}$ and $\Im(\Psi) = \Psi_{Im}$. Finally, taking the complex conjugate yields: $\Psi^* = \Psi_{Re} - i\Psi_{Im}$. The flux operator, j , can be rewritten in the following way, using simple algebraic manipulations:

$$\begin{aligned} j &= -\frac{i\hbar}{2m} (\Psi^* \nabla \Psi - \Psi \nabla \Psi^*) \\ &= -\frac{i\hbar}{2m} [(\Psi_{Re} + i\Psi_{Im})^* \nabla (\Psi_{Re} + i\Psi_{Im}) - (\Psi_{Re} + i\Psi_{Im}) \nabla (\Psi_{Re} + i\Psi_{Im})^*] \\ &= -\frac{i\hbar}{2m} [\Psi_{Re} \nabla \Psi_{Re} + i\Psi_{Re} \nabla \Psi_{Im} - i\Psi_{Im} \nabla \Psi_{Re} + \Psi_{Im} \nabla \Psi_{Im} \\ &\quad - \Psi_{Re} \nabla \Psi_{Re} + i\Psi_{Re} \nabla \Psi_{Im} - i\Psi_{Im} \nabla \Psi_{Re} - \Psi_{Im} \nabla \Psi_{Im}] \\ &= -\frac{i\hbar}{2m} [2i\Psi_{Re} \nabla \Psi_{Im} - 2i\Psi_{Im} \nabla \Psi_{Re}] = \frac{\hbar}{m} [\Psi_{Re} \nabla \Psi_{Im} - \Psi_{Im} \nabla \Psi_{Re}] \end{aligned}$$

Taking the imaginary part of the wavefunction disregards the real part. Hence, multiplying j by i and taking the imaginary part still yields j . Furthermore, by doing so, terms, which do not hold an i , can be added as long as the imaginary part of j is taken.

Exploiting this yields the following result:

$$\begin{aligned}
j &= \frac{\hbar}{m} \Im [i (\Psi_{Re} \nabla \Psi_{Im} - \Psi_{Im} \nabla \Psi_{Re})] \\
&= \frac{\hbar}{m} \Im [(\Psi_{Re} \nabla \Psi_{Re} + \Psi_{Im} \nabla \Psi_{Im}) + i (\Psi_{Re} \nabla \Psi_{Im} - \Psi_{Im} \nabla \Psi_{Re})] \\
&= \frac{\hbar}{m} \Im [\Psi_{Re} \nabla (\Psi_{Re} + i\Psi_{Im}) - i\Psi_{Im} \nabla (\Psi_{Re} + i\Psi_{Im})] \\
&= \frac{\hbar}{m} \Im [(\Psi_{Re} - i\Psi_{Im}) \nabla (\Psi_{Re} + i\Psi_{Im})] = \frac{\hbar}{m} \Im [(\Psi_{Re} + i\Psi_{Im})^* \nabla (\Psi_{Re} + i\Psi_{Im})] \\
&= \frac{\hbar}{m} \Im (\Psi^* \nabla \Psi)
\end{aligned}$$

which was to be shown. Similarly, taking the real part of the wavefunction disregards the imaginary part and using $-i \cdot i = 1$ yields:

$$\begin{aligned}
j &= \Re \left[\Psi_{Re} \frac{\hbar}{m} \nabla \Psi_{Im} - \Psi_{Im} \frac{\hbar}{m} \nabla \Psi_{Re} \right] \\
&= \Re \left[i \left(\Psi_{Re} \left(-\frac{i\hbar}{m} \nabla \right) \Psi_{Im} - \Psi_{Im} \left(-\frac{i\hbar}{m} \nabla \right) \Psi_{Re} \right) \right] \\
&= \Re \left[i \left(\Psi_{Re} \left(-\frac{i\hbar}{m} \nabla \right) \Psi_{Im} - \Psi_{Im} \left(-\frac{i\hbar}{m} \nabla \right) \Psi_{Re} \right) \right. \\
&\quad \left. + \left(\Psi_{Re} \left(-\frac{i\hbar}{m} \nabla \right) \Psi_{Re} - \Psi_{Im} \left(-\frac{i\hbar}{m} \nabla \right) \Psi_{Im} \right) \right] \\
&= \Re \left[\Psi_{Re} \left(-\frac{i\hbar}{m} \nabla \right) (\Psi_{Re} + i\Psi_{Im}) - i\Psi_{Im} \left(-\frac{i\hbar}{m} \nabla \right) (\Psi_{Re} + i\Psi_{Im}) \right] \\
&= \Re \left[(\Psi_{Re} - i\Psi_{Im}) \left(-\frac{i\hbar}{m} \nabla \right) (\Psi_{Re} + i\Psi_{Im}) \right] \\
&= \Re \left[(\Psi_{Re} + i\Psi_{Im})^* \left(-\frac{i\hbar}{m} \nabla \right) (\Psi_{Re} + i\Psi_{Im}) \right] \\
&= \Re \left[\Psi^* \left(-\frac{i\hbar}{m} \nabla \right) \Psi \right] = \Re (\Psi^* \hat{P} \Psi)
\end{aligned}$$

where the momentum operator in position space is provided by: $\hat{P} = -\frac{i\hbar}{m} \nabla$. Hence, the flux operator can be represented by eq. (D.2). This concludes the flux operator¹.

¹As a final remark to the flux operator, the name is motivated. The name arrives from the fact that the flux can easily be found by integrating eq. (D.1) over the position space, using Gauss divergence theorem and the definition of Flux [29]: $\int_V \frac{\partial}{\partial t} P d\mu_V = - \int_V \operatorname{div}(j) d\mu_V = - \int_S j \cdot n_S d\mu_S = \operatorname{Flux}(j)$, where n_S is the orthogonal vector to the surface S .

E. Accuracy of Strang-Marchuk Splitting

This section derives the accuracy of the Strang-Marchuk algorithm. As mentioned in section 2.1.1, eq. (2.10) is derived in this section. Substituting eq. (2.7) into eq. (2.8) yields:

$$\begin{aligned}
 |\Phi_{\text{SM}}^{(2)}(\Delta t)\rangle &= |\Psi(t_0)\rangle - \frac{\Delta t}{2} \frac{i\hat{V}}{\hbar} |\Psi(t_0)\rangle - \frac{(\Delta t/2)^2}{2!} \frac{\hat{V}^2}{\hbar^2} |\Psi(t_0)\rangle - \Delta t \frac{i\hat{T}}{\hbar} \left(|\Psi(t_0)\rangle \right. \\
 &\quad \left. - \frac{\Delta t}{2} \frac{i\hat{V}}{\hbar} |\Psi(t_0)\rangle - \frac{(\Delta t/2)^2}{2!} \frac{\hat{V}^2}{\hbar^2} |\Psi(t_0)\rangle \right) - \frac{\Delta t^2}{2!} \frac{\hat{T}^2}{\hbar^2} \left(\right. \\
 &\quad \left. |\Psi(t_0)\rangle - \frac{\Delta t}{2} \frac{i\hat{V}}{\hbar} |\Psi(t_0)\rangle - \frac{(\Delta t/2)^2}{2!} \frac{\hat{V}^2}{\hbar^2} |\Psi(t_0)\rangle \right) + \mathcal{O}(\Delta t^3) \\
 &= |\Psi(t_0)\rangle - \frac{\Delta t}{2} \frac{i\hat{V}}{\hbar} |\Psi(t_0)\rangle - \Delta t \frac{i\hat{T}}{\hbar} |\Psi(t_0)\rangle - \frac{(\Delta t/2)^2}{2!} \frac{\hat{V}^2}{\hbar^2} |\Psi(t_0)\rangle \\
 &\quad - \frac{\Delta t^2}{2!} \frac{\hat{T}^2}{\hbar^2} |\Psi(t_0)\rangle - \frac{\Delta t^2}{2} \frac{\hat{T}\hat{V}}{\hbar^2} |\Psi(t_0)\rangle + \mathcal{O}(\Delta t^3) \tag{E.1}
 \end{aligned}$$

and substituting eq. (E.1) into eq. (2.9) yields:

$$\begin{aligned}
 |\varphi_{\text{SM}}^{(2)}(\Delta t/2)\rangle &= |\Psi(t_0)\rangle - \frac{\Delta t}{2} \frac{i\hat{V}}{\hbar} |\Psi(t_0)\rangle - \Delta t \frac{i\hat{T}}{\hbar} |\Psi(t_0)\rangle - \frac{(\Delta t/2)^2}{2!} \frac{\hat{V}^2}{\hbar^2} |\Psi(t_0)\rangle \\
 &\quad - \frac{\Delta t^2}{2!} \frac{\hat{T}^2}{\hbar^2} |\Psi(t_0)\rangle - \frac{\Delta t^2}{2} \frac{\hat{T}\hat{V}}{\hbar^2} |\Psi(t_0)\rangle - \frac{\Delta t}{2} \frac{i\hat{V}}{\hbar} \left(|\Psi(t_0)\rangle \right. \\
 &\quad \left. - \frac{\Delta t}{2} \frac{i\hat{V}}{\hbar} |\Psi(t_0)\rangle - \Delta t \frac{i\hat{T}}{\hbar} |\Psi(t_0)\rangle - \frac{(\Delta t/2)^2}{2!} \frac{\hat{V}^2}{\hbar^2} |\Psi(t_0)\rangle \right. \\
 &\quad \left. - \frac{\Delta t^2}{2!} \frac{\hat{T}^2}{\hbar^2} |\Psi(t_0)\rangle - \frac{\Delta t^2}{2} \frac{\hat{T}\hat{V}}{\hbar^2} |\Psi(t_0)\rangle \right) - \frac{(\Delta t/2)^2}{2!} \frac{\hat{V}^2}{\hbar^2} \left(\right. \\
 &\quad \left. |\Psi(t_0)\rangle - \frac{\Delta t}{2} \frac{i\hat{V}}{\hbar} |\Psi(t_0)\rangle - \Delta t \frac{i\hat{T}}{\hbar} |\Psi(t_0)\rangle - \frac{(\Delta t/2)^2}{2!} \frac{\hat{V}^2}{\hbar^2} |\Psi(t_0)\rangle \right. \\
 &\quad \left. - \frac{\Delta t^2}{2!} \frac{\hat{T}^2}{\hbar^2} |\Psi(t_0)\rangle - \frac{\Delta t^2}{2} \frac{\hat{T}\hat{V}}{\hbar^2} |\Psi(t_0)\rangle \right) + \mathcal{O}(\Delta t^3) \\
 &= |\Psi(t_0)\rangle - \Delta t \frac{i\hat{T}}{\hbar} |\Psi(t_0)\rangle - \Delta t \frac{i\hat{V}}{\hbar} |\Psi(t_0)\rangle - \frac{\Delta t^2}{2} \frac{\hat{T}^2}{\hbar^2} |\Psi(t_0)\rangle \\
 &\quad - \frac{\Delta t^2}{2} \frac{\hat{V}^2}{\hbar^2} |\Psi(t_0)\rangle - \frac{\Delta t^2}{2} \frac{\hat{T}\hat{V}}{\hbar^2} |\Psi(t_0)\rangle - \frac{\Delta t^2}{2} \frac{\hat{V}\hat{T}}{\hbar^2} |\Psi(t_0)\rangle + \mathcal{O}(\Delta t^3)
 \end{aligned}$$

$$\begin{aligned} &= |\Psi(t_0)\rangle - \frac{i\Delta t}{\hbar} (\hat{T} + \hat{V}) |\Psi(t_0)\rangle \\ &\quad - \frac{\Delta t^2}{2\hbar^2} (\hat{T}^2 + \hat{T}\hat{V} + \hat{V}\hat{T} + \hat{V}^2) |\Psi(t_0)\rangle + \mathcal{O}(\Delta t^3) \end{aligned} \quad (\text{E.2})$$

and eq. (E.2) is provided in the main text as eq. (2.10), which was to be shown.